

Elastic and Inelastic Finite Element Analysis of Tube
to Tubesheet Junction for C2- Hydrogenation Reactor
Subject to Pressure and Temperature Actions

by

Khosrow Behseta

Thesis submitted in fulfillment of partial
requirements for the degree of

Doktor der technischen Wissenschaften

at the

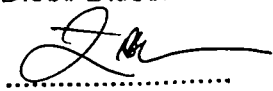
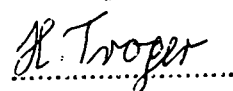
Institute of Pressure Vessel and Plant Technology
Department of Mechanical Engineering
Vienna University of Technology

Under Supervision of

Professor Dr. J. L. Zeman

2006

Diese Dissertation haben begutachtet:

Acknowledgements

I would like to thank Professor Dr. J. L. Zeman , whose guidance and supervision made this work possible.

It has been a great opportunity and valuable experience to work under close supervision of Professor Zeman for purpose of applying complex code rules to very sophisticate industrial equipment which is licensed by an international company.

I also would like to thank Professor Dr. H. Troger for his review of the work.

Moreover, many thanks to Dr. Franz Rauscher, Dr. Reinhard Preiss, Dr. Sebastian Schindler and Mr. M. Moosavi for their valuable hints on various subjects in regard to the ANSYS program applications on this specific work.

Last but not the least I am great full to my wife Miss Melika Bahadori whose consistent support during my study gave me confidence of facing various situations.

ABSTRACT

Elastic and inelastic finite element analyses have been carried out for the shell to tubesheet junction of a C2- Hydrogenation reactor subject to pressure and temperature actions.

Three geometrically different models have been tested to select the most efficient one for applying the analysis. These models are symmetrical and differ from each other by the amount of tube to tubesheet perforations and the type of the supporting tubes. It has been shown that a tubesheet FE model with full perforation supported by combination of the link and three- dimensional elements produces quite reasonable results as compared to other proposed models.

FE elastic analysis was carried out for tubesheet thickness as per datasheet, and also for reduced tubesheet and shell thicknesses. Results indicate that the lower thickness can be employed and additional thickening of the tubesheet and adjacent shells is not required. Inelastic analyses for the gross plastic deformation and progressive plastic deformation design checks have been carried out for the data sheet original thickness as well as the reduced thicknesses. Results indicate that in either case larger pressure in comparison with data sheet values can be carried safely by tubesheet and adjacent shells.

Moreover, employing Melan's shakedown theorem, it is shown that the residual stress field created during a loading and unloading cycle will not grow during successive load and unload cycles once the tube sheet is subject to cyclic actions and, hence, the tubesheet shakes down to completely elastic behavior.

Fatigue analysis for both welded and unwelded region of tubesheet and shell junction at the groove location have indicated that the number of life cycles for this reactor is much larger than the number of operating cycles anticipated to occur during the reactor life.

Radii effect analysis was performed in order to study the effect of radii size on the magnitude of the stresses. Results of analysis indicate that small radii result in larger stresses, which increase of this transition radius results in decrease of stresses down to a minimum, and further increase leads to an increase of stresses. The optimum radius size has been reported.

A manual calculation according to ASME Sec. VIII and EN 13445-3 Appendix 13 and Annex J was performed to show the difference in results obtained according to these codes.

Statement of the Problem

Various codes and standards give quite different values for the thickness of tubesheets of heat exchangers, and, based on this, fabrication time and overall price will be quite different.

It has been suggested that considerable reduction in the cost of fixed tubesheet heat exchangers can be obtained by employing the Direct Route in Design by Analysis, according to EN 13445-3 Annex B.

The purpose of this work is the comparison of different results for various codes and standards with the direct route approach, which requires linear-elastic ideal-plastic Finite Element calculations.

The junction of a tubesheet to the shell of a fixed tubesheet heat exchanger for a hydrogenation reactor of an olefin plant is to be modeled by means of ANSYS 8.1 software, in order to carry out the various finite element analyses that are required to be performed in this method.

The results for the specified tubesheet thickness, based on ASME section VIII, Division 1 and 2, and the standard EN 13445, Clause 13 and Annex J, shall be compared with that of the Direct Route in Design by Analysis. In this investigation for the Direct Route in Design by Analysis two constitutive laws are required in the relevant design checks: A linear- elastic and a linear-elastic ideal-plastic constitutive law.

Moreover, the effect of various radii sizes and shell thicknesses at the junction is to be investigated because of their importance especially for fatigue life calculations. In this investigation, linear analyses are to be performed for pressure and temperature loadings, whilst for the determination of the GPD limit pressure and for the shakedown design check a combination of pressure and temperature has been considered.

Due to the base load operation, this reactor is considered not to be subject to cyclic loading and, formally, in a classical admissibility check no fatigue calculation is required. However fatigue checks are required in accordance with the requirements of EN 13445-3, the Direct Route does require a detailed fatigue design check even if fatigue is not governing the design, is not considered to be a problem.

Table of Contents

1. Introduction
2. Basic data and mechanical properties
 - 2.1) Dimensions and design data
 - 2.2) Basic material data
3. Code descriptions and results of code calculations
 - 3.1) ASME Section VIII
 - 3.2) EN 13445-3 clause 13 and annex J
 - 3.3) Results and discussions of results of codes calculations
4. Finite element models and boundary conditions
 - A) Model selection
 - B) Displacement boundary conditions
 - C) Load boundary conditions and load cases
5. Elastic analyses
 - 5.1) Model elastic calculation
 - 5.2) Results and discussions of results
 - 5.3) Fatigue considerations
6. Inelastic analyses
 - A) Gross plastic deformation design check
 - B) Progressive plastic deformation design check
7. Discussions of the results
8. Radii effect
9. Reduced thickness analysis
10. Discussions and comparison of the result
11. Conclusions
12. Appendices
13. References

1. Introduction

Study of plane surfaces bent to a simple geometry has a long history, going back to Poisson who defined extension of inner and outer fibers of a plate in terms of the radius of curvature for the purpose of arriving at bending equations.

His work has been extended by many others to cover plates of various shapes subject to different loads and with different edge supports. Results of these efforts for circular solid flat plate with various edge conditions was presented among others by Timoshenko[1].

Timoshenko formulated the deflection equation by studying bending of a flat plate due to distributed loadings. He considered equilibrium, compatibility and elasticity equations for this purpose.

The result of his equation for the deflection of a solid flat circular plate made of linear – elastic material uniformly loaded and with clamped edge is

$$w = qa^4 / (16 \cdot D) \quad (1.1)$$

There w is the maximum deflection, q the uniformly distributed load, a the plate radius, and D is the plate flexural rigidity, $D = Ee^3 / 12 (1 - \nu^2)$, with e the plate thickness.

With regard to the application of this equation to a fixed tubesheet heat exchanger some factors require specific attention. These factors are:

- (1) The effect of plate perforation.
- (2) The effect of an imperforated rim with pressure loading as it interacts with the perforated part of the plate.
- (3) The effect of the staying action of the tubes specifically those close to the rim.
- (4) The effect of differential thermal expansion due to different temperatures and/ or different materials, tubes, tubesheets, shells.

These considerations have been subject of extensive studies by many researchers, the effect of perforation on flat plate deflection and resulting stresses subject of analytical and experimental work in the early 1960's.

Gardner [2-4] proposed to replace the perforated plates with a solid plate with elastic constants appropriately adjusted. A review of the research including extensive literature survey is given in [6], with the milestone papers [7-10] included in full.

Based on Gardner's work, ASME and other codes adopted his proposals for the calculation an effective modulus of elasticity and an effective Poisson's ratio.

In early 1980's, these curves were extended to lower thickness ranges with inclusion of more general features [9,10].

The lateral deflection of the plate with respect to the outer edge of the imperforated rim is governed by the classical plate solution, given, in the present context, among others by Soler[11][12] in the form

$$D \nabla^4 w = K * Q \quad (1.2)$$

where D is the perforated plate effective stiffness, K an elastic foundation parameter reflecting the staying effect of the tube bundle, and Q the imposed loading or any other action that acts like an imposed loading.

The solution of equation (1.2) involves Bessel (Ber and Bei) functions and a parameter Xa , which represents the ratio of the axial stiffness of the tube bundle to the bending rigidity of the perforated plate, having the form

$$Xa^4 = 24(1 - \nu^{*2}) (nE (d - t)t) (a / h)^3 / (E^* La) \quad (1.3)$$

In the equation above E^* and ν^* are the effective tubesheet modulus of elasticity and Poisson's ratio. L is the tube free length between tubesheet inside faces, n the number of tubes, E the tube modulus of elasticity, and d and t are the tube outer diameter and the thickness, respectively. H is the tubesheet thickness and a the radius of the perforated region. A manual computation is possible with the aid of the series of charts from which values of the Bessel functions versus Xa can be obtained. Staying action of tubes has been considered by replacing tubes by equivalent elastic foundation modulus.

This approach is employed in many codes and standards like ASME, CODAP, EN 13445 – 3, Clause 13, etc. A different approach is used in Annex J of EN 13445 – 3[14], an approach based on limit analysis concepts.

Another, very different, very general approach is specified in Annex B of EN 13445 – 3, the Direct Route to Design by Analysis, which allows for the usage of finite element method (FEM) software in specified design checks. Out of the number of design checks defined in Annex B three are of relevance here. These checks are:

- The gross plastic deformation design check (GPD – DC).
- The progressive plastic deformation design check (PD – DC).
- The cyclic fatigue design check (F-DC)

In short these three design checks are related to the modes of failure for which the component should possess adequate safety margins. These failure modes are encumbered failure criteria based on limit load theory, shakedown theory, and fatigue theory.

The gross plastic deformation and progressive plastic deformation design checks cannot be dealt with in an elastic analysis, as the corresponding failure mechanism is inelastic. Ideally, these inelastic failure modes should be assessed by appropriate analyses that adequately model the mechanism of failure.

2. Basic Data and Mechanical Properties of the Considered Heat Exchanger

The considered C2–Hydrogenation reactor is the largest and heaviest heat exchanger in an Olefin plant. This special heat exchanger, considered here, is actually a chemical reactor with 3200 tubes. It is considered to be a long delivery equipment, due to its very large inside diameter and considerable time required for tubesheet drilling, tubes installation, and various welding steps.

Dimensions, properties, and basic material information, which are repeatedly referred to, are given below [15]:

2.1 Dimensions, design data and basic material type

Shell inside diameter = 4250 mm

Channel inside diameter = 4230 mm

Outside Tube Limit (OTL) = 4136 mm

Tube pitch = 69 mm

Tube pattern = 60°

Thickness of tubesheet = 135 mm

Shell thickness channel side = 90 mm

Shell thickness shell side = 70 mm

Corrosion allowance = 3 mm, with the exception of tubes, for which zero is specified

Design fluid temperature on tube side = -4/190°C

Design fluid temperature on shell side = -4/145°C

Design pressure shell side = 1 MPa

Design pressure tube side = 4 MPa

Shell side test pressure = 6 MPa

Tube side test pressure = 1.5 MPa

Shell side mean wall temperature = 50°C

Tubesheet mean wall temperature = 100°C

Calculated temperature for selection of material properties:

Shell material channel side = 190°C

Shell material tube side = 145°C

Tubesheet material = 167.5°C

Tube material = 167.5 °C

Basic materials:

Tube material: SA 334 Gr. 1

Tube sheet material: SA 266 Cl. 2

Lower shell material: SA 516 Gr. 70

Upper shell material: SA 516 Gr. 70

Figure (2.1) below indicates some additional dimensions, as given on the data sheet of the considered heat exchanger. All thicknesses are uncorroded actual minimum permissible thicknesses after manufacture.

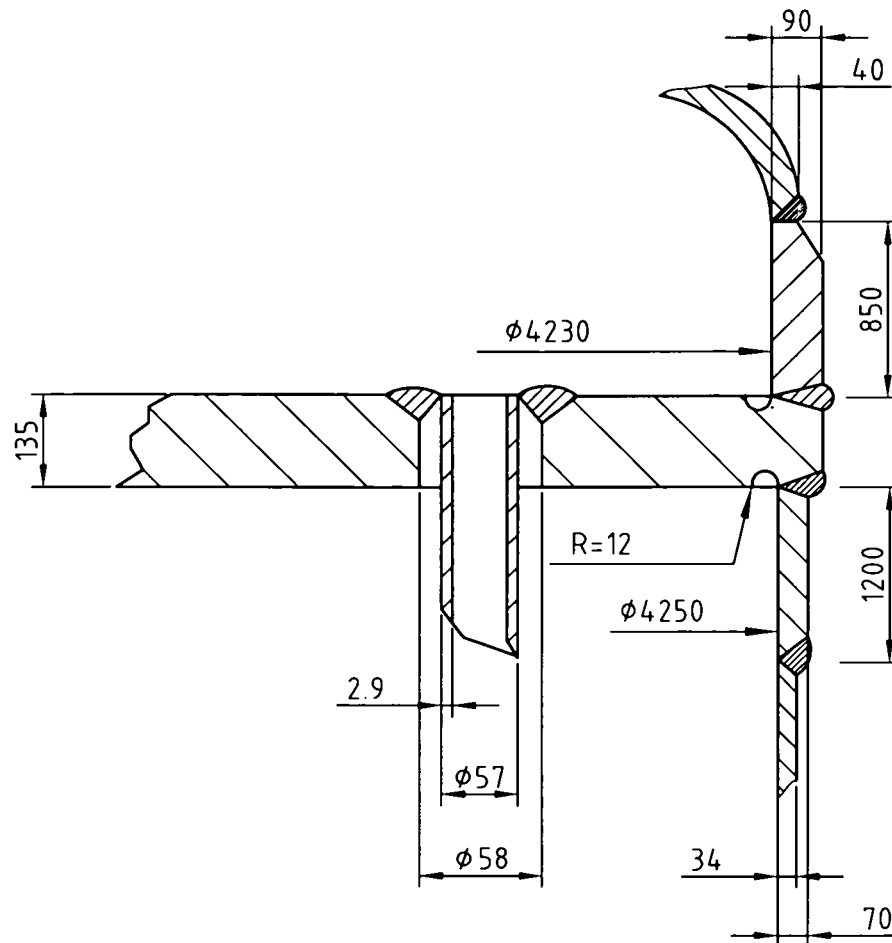


Fig (2.1) Basic dimensions and mechanical features

(2.2) Basic Material Data

- (A) The material physical properties are extracted from EN 13445-3 Annex O and have been cross-checked with ASME Sec II, Part D. Values are reported at the calculation temperature. In this regard E is the modulus of elasticity, σ is the allowable stress, and α is the mean coefficient of linear thermal expansion.
- (B) Allowable stresses are calculated based on EN 13445, Clause 6, using yield and tensile properties reported by ASME Sect. II, Part D at calculation temperature. Table (2.2.1), (2.2.1.A) and (2.2.2) below provide the material information, table (2.2.3) gives the allowable stress values based on ASME Section VIII Division I. Table (2.2.4) gives the allowable stress intensity according to EN 13445-Clause 6.

Table (2.2.1) Material Properties Data at Calculated Temperature^e

Mat	E(MPa)	α^d (1/°C) .10 ⁻⁶	Rm (MPa)	Rp,0.2/ 20 °C (MPa)	Rp,0.2/ tcalc (MPa)	t _{cal} ^a (°C)
SA 516 Gr 70 ^b	192000	12.7	485	260	225.75	190
SA 516 Gr 70 ^c	195000	12.42	485	260	232	145
SA 266 Cl 2	193875	12.51	485	250	217.5	167.5
SA 334 Gr 1	193875	12.51	380	205	181.5	167.5

^a Calculation temperatures are :

- Fluid design temperature for shell material channel side.
- Fluid design temperature for shell material shell side.
- Average design temperature of shell and tube sides for tube sheet and tubes.

^b Channel side.

^c Shell side.

^d α depends on t_{cal}

^e Rm is the ultimate stress at 20°C, Rp 0.2/20 is the material yield strength at 20°C, or the 0.2% - proof stress, and Rp,0.2/tcalc is the material yield strength, or the 0.2 %- proof stress, at calculation temperature.

Table (2.2.1.A) Variation of Material Yield Strength, in MPa, with Temperature

T °C Material	up to 40	50	65	100	108	125
SA 516 Gr 70	260	255	246	239	238	235
SA 266 Cl 2	250	242	233	227	226	223
SA 334 Gr 1	205	201	195	189	188	186
SA 537 Cl 1 ^a	310	303	292	283	282	279

^a $64 < t \leq 100$ where t is thickness.

Table (2.2.2) Material Properties Defined for DBA (MPa)^{a,d}

Material	$R_{p0.2}$ /t metal	$R_{m/20}$	$R_{p0.2}/t_{calc}$ $/R_m$	γ_R	RM	$RM_{d,red}$ ^f
SA 516Gr70 ^b	238	485	.49	1.25	190	165
SA 516Gr70 ^c	255	485	.53	1.25	204	176.6
SA 266CL2	226	485	.47	1.25	180.8	156.6
SA 334Gr1	188	380	.49	1.25	150.4	130.2
SA 537Cl2 ^e	282	485	.58	1.25	225.6	195

^a For $RM = R_{p0.2}/t_{calc}$

^b Channel side shell

^c Shell side shell

^d Symbols according to EN-13445 Annex B.

^e Proposed material for upper shell to make it stronger.

^f Reduced design value for usage with Mises yield condition.

Table (2.2.3) Material allowable stress (MPa) from ASME Div 1^a

MAT	Allowable stress in tension (MPa)	Allowable stress in shear (MPa)	Allowable stress in bending - Pressure (MPa)	Allowable stress in bending- Pressure & Temp. (MPa)	t _{cal} (°C)
SA 266CL. 2	138	110.34	275.86	552	167.5
SA 334Gr. 1	108.2	86.62	216.55	432.8	167.5
SA 516Gr: 70	138	110.34	275.86	552	190

^a Calculation temperatures are :

- Fluid design temperature for shell material in channel side.
- Fluid design temperature for shell material shell side.
- Average design temperature of shell and tube sides for tubesheet and tubes.

Table (2.2.4) Material allowable stress(MPa) from EN-13445: DBF

	allow Stress value- Tension (MPa)	Allowable stress in shear (MPa)	Allowable stress in bending- Pressure (MPa)	Allowable stress in bending- Pressure & Temperature (MPa)	t _{cal} ^a (°C)
SA 266 Cl. 2	145	116	290	435	167.5
SA 334 Gr. 1	121	96.8	242	363	167.5
SA 516 Gr. 70	150.5	120.4	301	451.5	190

^a Calculation temperatures are :

- Fluid design temperature for shell material in channel side.
- Fluid design temperature for shell material shell side.
- Average design temperature of shell and tube sides for tube sheet and tubes.

3. Code Description and Results of Manual Calculations

The methods for calculation of tubesheets, as given below in the considered codes, use the concept of the equivalent solid plate. In this method the perforated plate is replaced by a solid plate that is geometrically identical to the perforated plate but has modified values of the elastic constants - modulus of elasticity and Poisson's ratio.

3.1 ASME Sec. VIII[13]:

In this code, the basic equations with regard to fixed tubesheets are provided according to the classical plate theory with modifications for the plate perforation.

A. Divison 1:

For fixed tubesheets, Div 1 covers, in article AA-2.6, the effect of plasticity at the tube sheet to channel or shell joints. This article suggests that if loading is such that high discontinuity stresses exist at the channel-to-tubesheet and/or shell-to-tubesheet joints, to alleviate this condition a decision may be made to change the geometries of the shells or the tubesheet in order to meet all stress limits given in AA-2.4. These stress limits given in AA- 2.4 are limits on tubesheet shear and bending stresses and tube streses in the outermost tube row. These limitations are:

$$|\sigma| \leq 1.5 \Omega S$$

$$|\tau| \leq 0.8 S$$

where

σ is the bending stress in the tube sheet,

τ is the average shear stress in the tubesheet at the outer edge of the perforated region,

S is the allowable stress for the tubesheet material,

Ω is the allowable stress amplification factor, (4/3) for pressure loading and (8/3) for pressure and temperature loadings. For the value of the above parameters, see table (3.3.1).

In certain cases, when the tube sheet stress level is below the limit, but either or both of the shell or channel bending plus membrane stresses exceed their limits, an additional "elastic-plastic" solution step may be taken. This permits an adjustment of the shell and/ or channel modulus of elasticity, which in turn affects the rotation of the joint. Adjustment of the modulus of elasticity reflects the anticipated load shift resulting from plastic action at the joint.

This code also emphasizes that the elastic-plastic procedure shall only be used for pressure loading. However, it is indicated that the introduction of a reduced effective modulus has the effect of reducing the shell or channel stress in the

elastic-plastic iteration; however due to load shifting, this usually leads to an increase in tubesheet stress.

Results of manual calculations according to the code procedure are covered in the table given below.

B. Div 2:

The procedure presented in this code for a fixed tubesheet is also based on the concept of the equivalent solid plate with basic plate theory and with additional consideration of radial stresses coming from the pressure acting at the inside of the tubes.

Article 4-931.1 gives the mechanical and pressure load on circular plates. This article gives the stress intensity, based on stresses across the minimum ligament width and through the thickness of the plate. Equations (1) and (2), of Article 4.931, give the stresses across the minimum ligament width and through the thickness of the plate. These equations are given below. The larger value calculated according to these equations should be selected. The following descriptions are used

$$S = (P/h) \sqrt{[(\Delta p R^*/t) + (w/\pi t R^*)^2 + (\sigma_r)^2]}, \quad (1)$$

or

$$S = (0.5)(P/h) \{ \sqrt{[(\Delta p R^*/t) + (w/\pi t R^*)^2 + (\sigma_r)^2]} + \sigma_r + (2P_i h / P) \}, \quad (2)$$

where S is the equivalent stress, called here stress intensity, P is the tube inside pressure, Δp is the differential pressure across tube sheet, R^* is the effective radius of perforated plate, h is the nominal width of ligament the minimum cross section, t is the thickness of tube sheet, w is the radial displacement of tubesheet edge, and σ_r is the radial stress averaged through the depth of the equivalent solid plate.

The first term in equations (1) and (2) under the square root reflects the effect of the transverse shear stress due to the mechanical and pressure loads. It is maximum in the outer most ligament of the perforated region. The averaged radial stress σ_r is the stress resulting from applied in- plane loading averaged over the thickness of the equivalent solid plate. It includes the stresses due to pressure in the tubes or perforations. No bending stresses are included.

By reviewing the article the following points can be highlighted:

A) Effect of tubesheet displacement and/or rotations due to shell movement is not clearly defined.

B) Article 4-904(c) states that staying action of tubes is not covered.

C) Article 4- 920(d) asks for a discontinuity analysis by considering the imperforated rim as a separate ring or cylinder based on Article 4-7, but requirements and details for such an analysis are not provided directly in the code.

D) The scope is limited to a tube sheet thickness to pitch ratio not smaller than 2.0- the ratio of the heat exchanger under discussion is out side of the scope. Due to overall consideration it was therefore decided not to provide the Div 2 calculations in this work.

3.2 EN 13445-3:

Among other types of heat exchangers, Clause 13 and Annex J provide rules for the design of the fixed tube type. The relations provided in Clause 13 are based on the classical elastic theory of thin plates and shells with the assumption of tubesheet staying on an elastic foundation created by tubes, similar to the ASME approach.

Annex J provides an alternative method based on limit analysis. This annex assumes constant shell thickness at the junction. The basic equations are still derived by classical plate theory with account for various stresses. The created stress field is then simply compared with allowable limits that are based on limit analysis theory.

The procedure tabulated in Appendix J for the calculation of staying effect of tubes is structurally undetermined for fixed tubesheets. This fact requires the calculation with various values, minimum, maximum, and, possibly intermediate values. It is the code recommendation that, by making series of assumptions, the most favorable final result should be used. This can affect the final conclusion.

3.3 Results and discussions of results of codes calculations

For the purpose of design work, the various loading conditions to be considered shall include the normal operating conditions, the start- up conditions, the shut-down conditions, the upset and the pressure test conditions, that may govern the design of the main components of the heat exchanger (i.e. tubesheets, tubes, shell, channel).

The related load cases are,

- Load case 1: Tube-side pressure ($p_t=4$ MPa) and shell-side pressure ($p_s=1$ MPa) acting simultaneously, without thermal expansion.
- Load case 2: Tube -side ($p_t=4$ MPa) and shell-side pressures($p_s =1$ MPa) acting simultaneously and with thermal expansion.
- Load case 3: Shell-side pressure ($p_s =1$ MPa) acting only, without thermal expansion.
- Load case 4: Tube-side pressure ($p_t=4$ MPa) acting only, without thermal expansion.
- Load case 5: Thermal expansion acting only.
- Load case 6: Tube-side pressure($p_t= 4$ MPa) acting only , with thermal expansion.
- Load case 7: Shell-side pressure acting only ($p_s =1$ MPa), with thermal expansion.
- Load case 8: Tube side pressure ($p_t= 6.6$ MPa), thermal expansion, no shell side pressure with shell side temperature of 50 °C. This load case is used for preparation of table (8.1.A.1).

For purpose of this work, only the load cases with most severe effect, as given below, have been considered. The load cases considered are:

Load case 1: Tube- side pressure($P_t=4$ MPa) and shell side pressure($P_s =1$ MPa) acting simultaneously with out thermal expansion.

Load case 2: Tube-side pressure ($P_t=4$ MPa) and shell side pressure ($P_s =1$ MPa) acting simultaneously and with thermal expansion.

All calculations have been carried out at corroded condition.

Table (3.3.1) gives tabulated results.

Table (3.3.1): Results of calculation according to codes(A)

	Load Case	$\sigma_{b,max}$ (MPa)	τ_{max} (MPa)	τ_a (MPa)	$\sigma_{b,a}$ (MPa)	τ_{max} / τ_a	$\sigma_{b,max} / \sigma_{b,a}$	Notes
EN 13445-3 Clause 13	Pressure	266.64	63	116	290	0.44	0.92	(F)
	Pres.+ Temp.	130.33	30.8	116	435	0.27	0.30	$f_{allow}= 3f$ (E)
Annex J	Pressure	-	-	-		0.88	0.51	(B) 0.39
ASME Sec. VIII Div. 1	Pressure	265.53	56	110	275.86	0.51	0.96	(C) , (D)
	Pres. + Temp.	115	40.2	110	552	0.68	0.36	

Notes:

- (A) $\sigma_{b,max}$ is the maximum calculated bending stress, (MPa),
 τ_{max} is the maximum calculated shear stress (MPa),
 τ_a is the allowable stress in shear (MPa),
 $\sigma_{b,a}$ is the allowable stress in bending (MPa).
- (B) Uniform wall thickness is assumed. The Annex J method is based on the calculation of load ratios for bending and shear, the ratios are for the imperforated region. The method presented does not contain effects of thermal stresses in this part of the check. The 0.39 is the optimum value of $\sigma_{b,max} / \sigma_{b,a}$. optimal for the whole structure
- (C) Curves for the effective elastic tube sheet constants do not depend on the tube sheet thickness.
- (D) ASME Sec.VIII, Div. 2 has not been considered, since the staying action of tubes is not covered. Also, curves for equivalent elastic properties are out of the graphs' limit.
- (E) f is the allowable stress in tension, see table (2.2.4).
- (F) The allowable stress in shear is $.8f$, the allowable stress in bending is $2f$.

Comparing shear stresses due to pressure only, the ASME procedure gives slightly larger values than the EN Standard, whereas for bending EN gives slightly larger values. It should be noted that the effective elastic tubesheet constants in ASME VIII/ 1, which do not depend on the tube sheet thickness, seem to be less accurate than those of EN 13445-3, which do depend on the tube sheet thickness.

4. FEA Models and Boundary Conditions

This chapter deals with the FE models used in the direct route approach of design by analysis, which is covered in chapter five.

A. Model Selection

The FEA has been carried out by ANSYS version 8.1. The primary step was to decide on the model geometry and its overall dimensions. Three different models were considered and, based on the results obtained, one was selected for the additional detailed investigations.

The investigated models are:

(I) Quarter of the size model (called full model) - Fig (4.1.1 – 4.1.5)

The geometry of this model has been constructed in a stepwise fashion in the following way:

- Bottom up, with consideration of the actual geometry and for $\frac{1}{4}$ of the tube sheet surface.
- The model covers all tubes in the region, tube sheet and connecting shells with grooves at the junctions.
- The model has been created basically by swap and extrude commands, at first the tubesheet layout was constructed and then relevant areas were extruded.
- All the three-dimensional tubes for half of their length and within the plane of 90° symmetry have been included in the model. This type of modeling has also been employed by Jones and Gordon[16].
- Solid 45 elements have been uniformly employed everywhere throughout the model with good aspect ratio at tubesheet, radii and connection points. Other parts have fair aspect ratios.
- Usage of long elements has been avoided everywhere.
- For this model true elastic constants have been used due to the very exact geometry.
- This model contains 501912 nodes and 254545 elements, which, although giving efficient geometry, requires considerable time and memory storage for numerical calculations of inelastic parts.

(II) One eighth of the size model(called link model) – Fig (4.2.1 – 4.2.2)

The second model was constructed in the following way:

- The geometry covers $\frac{1}{8}$ of the tubesheet surface.
- The model covers some of the pipes, tubesheet, grooves, and shells at the junction.
- This model has also been constructed by swap and extrude commands.
- The tubesheet for the three outermost rows of tubes is perforated and for the rest it is a solid plate.
- The perforated zone is fitted with three- dimensional tubes, and for the rest of the tubesheet link 2D elements have been placed at locations where in reality tubes are.

- The three- dimensional tubes have half of their length.
- Elements are solid 45 and link elements.
- For this model true elastic constants have been used for the tubesheet on the perforated and the rim region and reduced ones for non-perforated parts (of the tubesheet).
- The model is made of 18211 elements and 27280 nodes.

(III) Sector of tube sheet face (called sector model) – Fig. (4.2.3 – 4.2.4)

The third model has been constructed in the following way:

- The geometry is of a cake type.
- The models covers three-dimensional tubes, tubesheet, and connecting shells, with the grooves at the junctions.
- The model has been constructed by swap and extrude commands.
- The tubesheet has been modeled as a perforated plate.
- A large portion of the perforated zone has been fitted with three- dimensional tubes.
- Holes which are not equipped with 3D tubes are supported in vertical direction with link elements to simulate the missing pipes. The number of link elements for each hole is twelve.
- Solid 45 elements have been used everywhere in the model with good aspect ratios in the tubesheet and grooves and at the junction points, and with acceptable values elsewhere.
- True elastic constants have been used everywhere in the model.
- The model consists of 42482 elements and 82238 nodes.

In comparison with the simpler link model, this model is much more accurate, and since it covers all the holes in the region, the values of the elastic constants are the true values. Moreover, staying action of tubes are captured by both of the link and three-dimensional tubes.

(IV) Tested Models

Due to various considerations and trade-off between accuracy, simplicity, computational time, and memory requirements for selection of optimized model, each model has been tested for the same load case according to the data presented in section 2.

It is concluded that the sector type model is the most feasible one. Therefore, this model has been used for all the other aspects of this work. It should also be noted that for the full model, once it is read in, ANSYS requires additional memory space in form of RAM, so that this could be used as a scratch file. Often this required memory allocation had to be adjusted such that the program could read and run internal Boolean operations.

Table (4.1) and the graphs (4.1.1 to 4.2.4) below give the result of the displacement comparison for the various models.

Table (4.1) Model Comparison – Maximum Displacements (mm)
($P_{\text{tube}} = 4.0 \text{ MPa}$, $P_{\text{shell}} = 1.0 \text{ MPa}$, ambient temperature)

Model \ \nearrow	Tube Sheet	Tubes	Shell
Link	0.5	1.0	1.48
Full	0.329	1.403	1.43
Sector	0.324	1.309	1.27

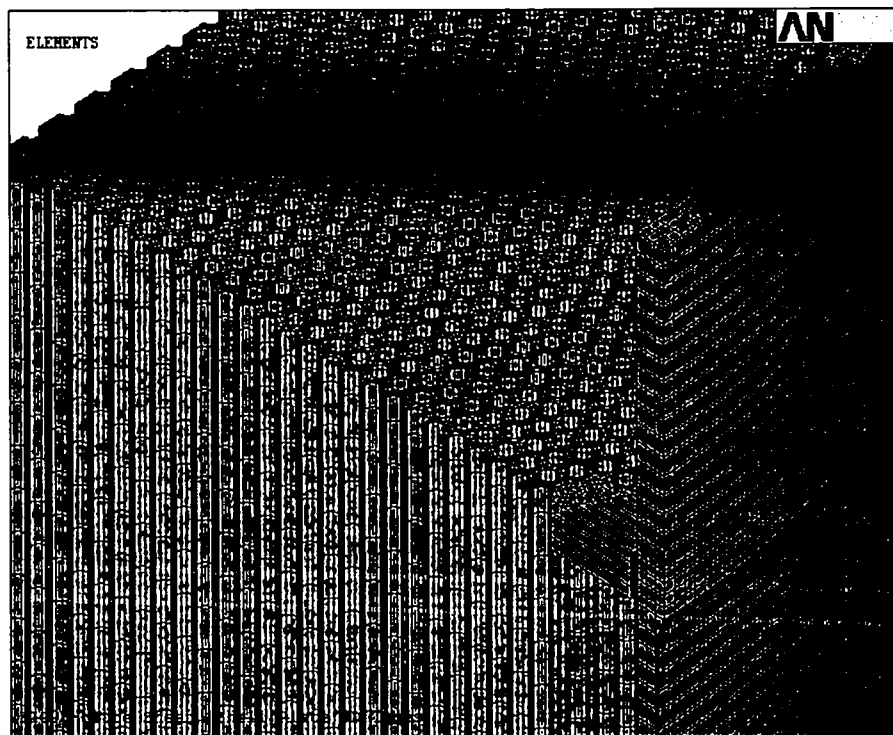


Fig. (4.1.1): Full model: geometry

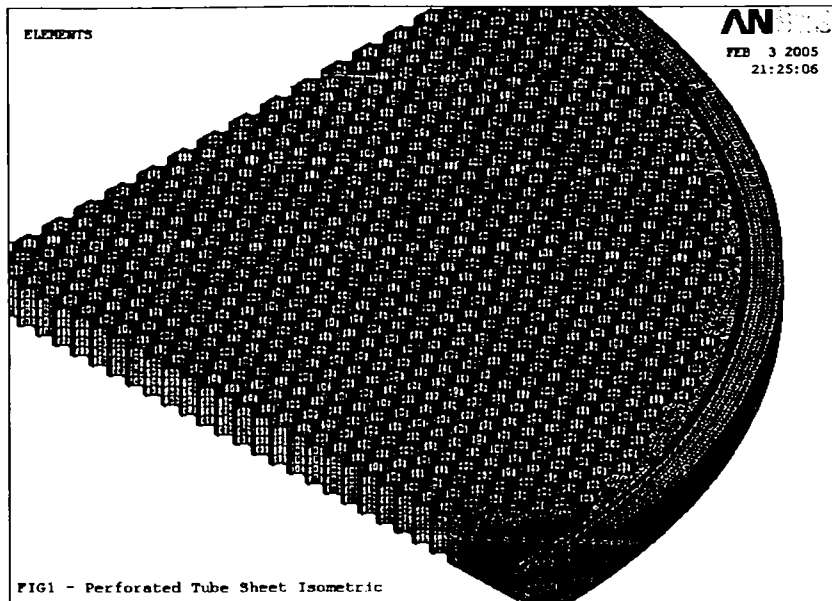


Fig. (4.1.2): Full Model: Tubesheet

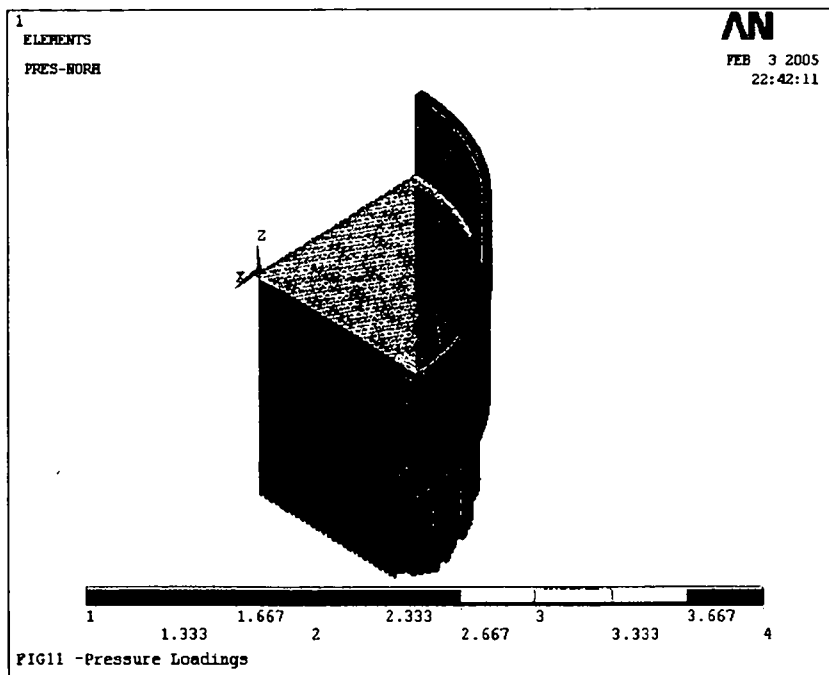


Fig. (4.1.3): Full Model: Pressure Loadings

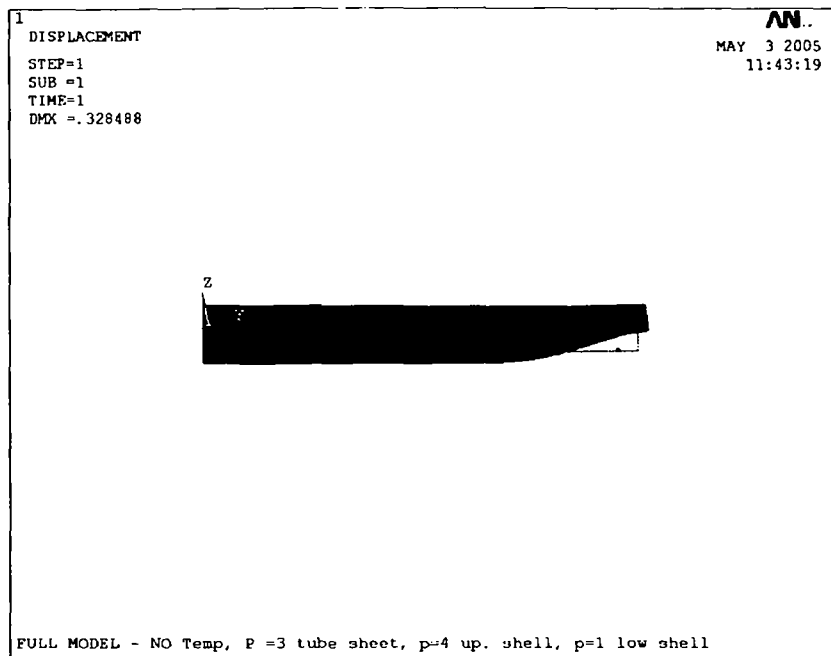


Fig. (4.1.4A): Full Model :Tubesheet Displacement

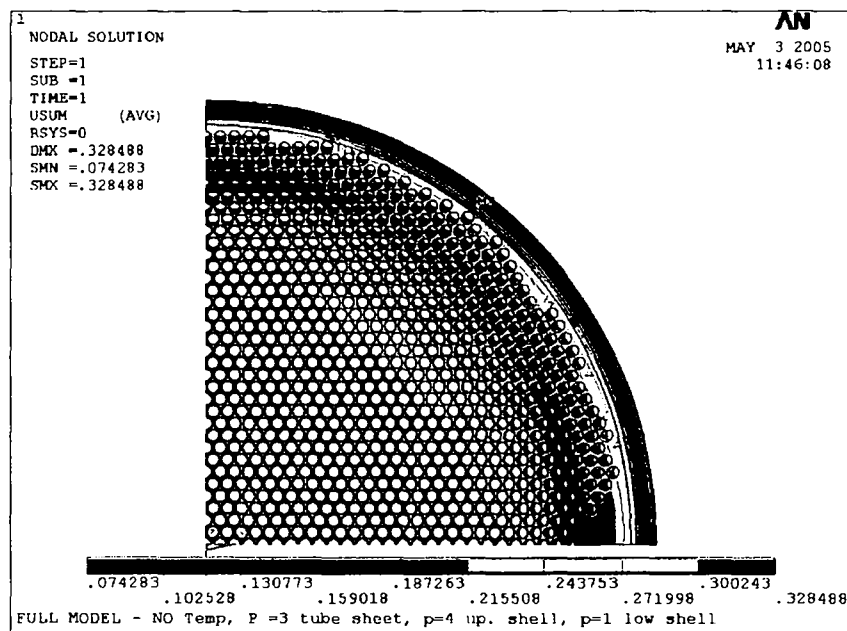


Fig. (4.1.4B): Full Model: Tubesheet Displacement

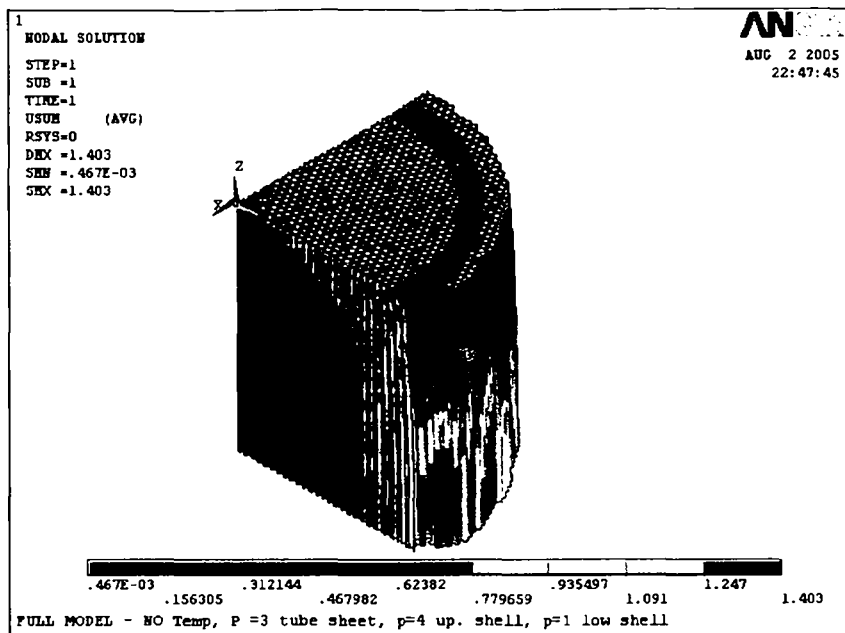


Fig. (4.1.4): Full model: Tube displacement

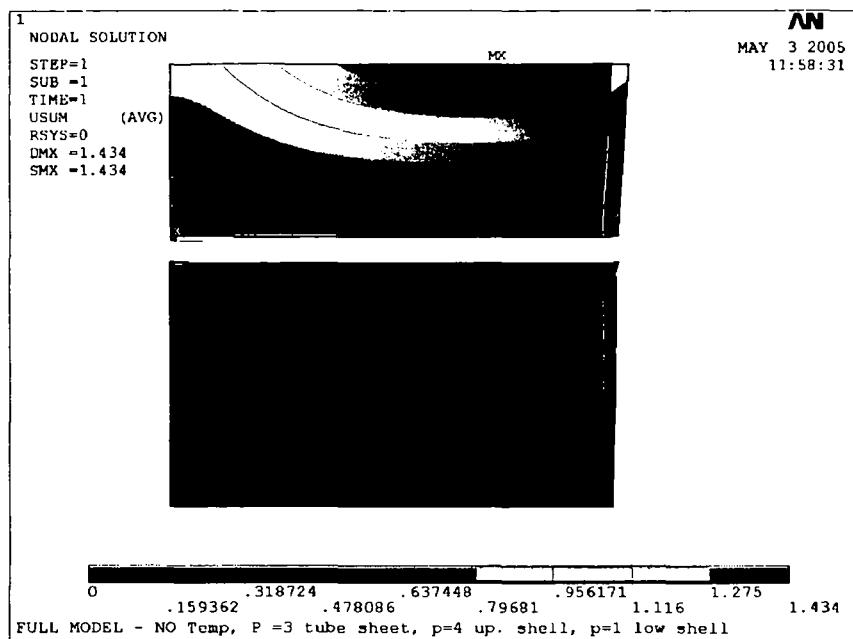


Fig. (4.1.5): Full model: Shell displacement

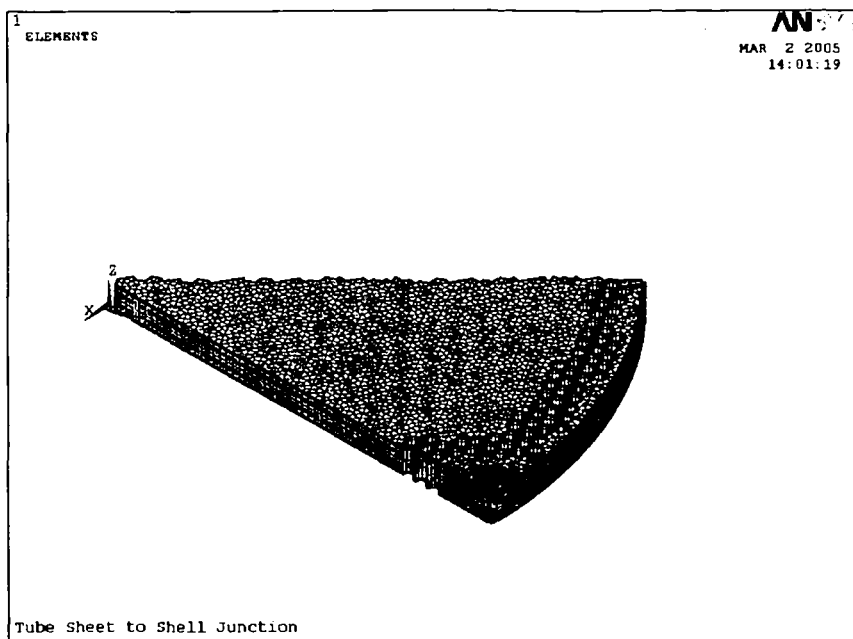


Fig. (4.2.1.A): Link Model: Tubesheet geometry

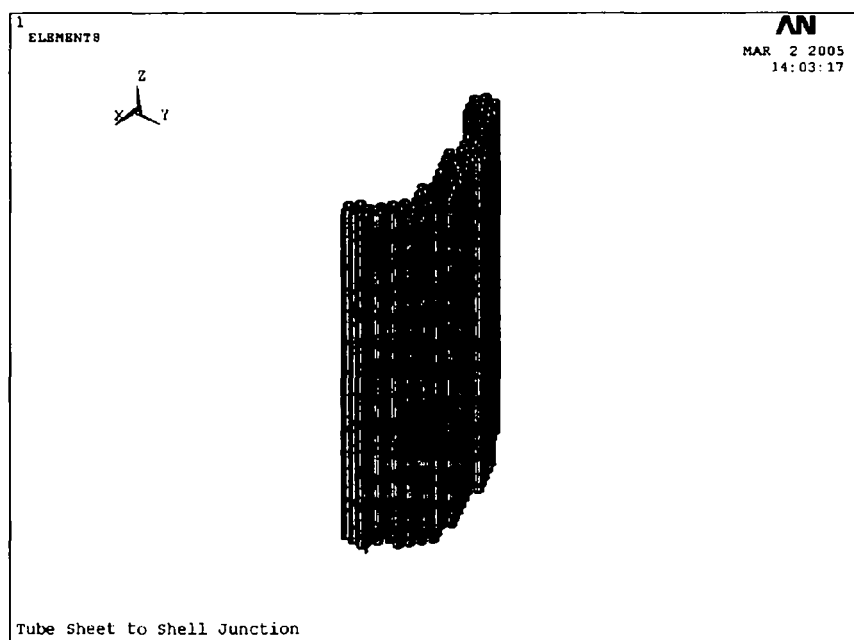


Fig. (4.2.1.B): Link Model: Tube geometry

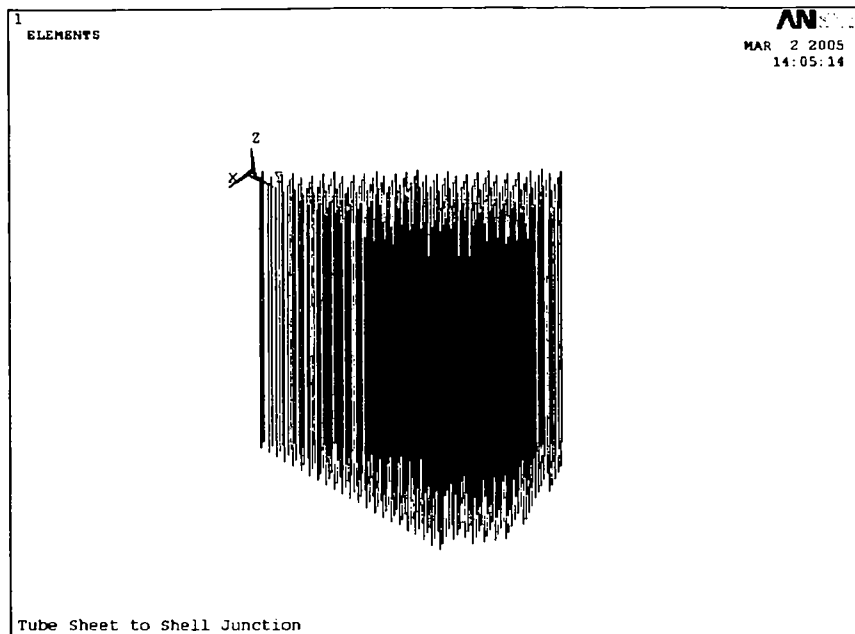


Fig. (4.2.1.C): Link Model: Link element geometry

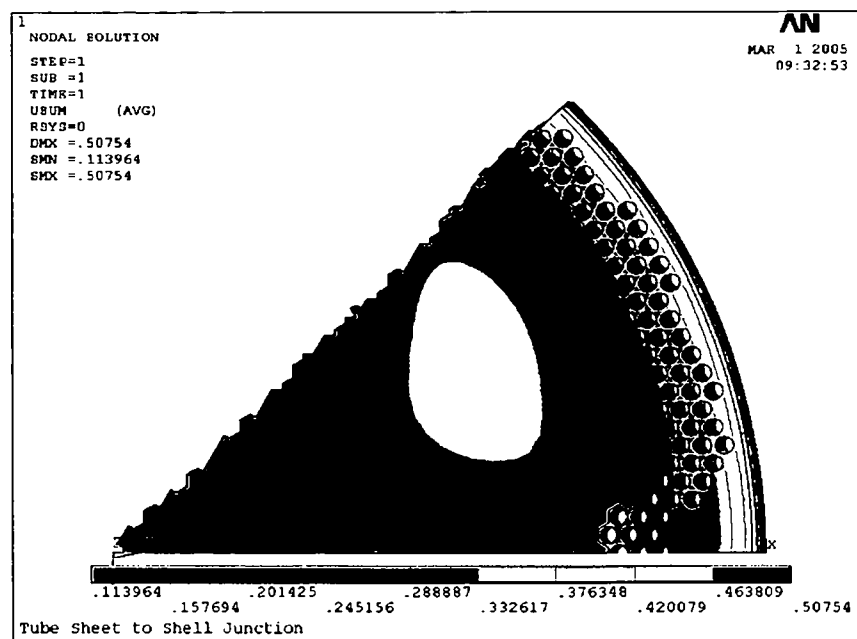


Fig. (4.2.2): Link model: Tubesheet displacement

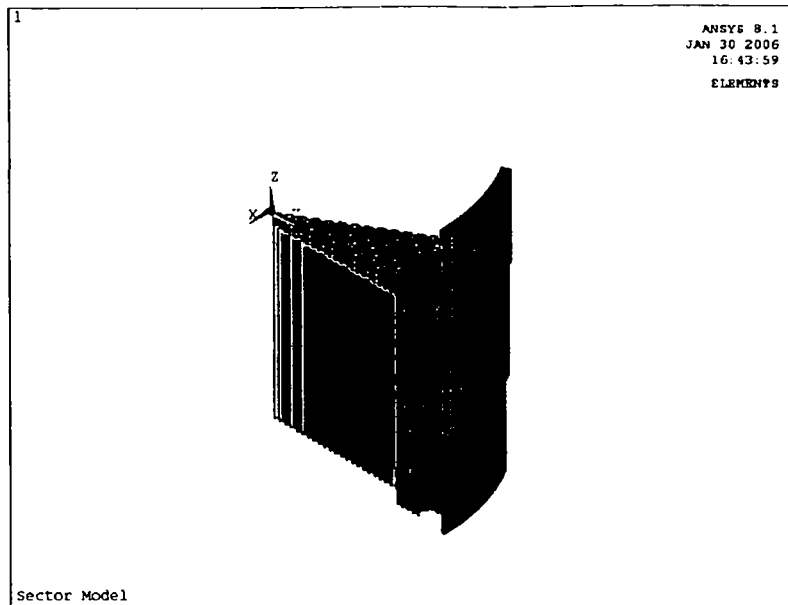


Fig. (4.2.3.A): Sector model: Geometry

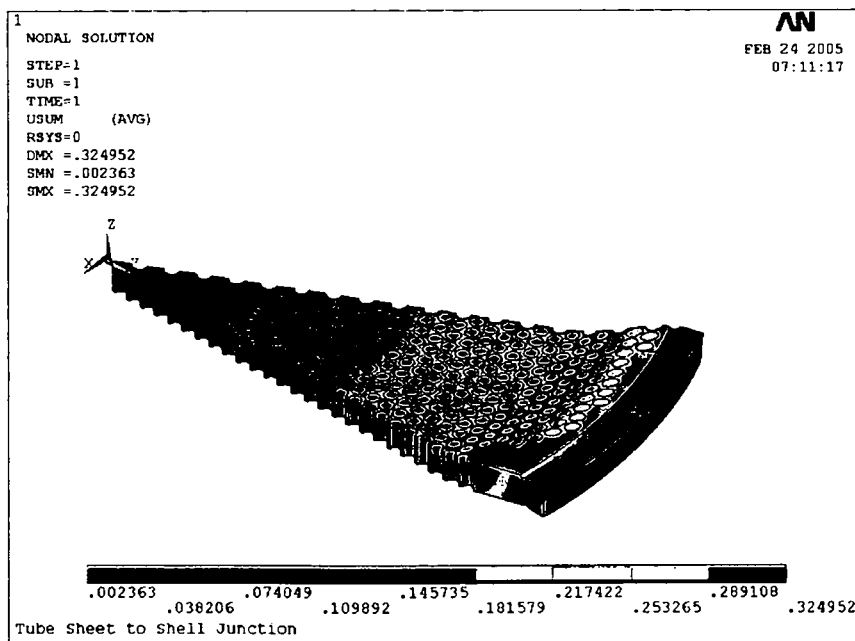


Fig. (4.2.4.B): Sector model: Tubesheet displacement (mm)

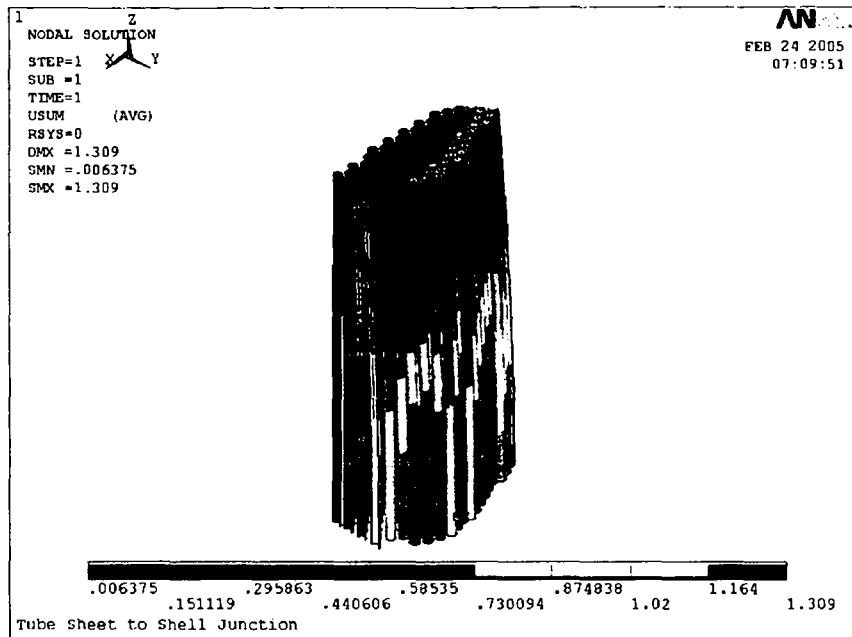


Fig. (4.2.4.C): Sector model: Tube displacement (mm)

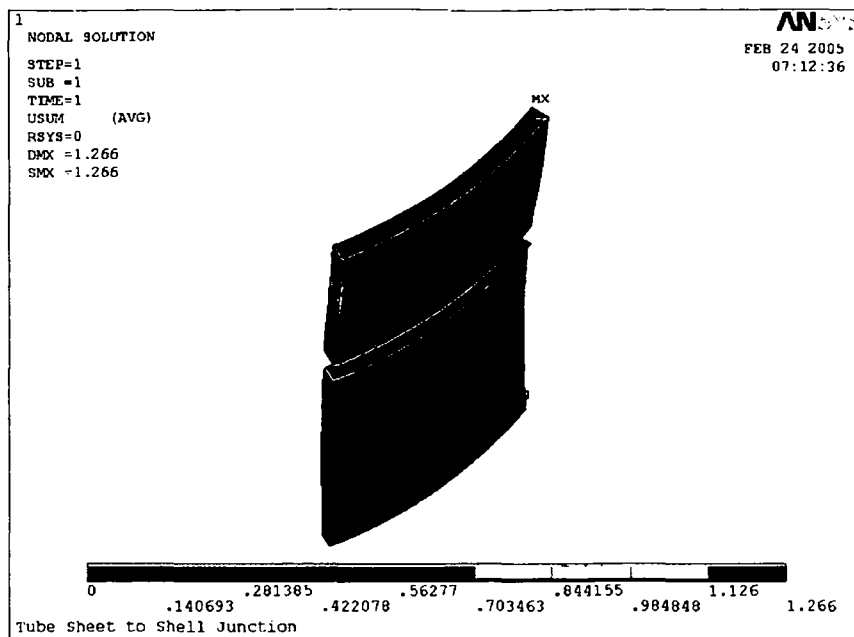


Fig. (4.2.4.D): Sector model: Shell displacement (mm)

(B) Displacement Boundary Conditions

All nodes of elements located at the edges of the tubesheet or shells have been assigned with symmetry boundary conditions. These nodes cannot rotate but they are allowed to have radial displacements.

3D pipes or link elements are fixed in vertical direction at the lower end, and they are attached to the tubesheet elements at the other end. For 3D tubes and link elements the fix points only prevent the vertical movements and all other displacements or rotations are free.

To take into account the effect of the head reaction to applied pressure, which imposes longitudinal stress on the channel side, vertical forces at the uppermost points have been introduced.

The value of these nodal forces is given by the quotient at the amount of longitudinal stresses and the available area.

For the shell-side shell, the nodes at the lower part are fixed in all aspects since these nodes are in the heat exchanger middle plane.

(C) Load Boundary Conditions and Load Cases

Actions at these boundary conditions are the pressure and the temperature that are applied in the various load cases.

For the inelastic analysis temperature effects have not been considered in the gross plastic deformation design checks since their incorporation is not required according to the code: Thermal stresses are self-equilibrating, and, therefore, they do not affect the results of a limit analysis investigation, and are thus not to be included in this check. The considered load cases are:

- Operating load case with design pressure and design temperature in elastic investigations.

- Pressure increase up to maximum allowable value according to the requirements of the direct route in design by analysis for gross plastic deformation checks (inelastic analysis).
- Pressure cycles up to maximum allowable value and back to zero, along with constant temperature distribution according to the requirements of the direct route in design by analysis for progressive plastic deformation design check (inelastic analysis).
- Pressure cycle up to the maximum value and back to zero along with constant temperature distribution for extracting maximum stresses as required in the fatigue design check (elastic analysis).

5. Elastic Analysis

Elastic analysis of the reactor has been carried out with regard to two separate goals. For the first goal the linear analysis has been carried out for the purpose of comparison between results obtained by FEA analysis and various code formulas. For the second goal the elastic analysis has been carried out to investigate the reactor performance under cyclic fatigue loading.

5.1 Model Elastic Calculation

Based on the data presented in part 4 of this work for the selected sector model, the elastic analysis with elastic material parameter at relevant temperature has been carried out. Detailed studies were carried out for five cases to observe tube sheet behavior under various loadings. The considered load cases are:

- **Load case 1: Pressure only (table 5.1).**

In this load case, the tubesheet, the tubes, and the upper shell, are subjected to 4 MPa pressure, and the lower shell to no pressure. All parts are at ambient temperature. In other parts of this work this load case is often referred to.

- **Load cases 2 and 3: Temperature only (table 5.2 and 5.3).**

Since EN 13445 Annex J for the tube sheet is based on mean temperatures instead of true temperature distributions, load case 3 has been performed to cover this condition. Load case 2 covers the temperature distribution according to the data sheet.

- **Load case 4: normal operating condition (table 5.4).**

For the combination of pressure and temperature see table 5.4. This table indicates the result of load case 4. In this load case tubesheet and tubes are subjected to 3 MPa pressure while the upper shell and the lower shell are subjected to 4 and 1 MPa respectively. All parts have a temperature distribution according to the data sheet.

- **Load case 5: Normal operating pressures but no temperature (table 5.5).**

This load case covers the pressure loading only: 3 MPa on the tubesheet, 4 MPa on the upper shell, and 1 MPa on the lower shell. This load case has been investigated for observing the amount of displacements due to pressure loadings (Table 5.5), and serves as a comparison for load case 4.

(5.1) Tables of Results of FEA Linear Analysis

Table (5.1):– pressure only(load case 1)

	tubesheet	tubes	upper shell	Lower shell
Maximum displacement (mm)	.725	2.805	1.247	.724
Max. Mises equivalent stress (MPa)	197.27	107.2	136.15	92.05

Table (5.2): Temperature distribution according to data sheet, no pressure (load case 2).

	tubesheet	tubes	upper shell	lower shell
Maximum displacement (mm)	2.188	2.16	3.02	1.6
Max. Mises equivalent stress (MPa)	95.2	76.3	77.8	64.4

Table (5.3): Mean temperature on tubesheet: temperature distribution else where: no pressure (load case 3).

	tubesheet	tubes	upper shell	lower shell
Max. displacement (mm)	2.04	2.04	3.04	1.6
Max. Mises equivalent stress (MPa)	99.73	86.9	68.89	59.2

Table (5.4): Normal operating condition (load case 4)
(pressure and temperature according to data sheet)

	Tubesheet	Tubes	Upper shell	Lower shell
Maximum Displacement (mm)	2.38	2.38	4.12	2.07
Max. Mises equivalent stress (MPa)	149.02	70.36	107.93	121.36

Table (5.5): Normal operating condition (load case 5)
(no temperature, pressure according to data sheet)

	Tubesheet	Tubes	Upper Shell	Lower shell
Maximum Displacement (mm)	0.65	2.46	1.16	0.65
Max. Mises equivalent stress (MPa)	181.7	87.26	131.99	102.7

Table (5.6) combines the results of the above tables, and below that table the results are discussed. The following graphs give details for each load case.

(5.1.1) Graphs for load case 4

Figures (5.1.1.1) to (5.1.1.11) show the relevant results. The load case considered is: pressure with 3.0 MPa on the tubesheet, 1 MPa on the lower shell, and 4.0 MPa on the upper shell, with temperature distribution according to the data sheet.

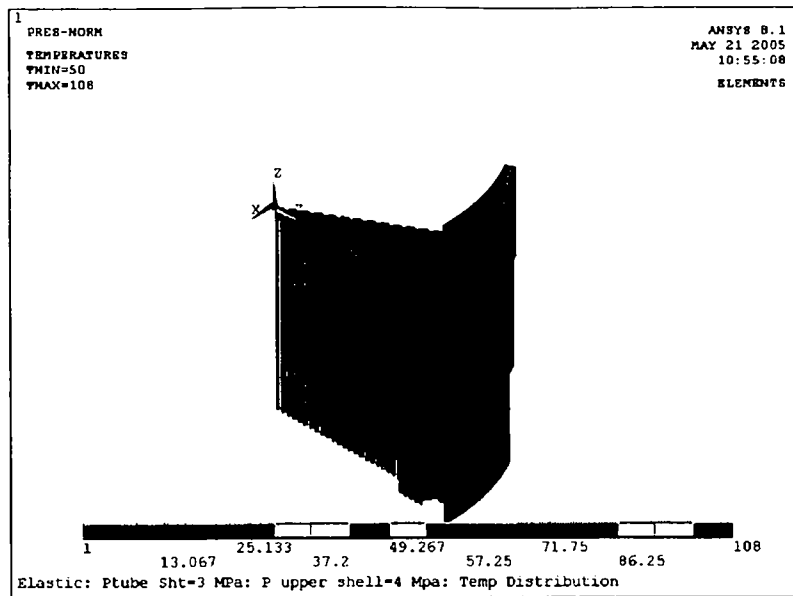


Figure (5.1.1.1): Loadings according to load case 4

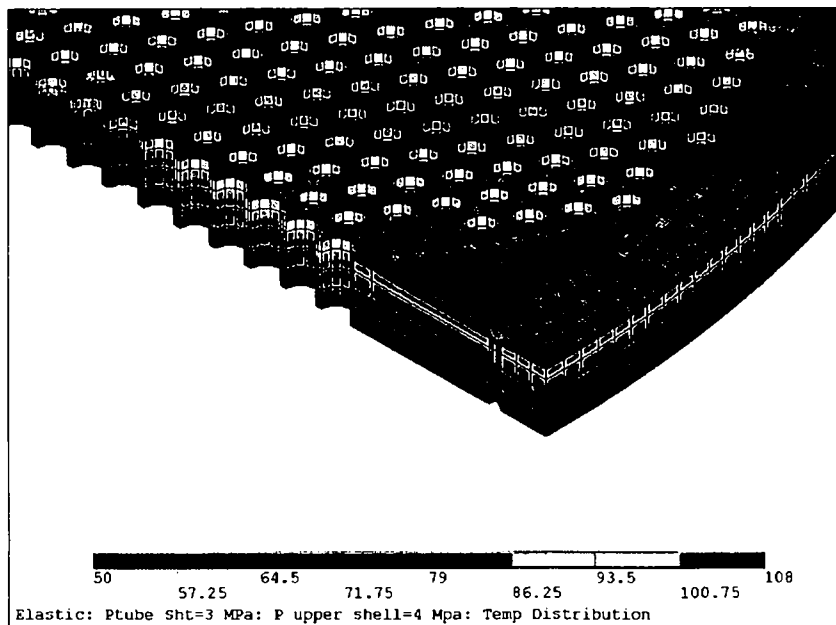


Figure (5.1.1.2): Tubesheet temperature distribution °C.

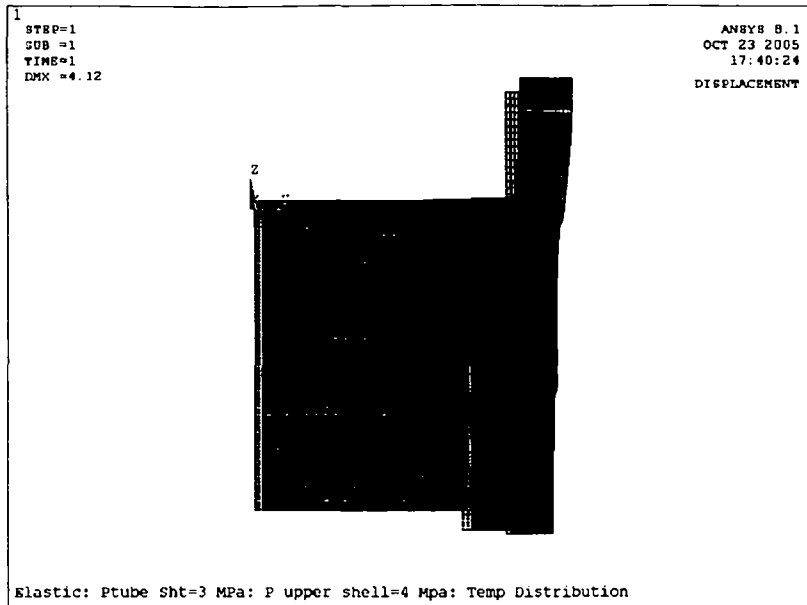


Fig. (5.1.1.3): Overall displacement, load case 4

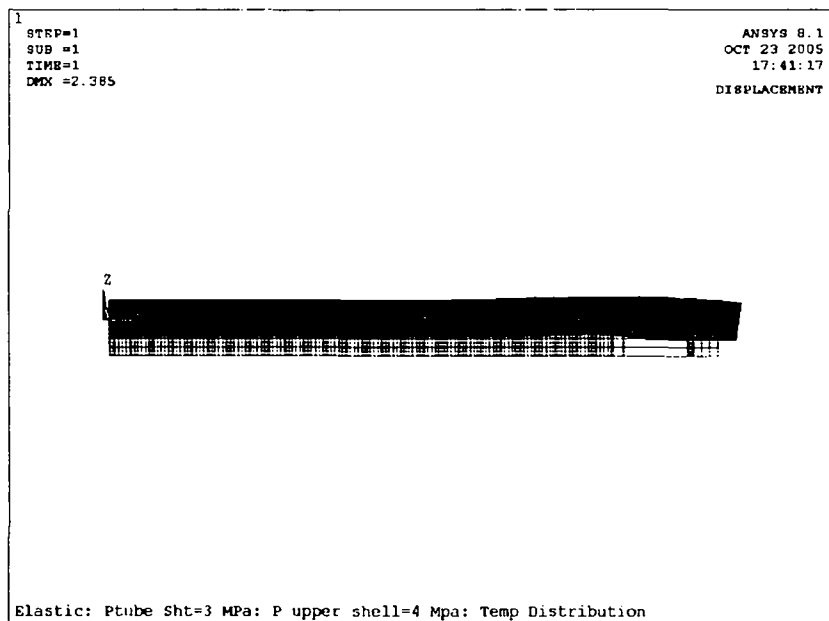


Fig. (5.1.1.4): Tubesheet displacement, load case 4

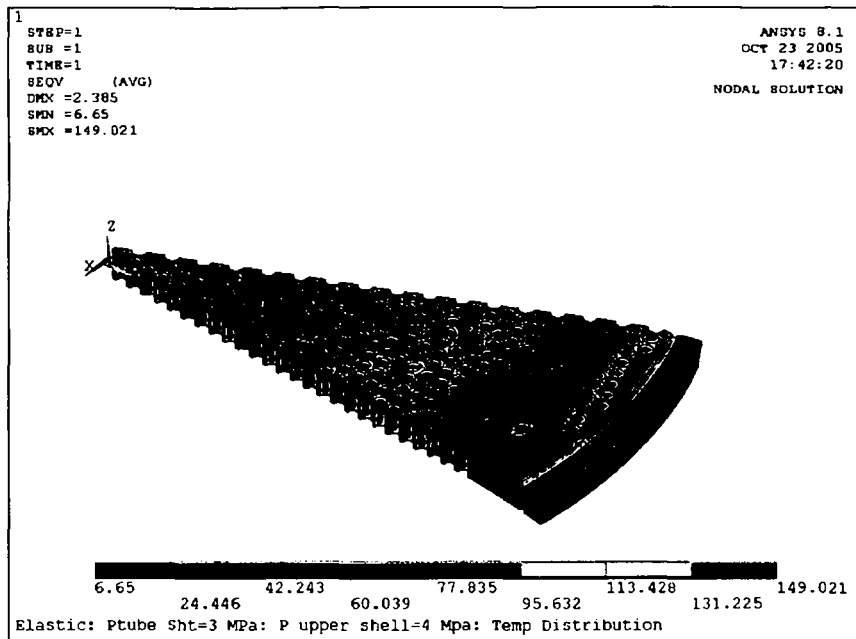


Fig. (5.1.1.5): Tubesheet, Mises equivalent stresses, load case 4

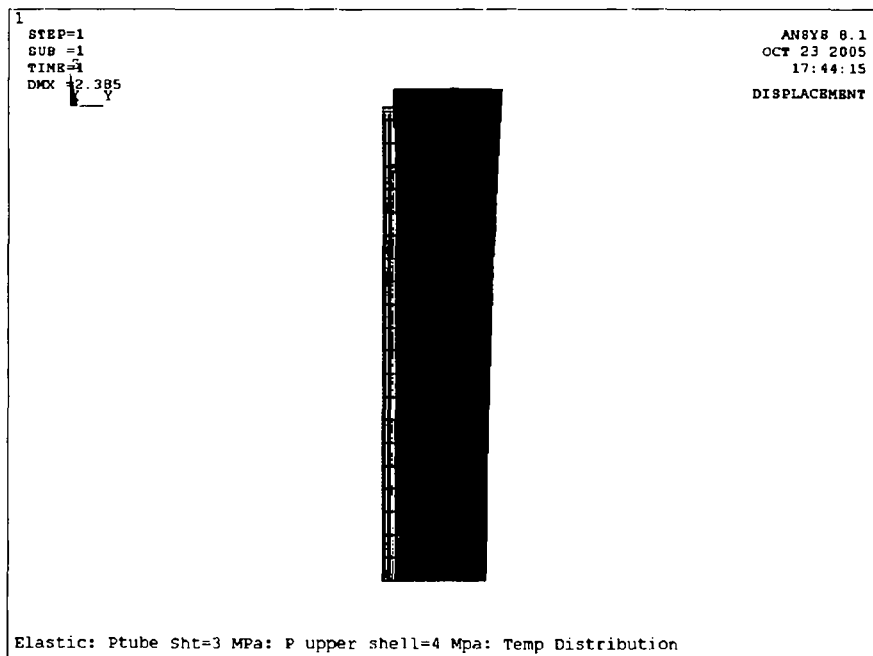


Fig.(5.1.1.6): 3D tube displacements, load case 4

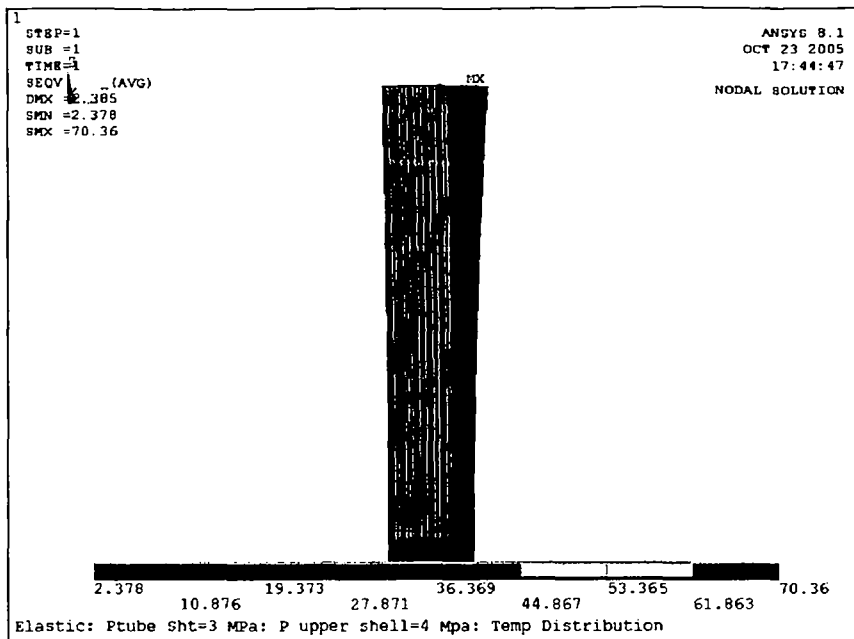


Fig. (5.1.1.7): 3D tubes: Mises equivalent stresses (MPa), load case 4

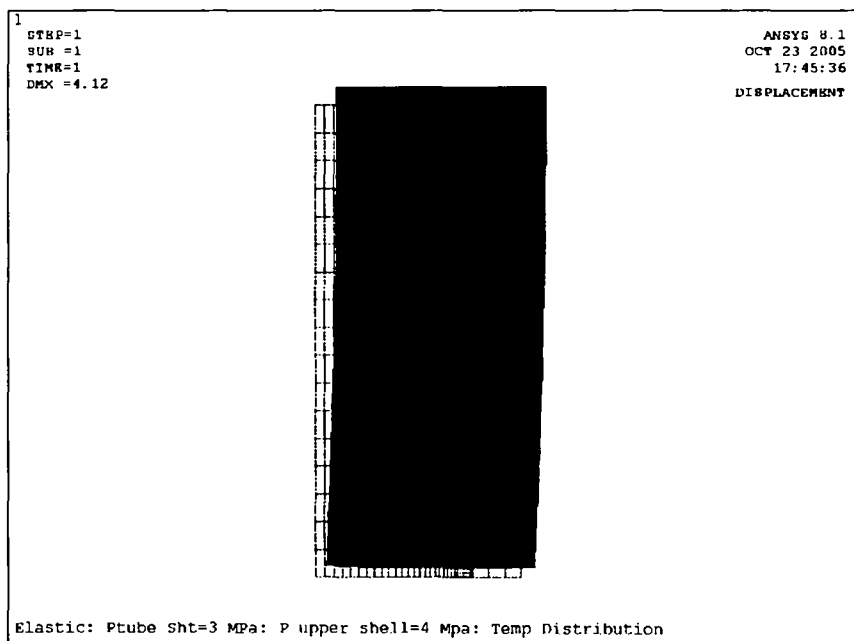


Fig.(5.1.1.8): Upper shell displacement (mm), load case 4

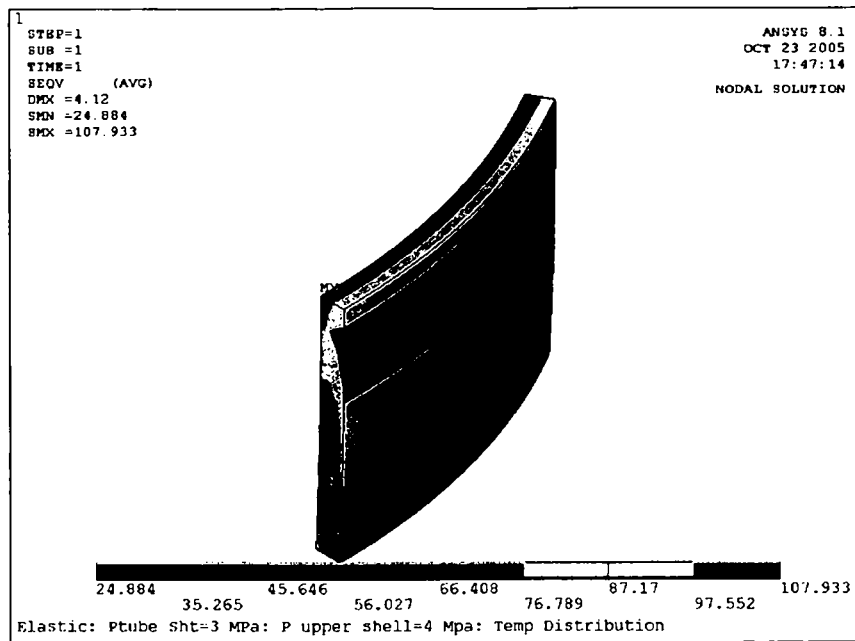


Fig.(5.1.1.9) :Upper shell, Mises equivalent stress (MPa), load case 4

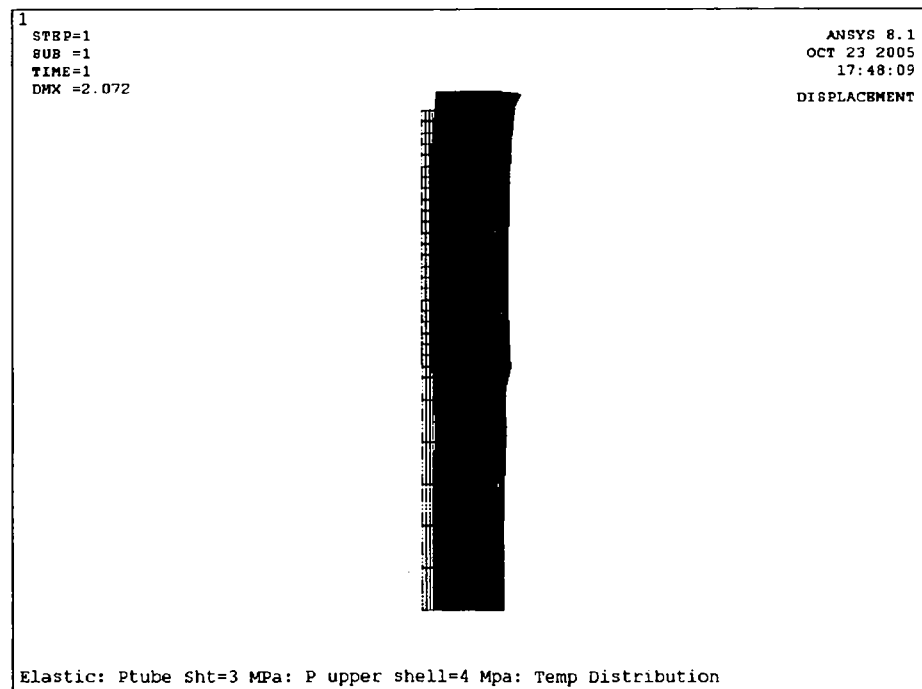


Fig.(5.1.1.10): Lower shell displacements (mm), load case 4

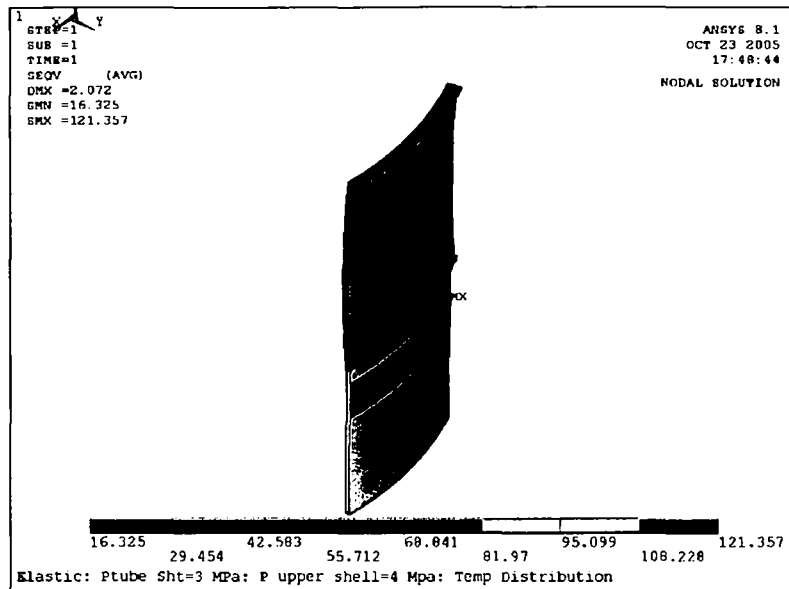


Fig. (5.1.1.11) Lower shell, Mises equivalent stress (MPa), load case 4

(5.1.2) Graphs for load case 1

Figures (5.1.2.1) to (5.1.2.10) show the relevant results of load case 1: 4.0 MPa on tubesheet, tubes, and upper shell. No pressure on the lower shell. Ambient temperature.

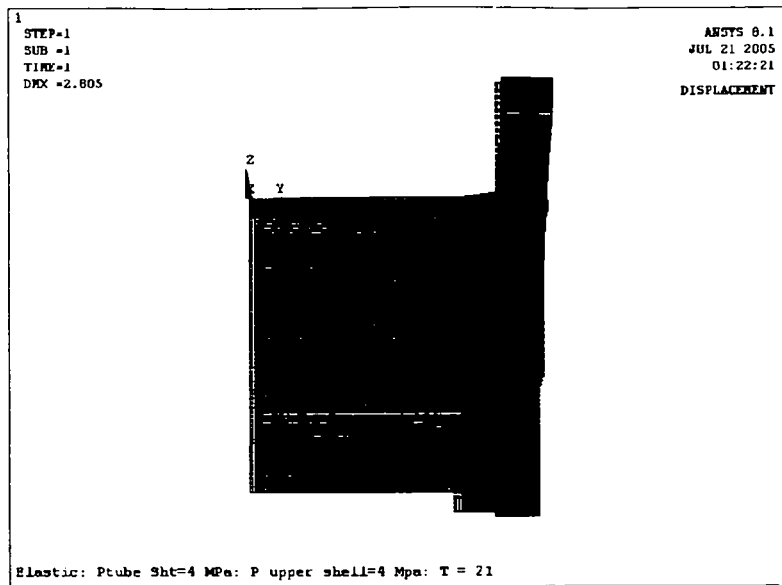


Figure (5.1.2.1): Overall displacement (mm), load case 1

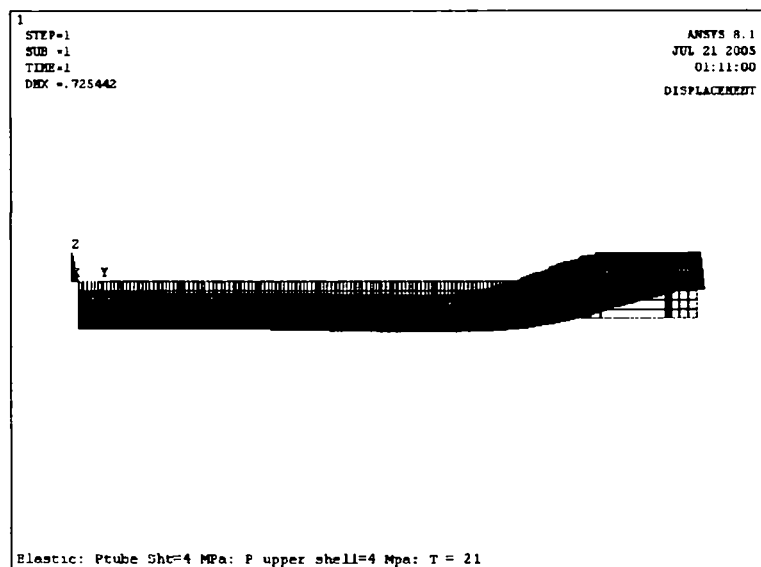


Figure (5.1.2.2): Tubesheet displacement (mm), load case 1

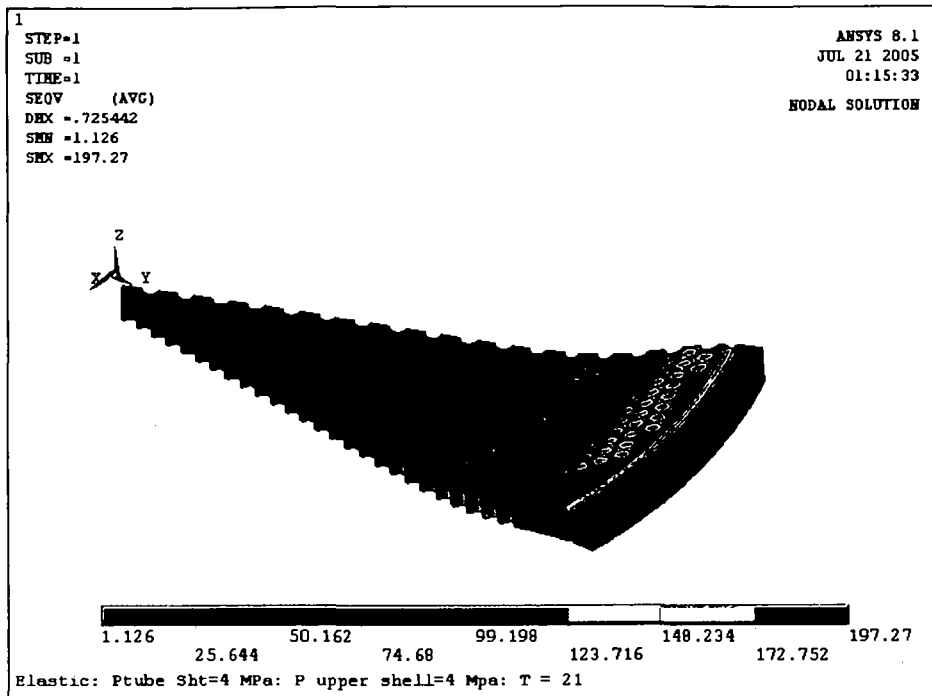


Figure (5.1.2.3): Tubesheet Mises equivalent stresses (MPa), load case 1

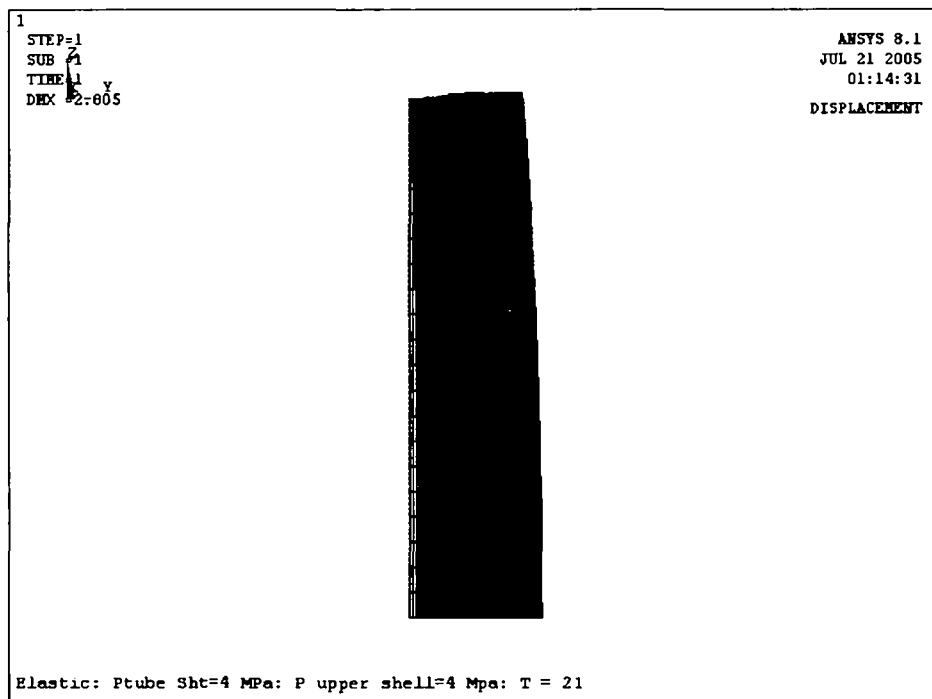


Figure (5.1.2.4): 3D tube displacements (mm), load case 1

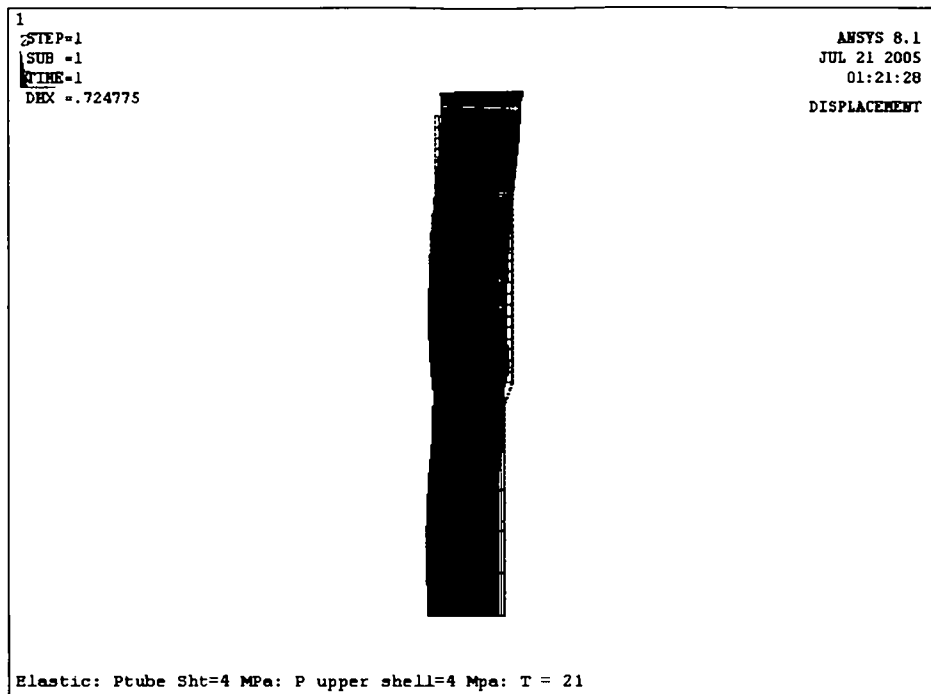


Figure (5.1.2.7): Lower shell displacement (mm), load case1

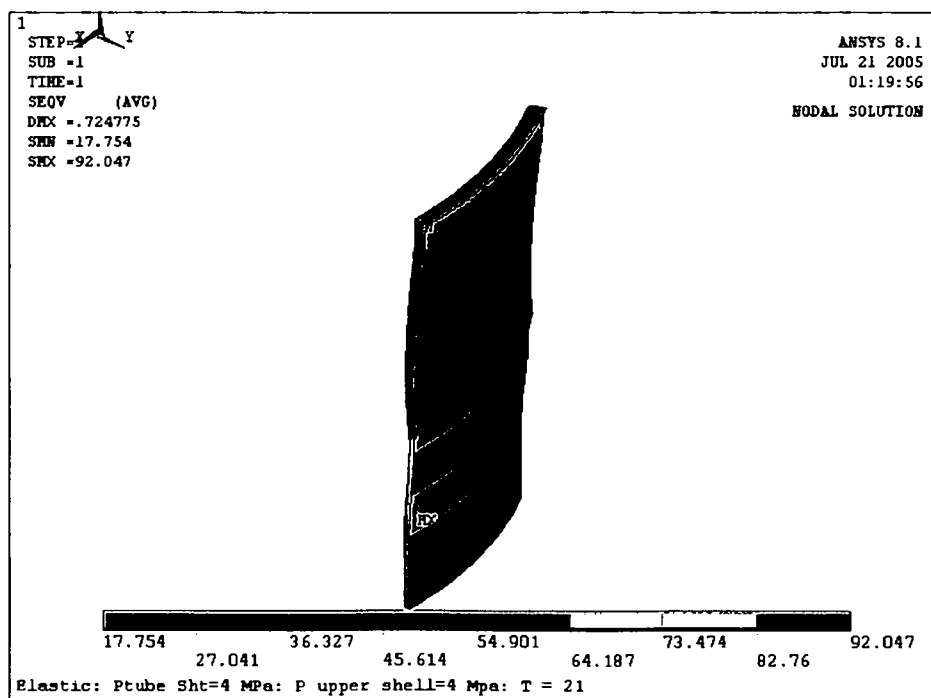


Figure (5.1.2.8): Lower shell Mises equivalent stresses (MPa), load case 1

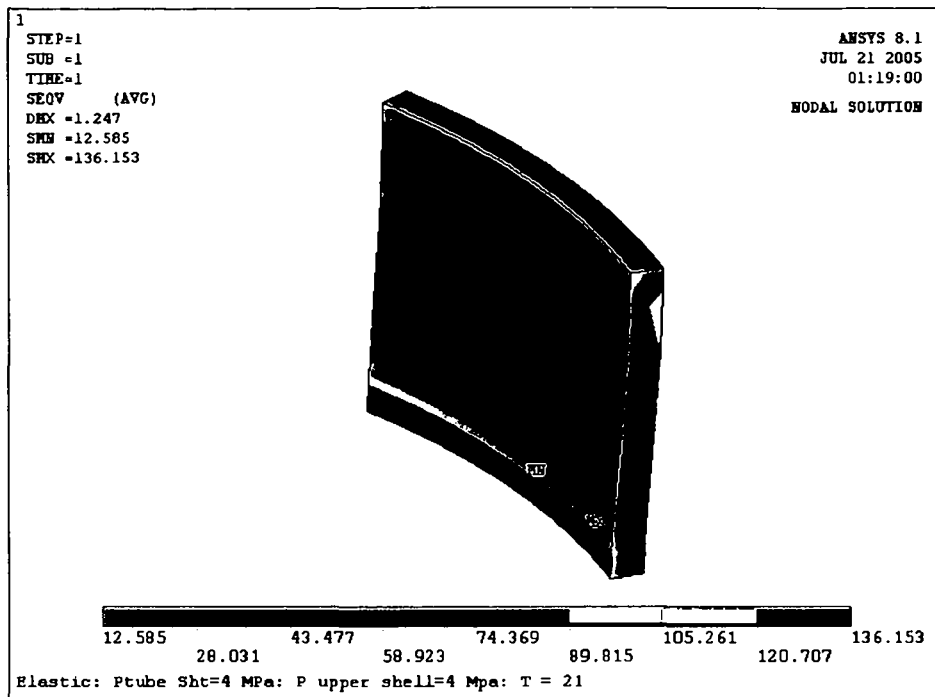


Figure (5.1.2.9): Upper shell Mises equivalent stresses (MPa) , load case 1

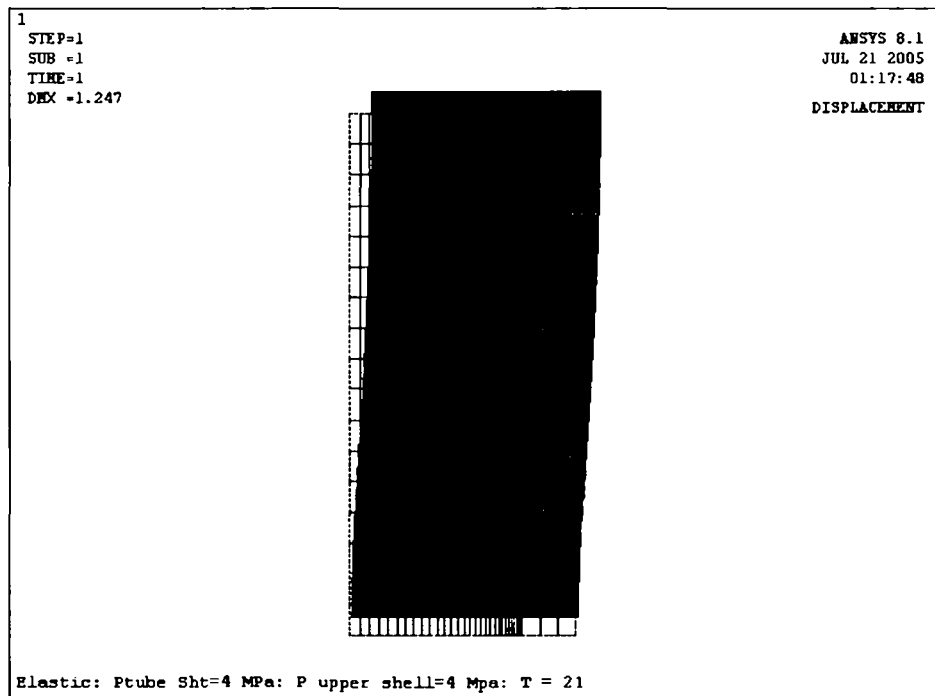


Figure (5.1.2.10): Upper shell displacement (mm), load case 1

(5.1.3) Graphs for load case 2

Figures (5.1.3.1) to (5.1.3.9) show the relevant results of load case 2: no pressure on tubesheet, tubes, upper and lower shell. Temperature distribution according to the data sheet.

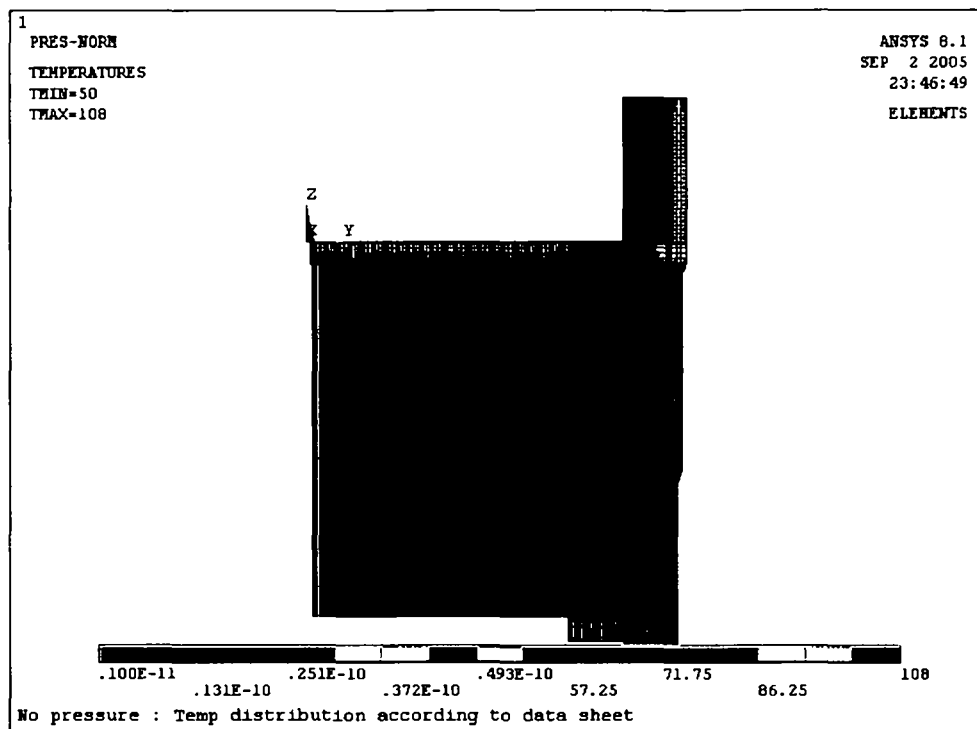


Figure (5.1.3.1): Overall loadings

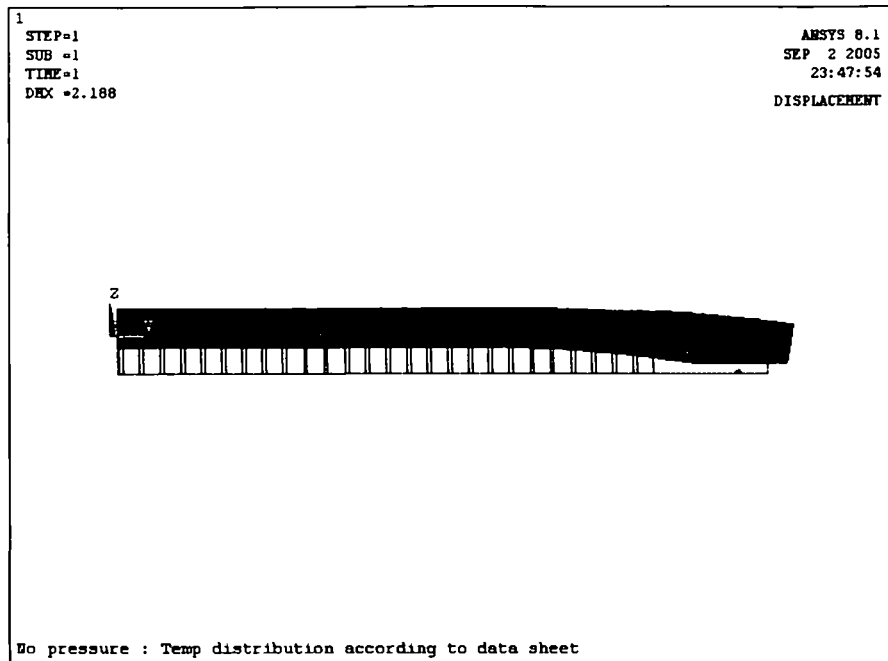


Figure (5.1.3.2): Tubesheet displacement (mm), load case 2

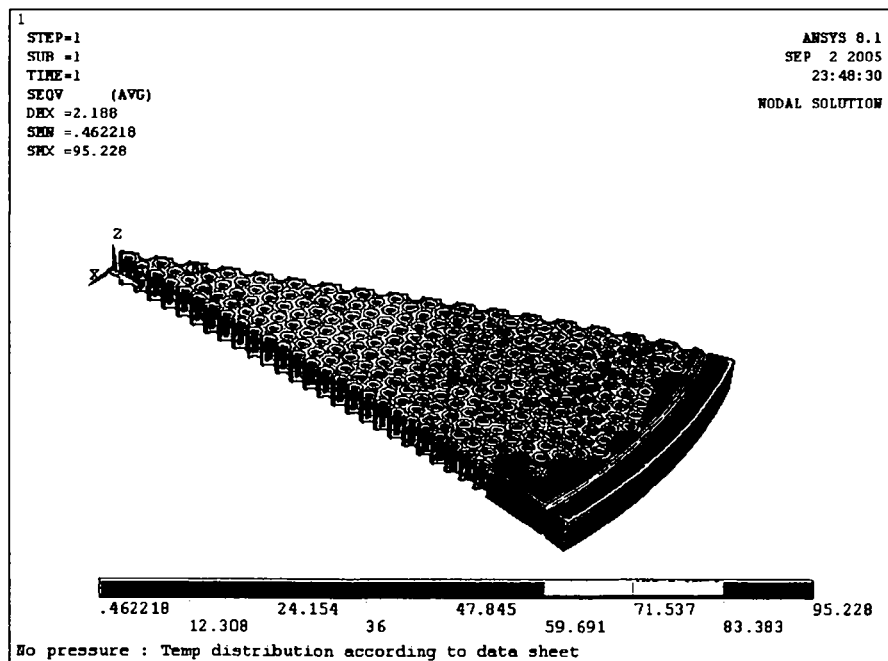


Figure (5.1.3.3): Tube sheet Mises equivalent stress (MPa), load case 2

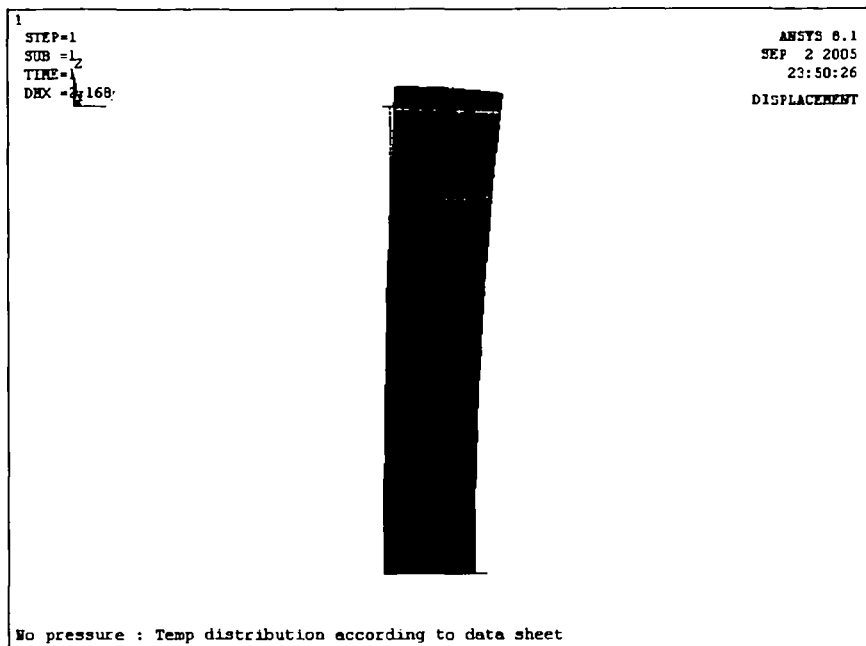


Figure (5.1.3.4): Tube displacement (mm), load case 2

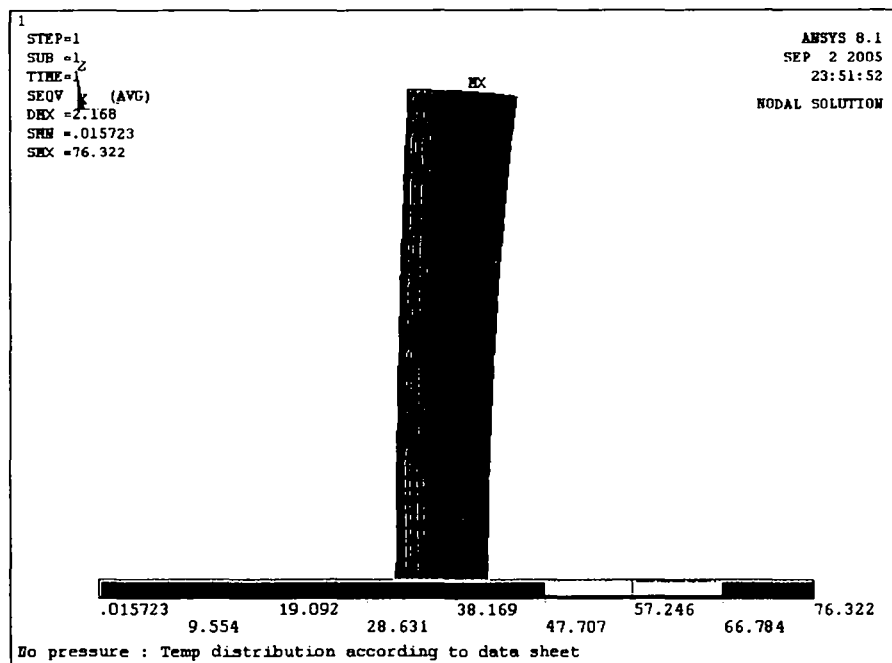


Figure (5.1.3.5): Tubes equivalent of Mises stress (MPa), load case 2

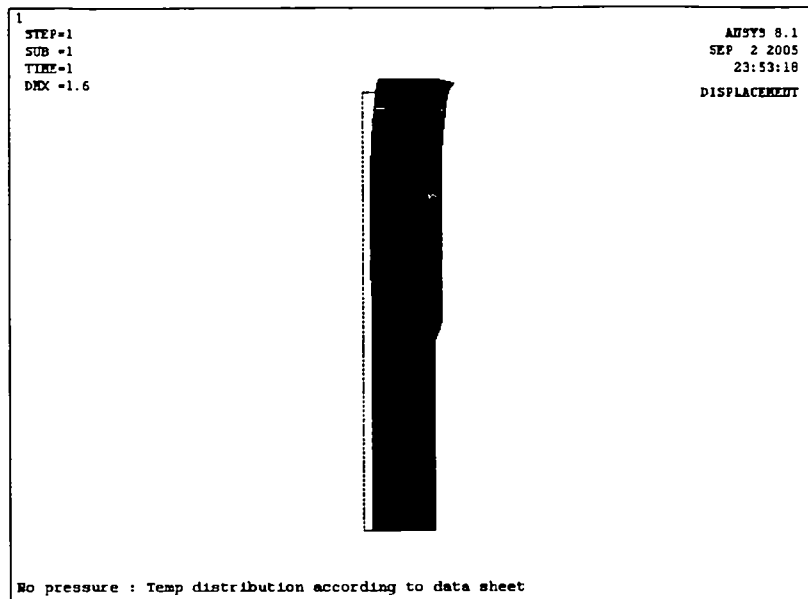


Figure (5.1.3.6): Lower shell displacements (mm), load case 2

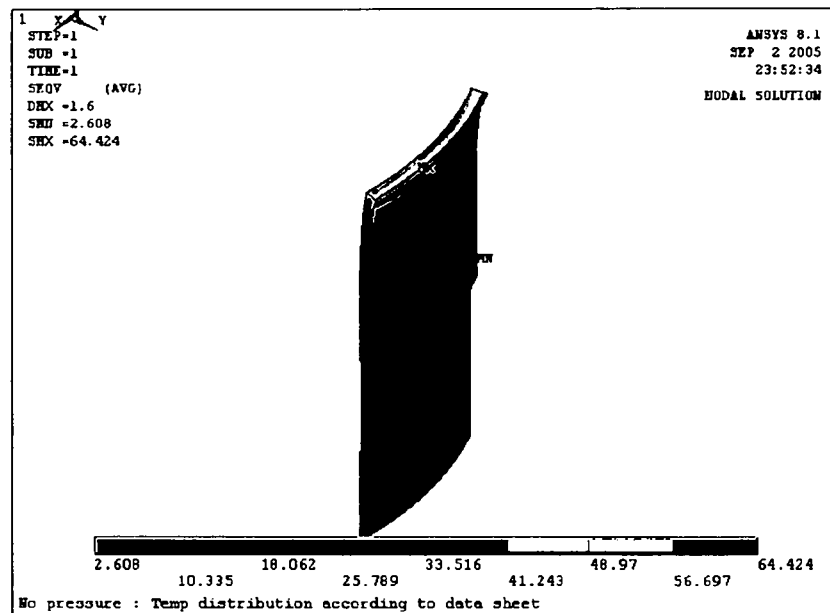


Figure (5.1.3.7): Lower shell Mises equivalent stress (MPa), load case 2.

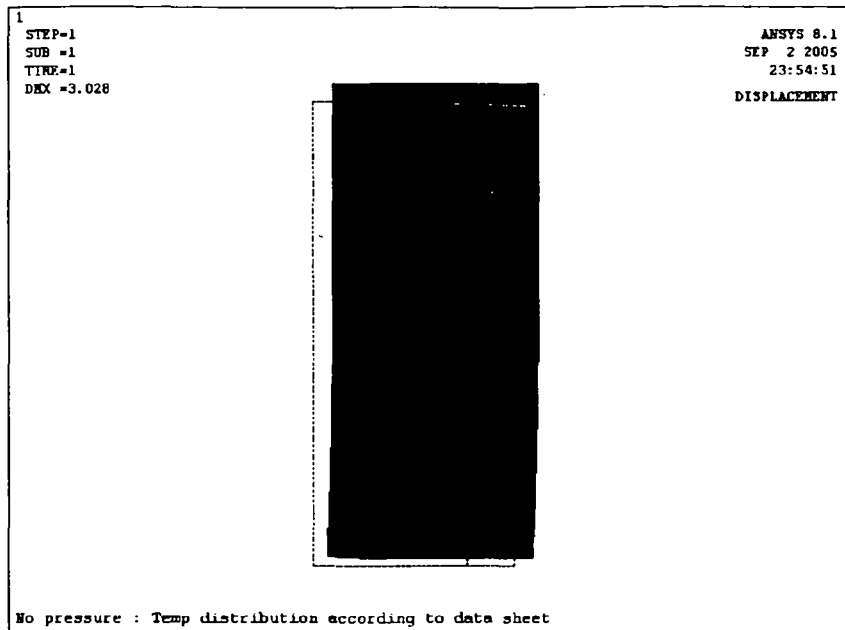


Figure (5.1.3.8): Upper shell displacement(mm), load case 2.

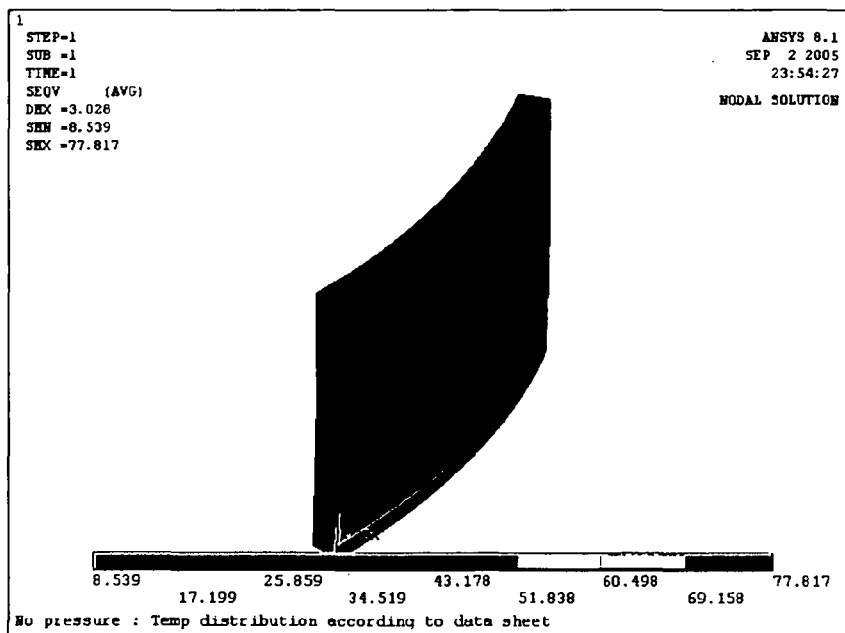


Figure (5.1.3.9): Upper shell Mises equivalent stress (MPa), load case 2

(5.1.4) Graphs for case 3 (no pressure and mean temperature)

Figures (5.1.4.1 to 5.1.4.9) show the various results for the case 3: no pressure, temperature distribution according to data sheet except for the tubesheet for which the mean temperature 79°C was used.

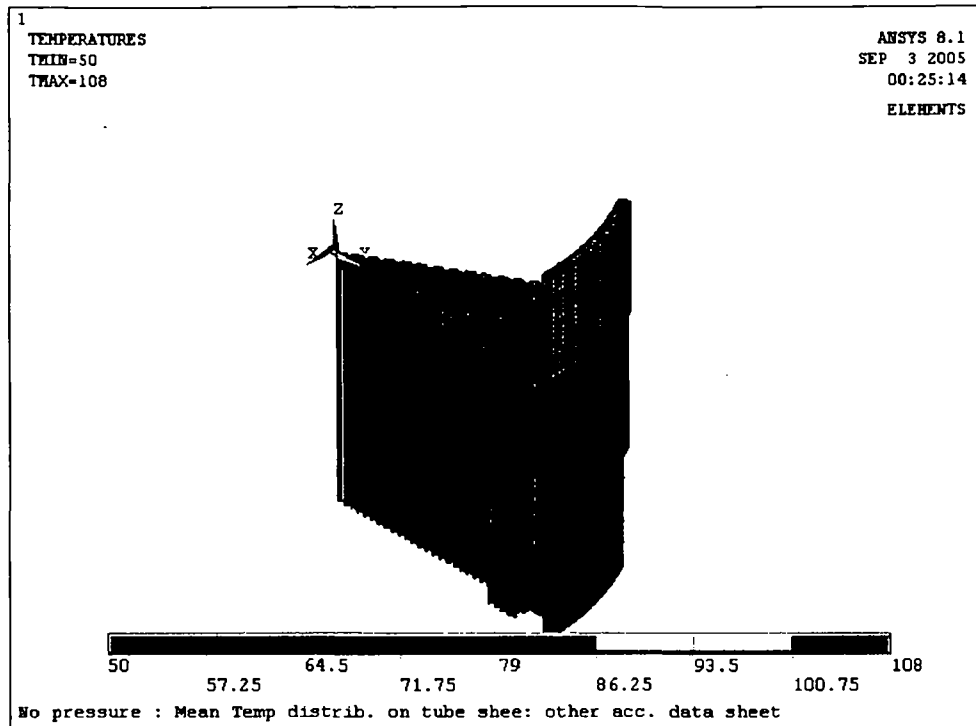


Figure (5.1.4.1): Geometry and loadings

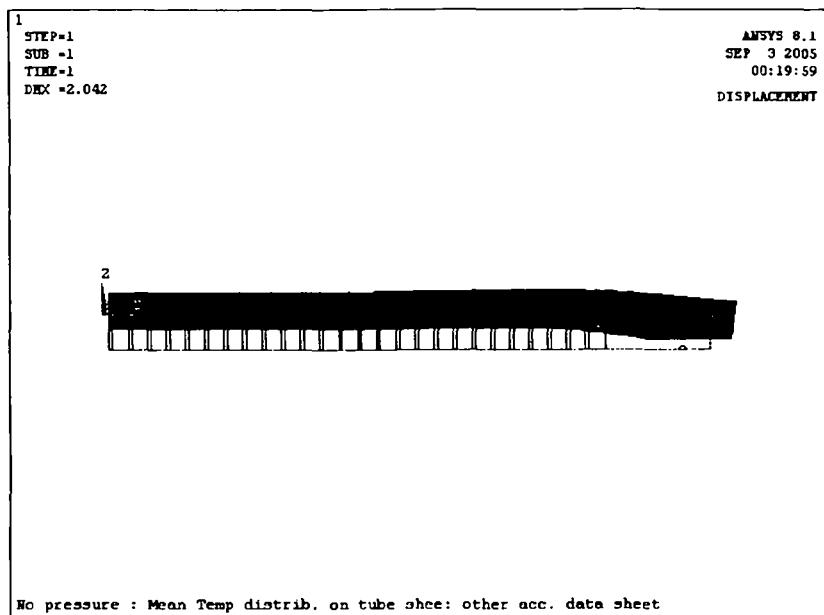


Figure (5.1.4.2): Tubesheet displacement (mm), load case 3

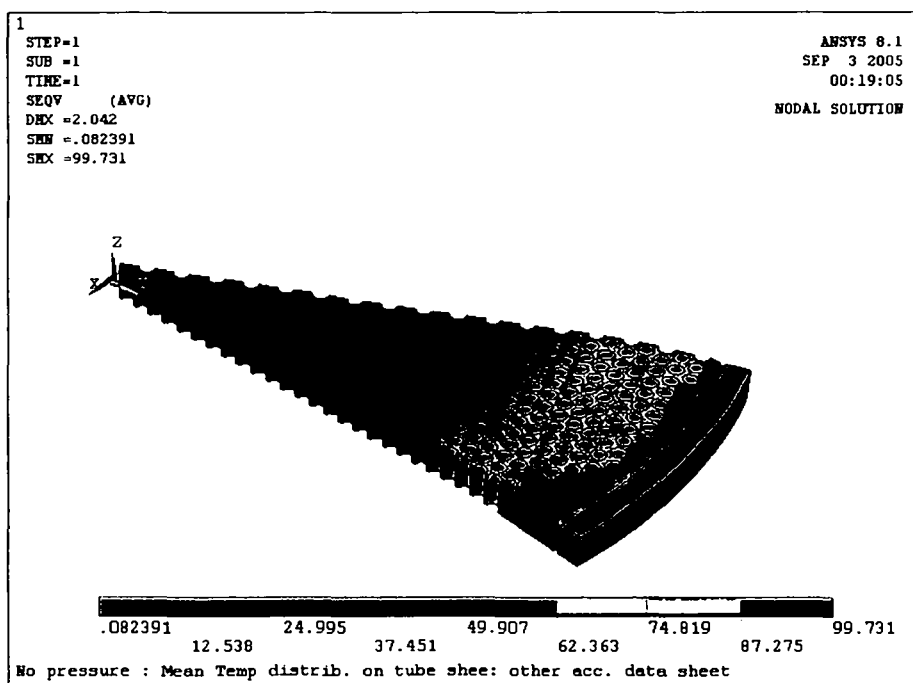


Figure (5.1.4.3): Tubesheet Mises stress (MPa), load case 3

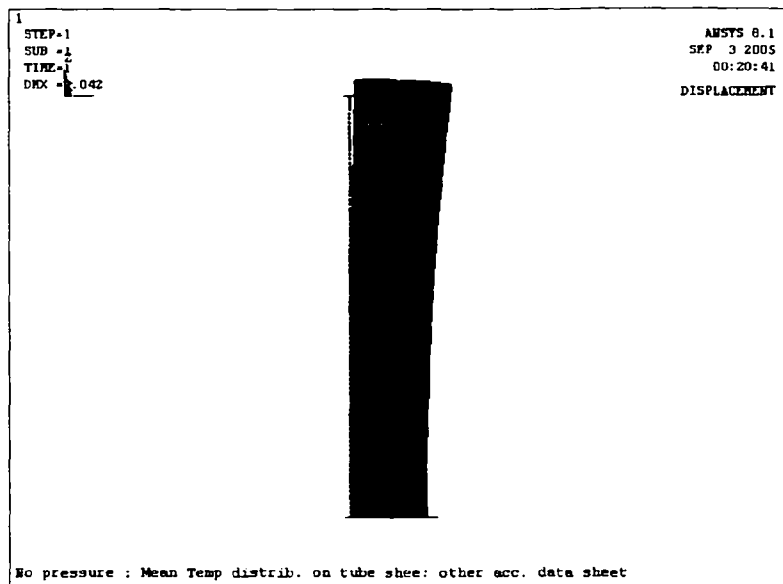


Figure (5.1.4.4): Tubes displacement (mm), load case 3.

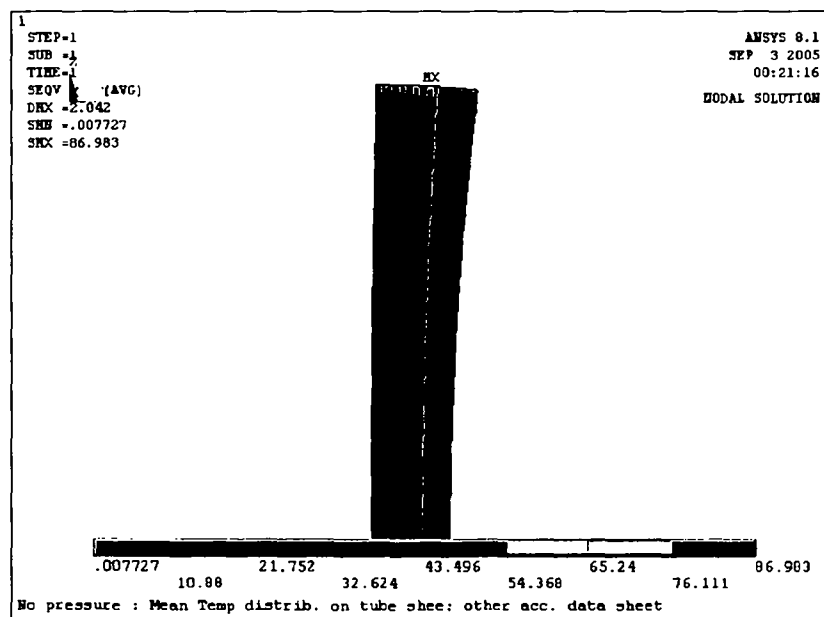


Figure (5.1.4.5): Tubes Mises equivalent stresses (MPa), load case 3

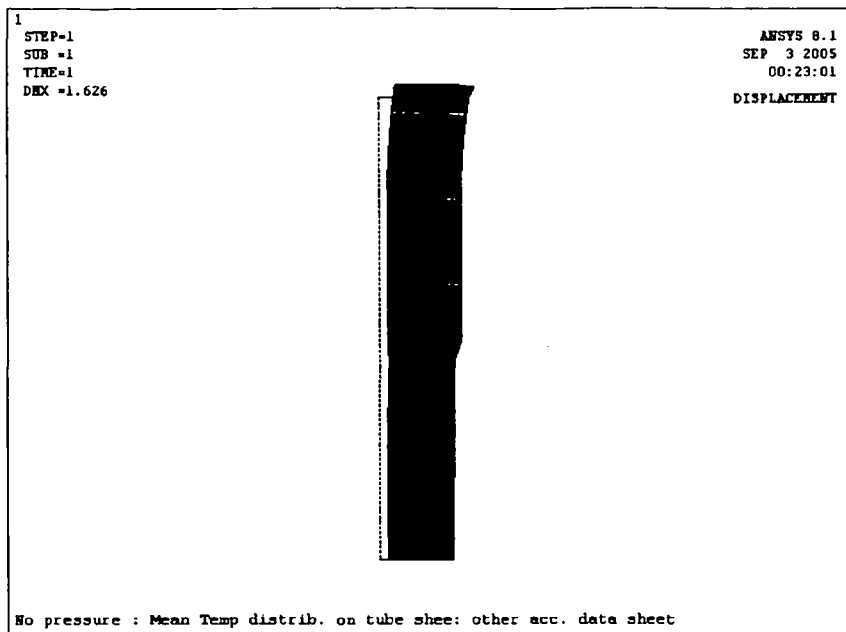


Figure (5.1.4.6): Lower shell displacement (mm), load case 3.

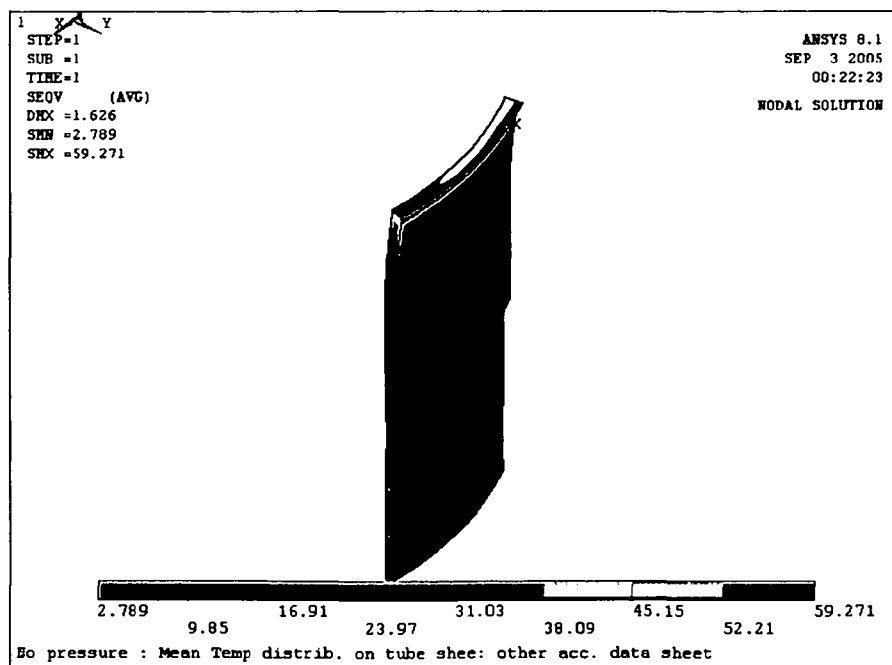


Figure (5.1.4.7): Lower shell Mises equivalent stress (MPa), load case 3.

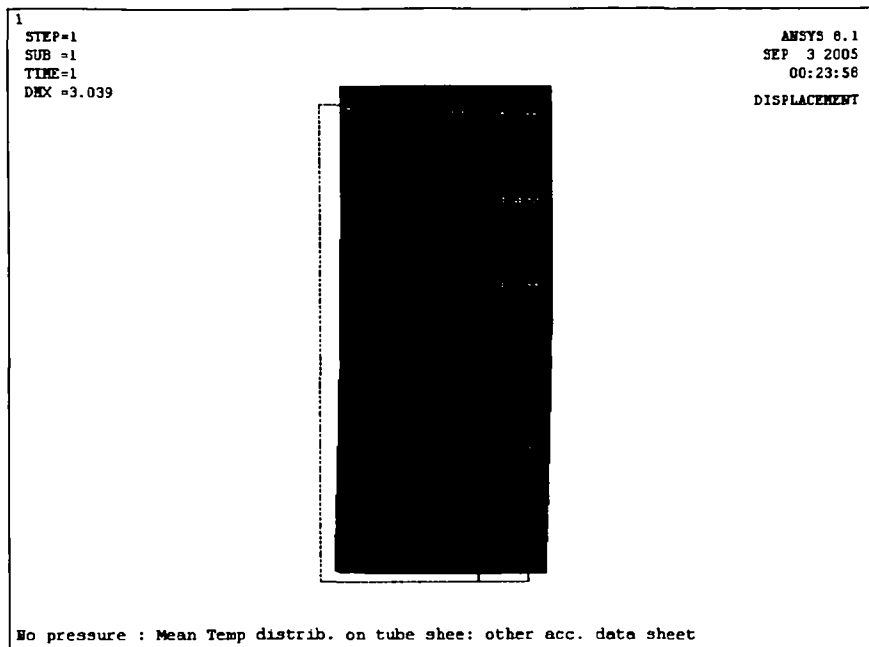


Figure (5.1.4.8): Upper shell displacement (mm), load case 3.

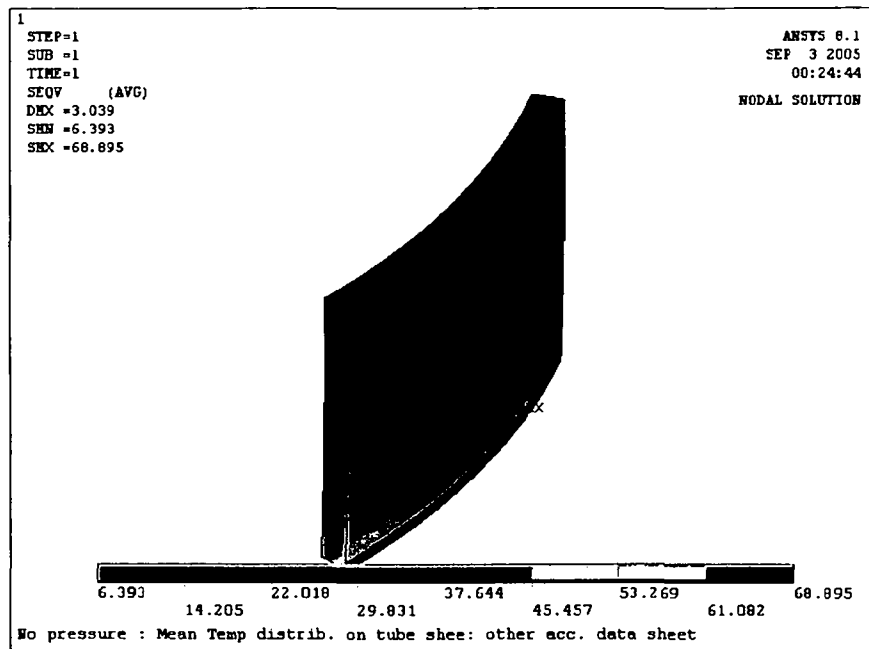


Figure (5.1.4.9): Upper shell Mises equivalent stress (MPa), load case 3

(5.1.5) Graphs for load case 5

Figures (5.1.5.1) to (5.1.5.9) show the various results for case 5: normal operating pressure according to data sheet and no temperature.

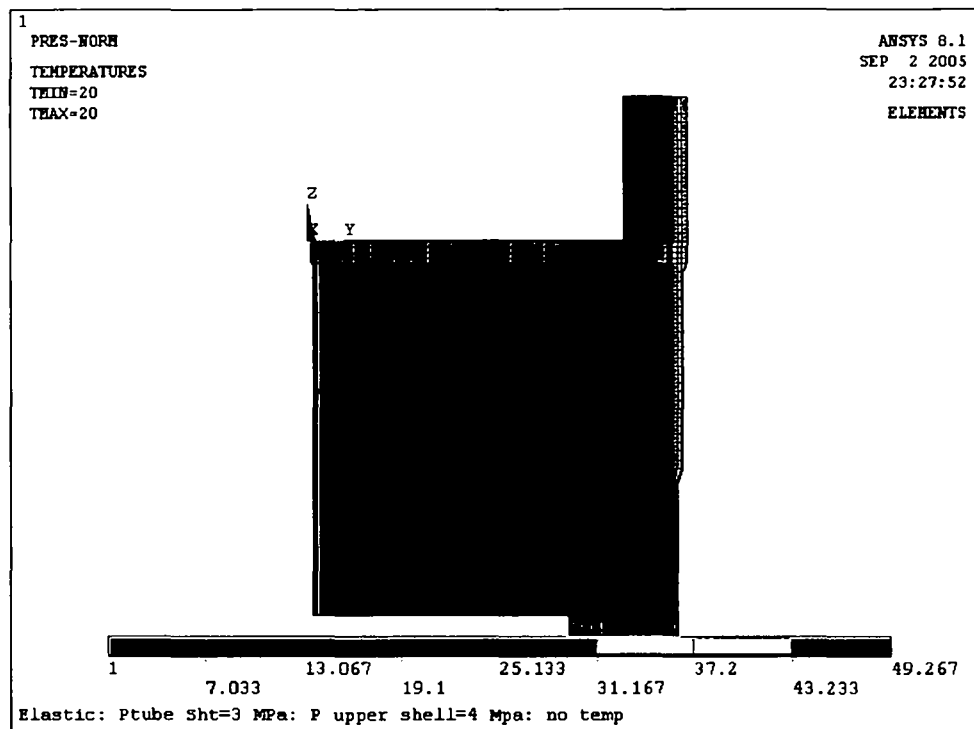


Figure (5.1.5.1): Geometry and loadings

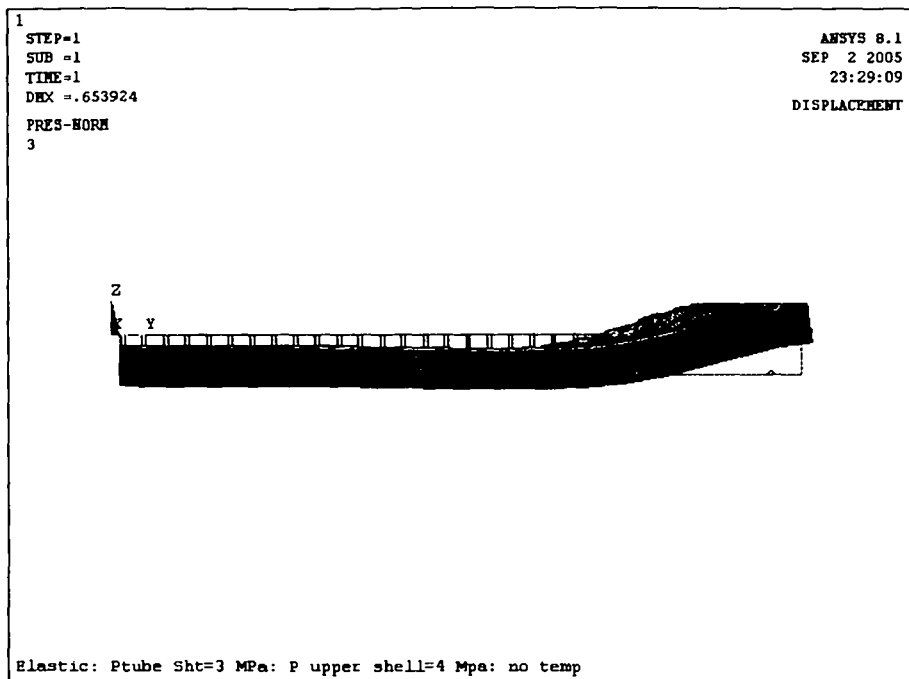


Figure (5.1.5.2): Tubesheet displacement (mm), load case 5

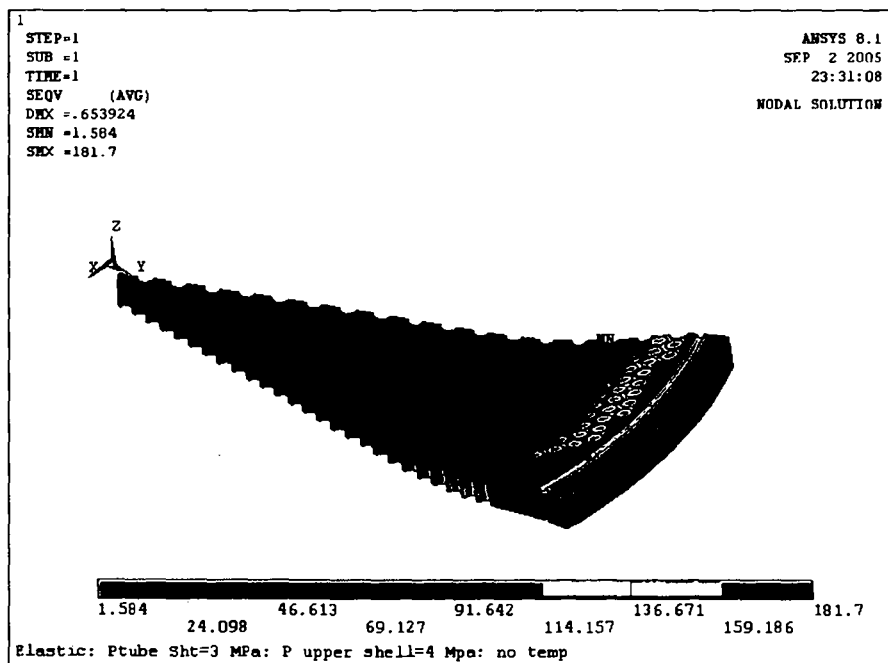


Figure (5.1.5.3): Tubesheet Mises equivalent stress (MPa), load case 5.

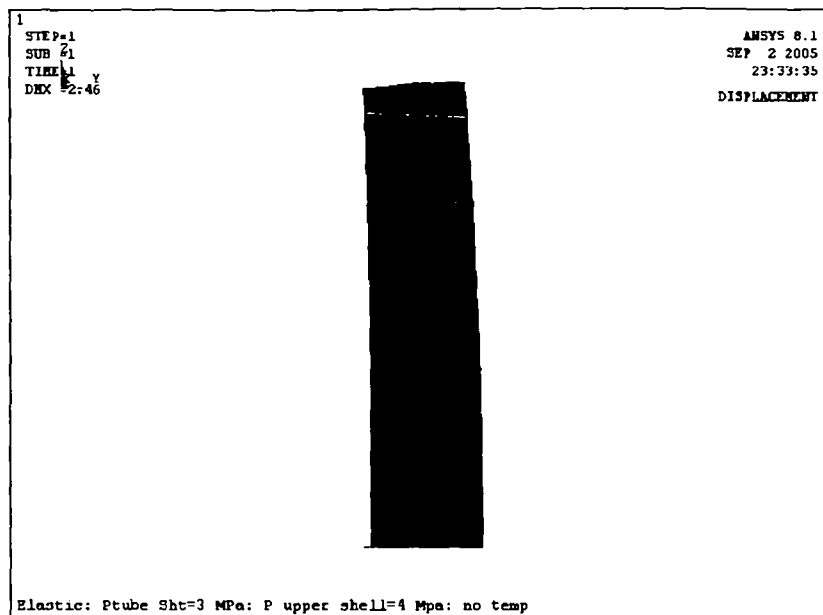


Figure (5.1.5.4): Tubes displacement (mm), load case 5

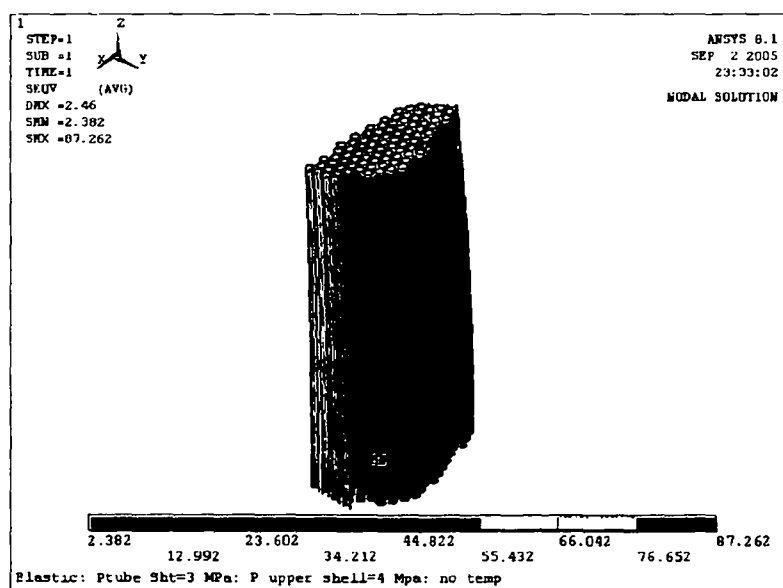


Figure (5.1.5.5): Tubes Mises equivalent stresses (MPa), load case 5.

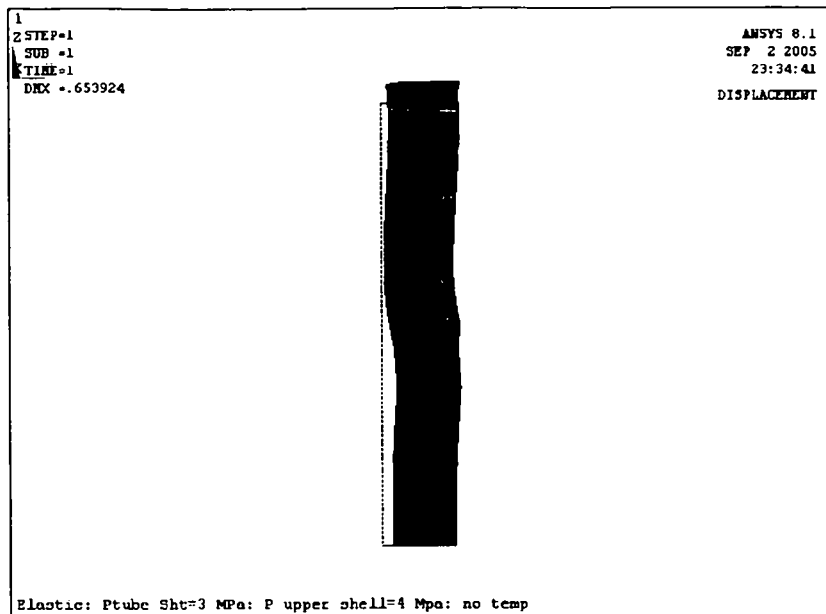


Figure (5.1.5.6): Lower shell displacement (mm), load case 5.

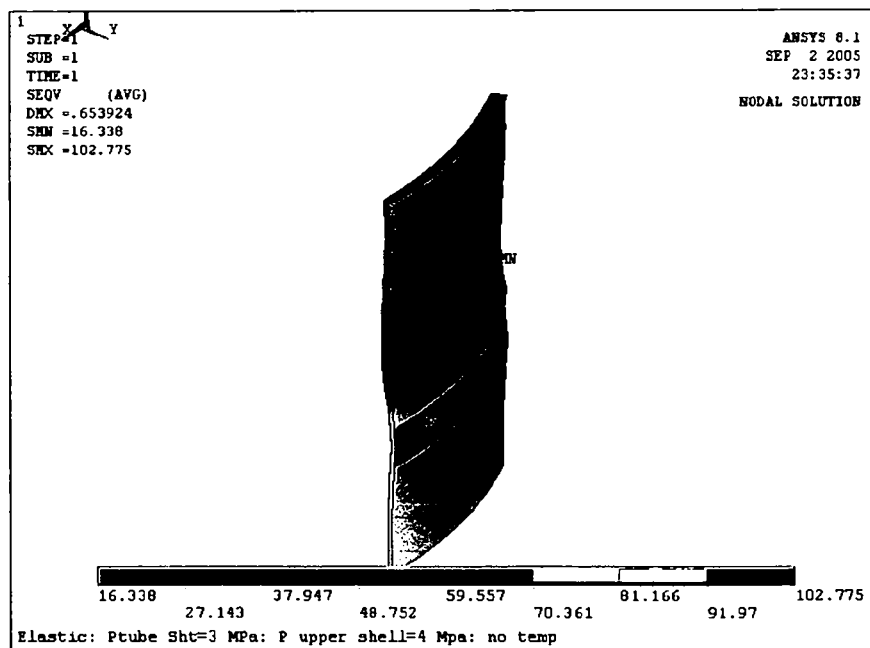


Figure (5.1.5.7): Lower shell Mises equivalent stress (MPa), load case 5.

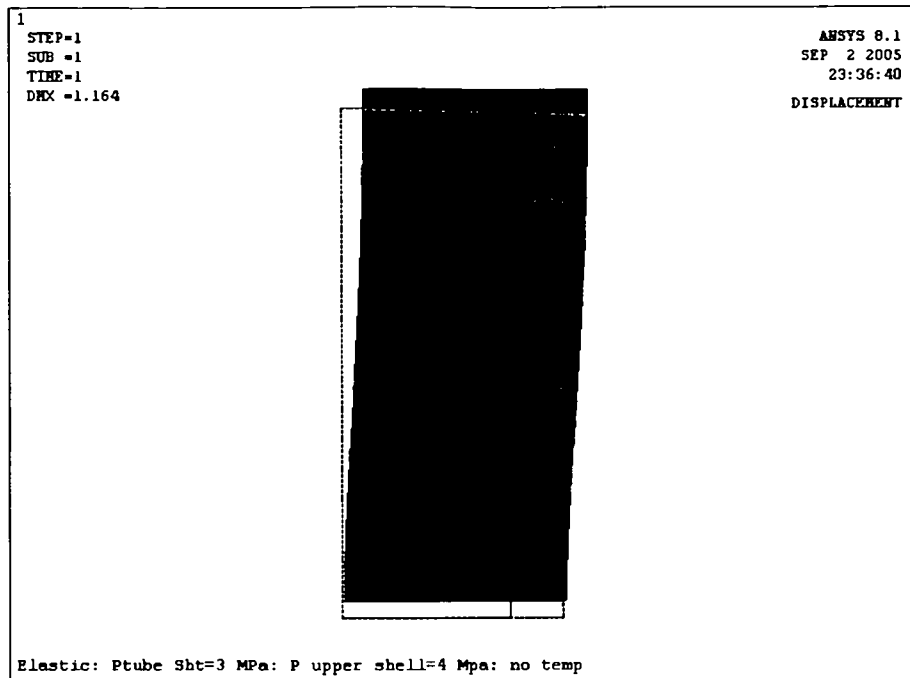


Figure (5.1.5.8): Upper shell displacement (mm), load case 5.

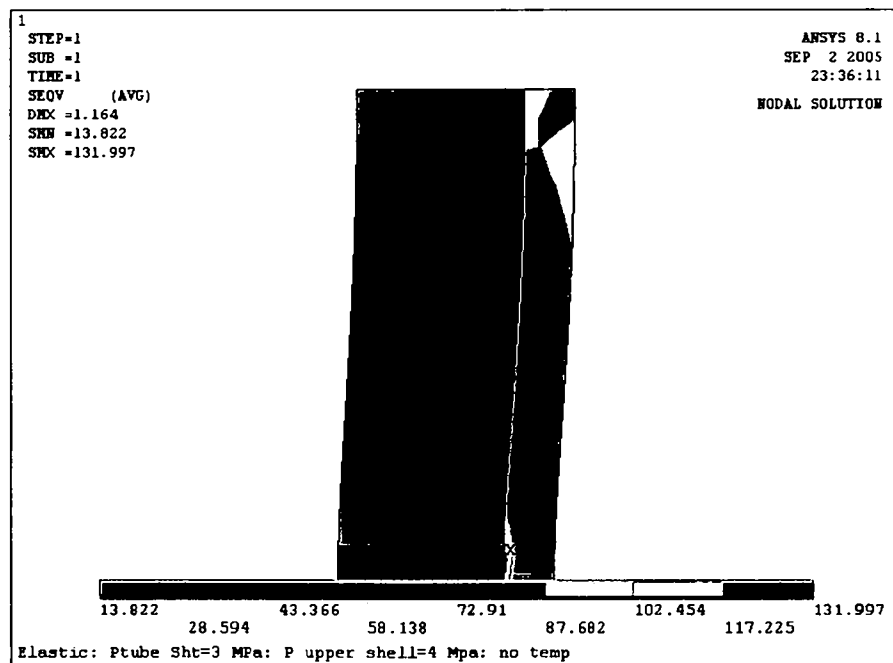


Figure (5.1.5.9): Upper shell Mises equivalent stress (MPa), load case 5

5.2 Results and discussion of results

To compare the results for the various load cases, table (5.6) has been prepared:

Table (5.6) Maximum Mises equivalent stress (MPa) and maximum deflection of various parts (mm) for all considered load cases

cases Items \ Load		Pressure only- no temp. (load case 1)	Temp. only data sheet (load case 2)	Temp. only- mean value (load case 3)	Normal operating pressure + temp. (load case 4)	Normal operating pressure, no temp. (load case 5)
Tube sheet	stress	197.27	95.2	99.73	149.02	181.7
	deflect.	.725	2.18	2.04	2.38	.65
3-D Tube	stress	107.2	76.32	86.9	70.36	87.262
	deflect.	2.805	2.16	2.04	2.38	2.46
Upper shell	stress	136.15	77.81	68.89	107.93	131.99
	deflect.	1.247	3.03	3.04	4.12	1.16
Lower shell	stress	92.05	64.4	59.2	121.36	102.7
	deflect.	.724	1.6	1.6	2.07	.65

To conclude the results for the above load cases the following conclusion can be noted, based on table (5.6) above:

Temperature imposes larger displacements in comparison to pressure but stresses due to pressure have larger values.

It should be noted that the values of thermal stresses are strongly affected by degree of the flexibility various parts.

It also can be observed, by examination of the results of tubesheet displacement as calculated under load case 4 and 5, that from the 2.38 mm of total tubesheet displacement under load case 4, 0.65 mm results from pressure loading and the rest is due to temperature.

The reactor behavior under various conditions can be described as follows:

- Tubesheet movement is greatly affected by the movement of the tubes and the attached shells.
- Tubes move up under temperature and few rows of them, close to the imperforated region, will bend as a result of the interaction of movement coming from the shells.
- Under temperature loading only, tubesheet moves up uniformly except in the rim area close to and at the grooves. At these locations some restriction comes from the adjoining shells.
- Under pressure loading only, tube sheet moves down except at the rim. The rim portion is dominated by rotation of the upper shell, which pushes the tubesheet in this region up.

- Rim of the tubesheet, which is extended below the upper shell, rotates slightly down due to the bending action enforcing by the upper shell movement.
- Upper shell extends itself in radial and axial directions. This displacement influences the tubesheet movement at and close to most of the regions.
- The lower shell with much lower pressure brings extra stiffness to the region, and it acts as a peripheral support for the tubesheet, preventing adjoining tubesheet axial displacement in the region of the attachment.

5.3 Fatigue Considerations

During the useful life of the reactor just a few operating cycles are expected to occur. Cycles could come from startups and shutdowns, process upsets, and cases related to overall plant load adjustments.

The variation in loads can cause fatigue damage, and cracks may grow and propagate to some critical size with possibilities of total failure. To check the effect of cyclic actions on the reactor, a fatigue calculation according to EN 13445-3 Section 18 and Annex P has been carried out.

According to Niemi [26] and Petershagen [27] at a notch such as a weld toe usage of 20 noded solid element with 3-point integration to model the nonlinear stress distribution across the plate thickness usually produces poor results. The correct linear stress distribution can be obtained using 8 node linear solid elements. This type of modeling is employed in the present FEA model.

The calculation has been performed for the critical regions of the reactor. These are locations in the various regions, welded and unwelded, with largest stresses coming from pressure and temperature actions, locations which are, therefore, the most susceptible to fatigue damage.

The selected locations for checking are the seam weld between tubesheet and the upper shell, and in the tubesheet material at the location of maximum local stress in the grooves on the channel side.

To start the calculation, a linear analysis has been performed for the load case with design pressure on the tube side ($p_t=4$ MPa) and no pressure on the shell side ($p_s=0$ MPa) and ambient temperature (LC 1) as well as one additional load case with design pressure on tube side ($p_t=4$ MPa), no shell side pressure ($p_s=0$ MPa) and temperature distribution according to the data sheet from 50 to 108 °C (LC 1A).

These load cases corresponds to the maximum allowable pressure in one case and maximum allowable pressure coupled with temperature distribution in the other case. The maximum principal stresses have been extracted from FEA calculations and fatigue calculation is performed for the governing case. Details with regard to fatigue check are given on the following sections.

5.3.1 Seam Weld Location (welded region)

5.3.1.1 Stresses

For welded regions the proper approach uses the range of the maximum absolute value of principal structural stresses normal or parallel to the weld joint direction. Values of principal stresses extracted from FEA calculations of the above load cases are given on table (5.3.1), (5.3.1.1), (5.3.2) and (5.3.2.1).

Figure (5.3.1) shows the geometrical location of node 68075 and other neighboring nodes at the surface. Node 68075 is located on the weld line joining the tube sheet to the upper shell.

Figures show a jump of principal stresses at the node 6807. The jump is caused in the post-processing, extrapolation from element interior points to surface points

and averaging values. The larger of the extrapolated value is used in the figure calculation.

Therefore, the largest of principal stresses from above or below of this node should be adapted for the further calculations.

Surface nodes above node 68075 belong to elements with SA 516 Gr 70 material and surface nodes, below 68075 are belong to elements with SA 226 Cl2 material properties. Figure (5.3.1) shows the geometric locations of nodes 68075, 70861, 70862, 70863, 68073, 68072 and 68069.

Node 68075 is directly located on the weld line joining tubesheet to the upper shell, node 70863 is located 150 mm above the node number 68075 and other nodes are in between with equal distance. Figure (5.3.2) shows the variation of the first principal stress at these nodes under LC1.

More over, nodes 68069, 68071 and 68073 are located with in the radii surface , they are located close to each other and are with in small distance from weld line node (68075).

Figure (5.3.3) shows the variation of the first principal stress at these nodes under LC1, table (5.3.1.) gives the principal stress values extracted from FEA out put for these nodes.

In regard to the surface nodes of the upper shell the result of quadratic extrapolations of these stresses, based on equation 5.3.1, given below, and according to figure 18.3 of section 18 of the code, is given in table (5.3.4). Whereas it is admissible to use directly the values of principal stresses taken at the node number 68075 (which is directly on the weld line), the code prescribes, for welded regions, the usage of structural stress, i.e. the neglecting of peak stresses obtained by extrapolation of stresses using neighboring nodes.

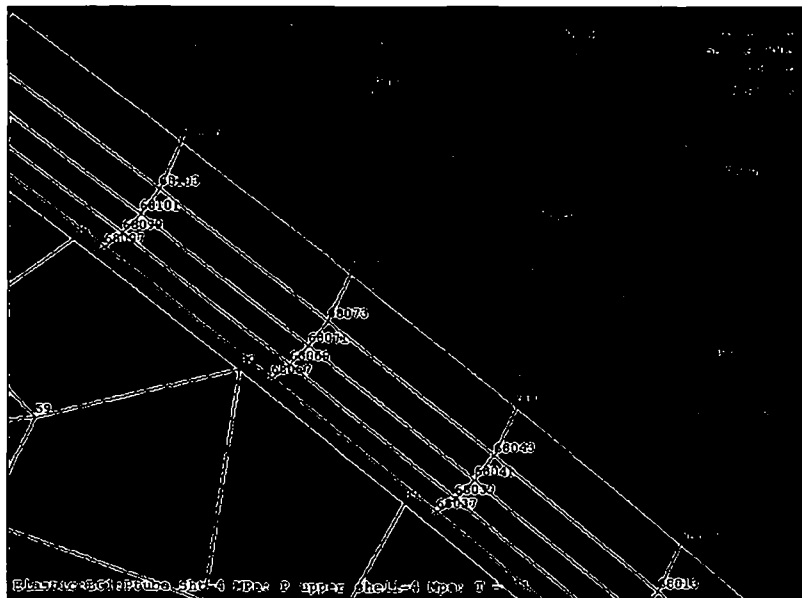


Figure (5.3.1): Geometrical locations of nodes 68075, 70861, 70862, 70863, 68073, 68071, 68069.

Table (5.3.1): Load case 1: Upper shell side(SA 516 Gr 70): Actual FEA nodal principal stresses at 150mm above and at the toe of the weld line (MPa).

FEA node number	σ_1	σ_2	σ_3
68075 (at the weld line)	176.84	73.489	34.908
70861 (50 mm above weld line)	149.31	54.555	-4.593
70862 (100 mm above weld line)	113.45	47.819	-3.631
70863 (150 mm above weld line)	93.182	47.316	-3.668

Table (5.3.1.1): Load case 1:Tube sheet side (SA 266 Cl2): Actual FEA nodal principal stresses at 17mm below and at the toe of the weld line (MPa).

FEA node number	σ_1	σ_2	σ_3
68075 (at the weld line)	267.49	109.65	64.02
68073 (9.8 mm below weld line)	265.47	109.16	64.516
68071 (14 mm below weld line)	253.55	101.19	51.714
68069 (17 mm below weld line)	218.8	87.1	40.73

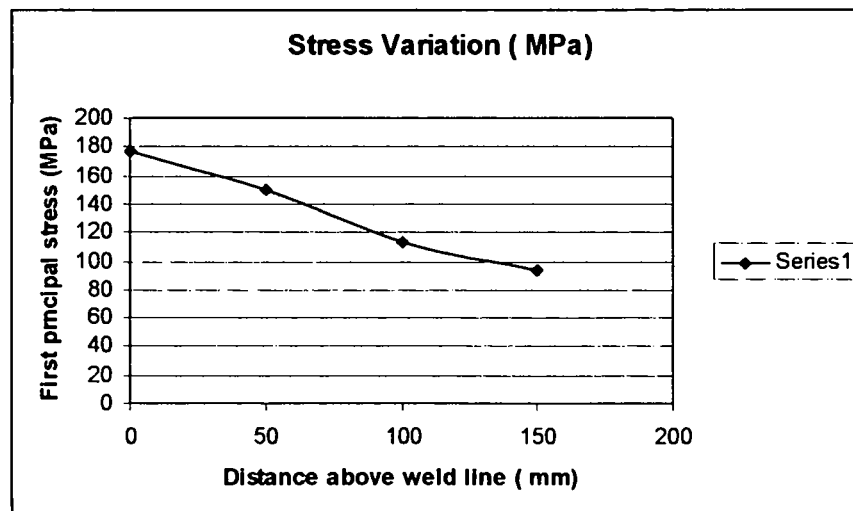


Figure (5.3.2):Load case 1: Stress variation according to node location for 68075, 70861, 70862, 70863

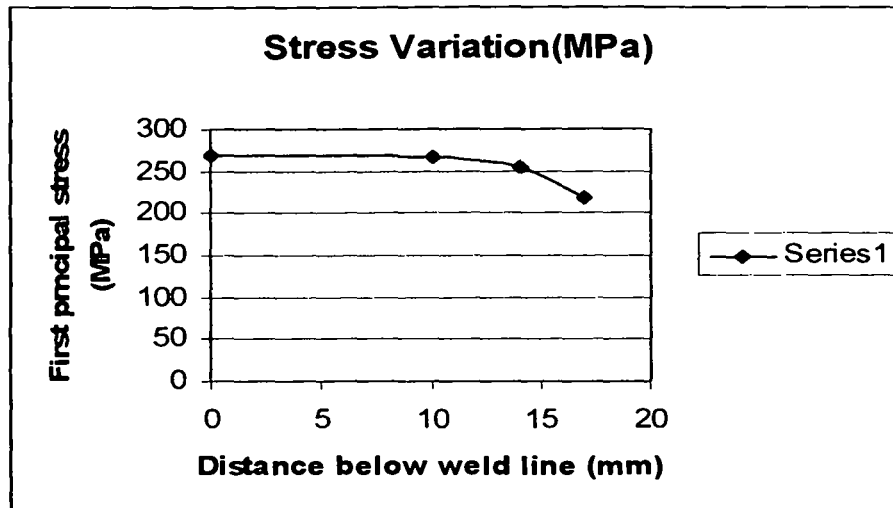


Figure (5.3.3): Load case 1: Stress variation according to node location for 68069,68071,68073 and 68075

Table (5.3.2): Load case 1A: Upper shell side (SA 516 Gr 70): Actual FEA nodal principal stresses at 150mm above and at the toe of the weld line (MPa).

FEA node number	σ_1	σ_2	σ_3
68075 (at the weld line)	138.03	21.83	4.75
70861 (50 mm above weld line)	106.44	-1.299	-4.188
70862 (100 mm above weld line)	65.483	1.0757	-3.838
70863 (150 mm above weld line)	45.19	9.68	-4.01

Table (5.3.2.1): Load case 1A: Tube sheet side (SA 266 Cl2): Actual FEA nodal principal stresses at 150mm above and at the toe of the weld line (MPa).

FEA node number	σ_1	σ_2	σ_3
68075 (at the weld line)	216.82	47.05	35.96
68073 (9.8 mm below weld line)	214.5	48.5	34.64
68071 (14 mm below weld line)	199.72	39.36	25.8
68069 (17 mm below weld line)	167.06	30.194	12.955

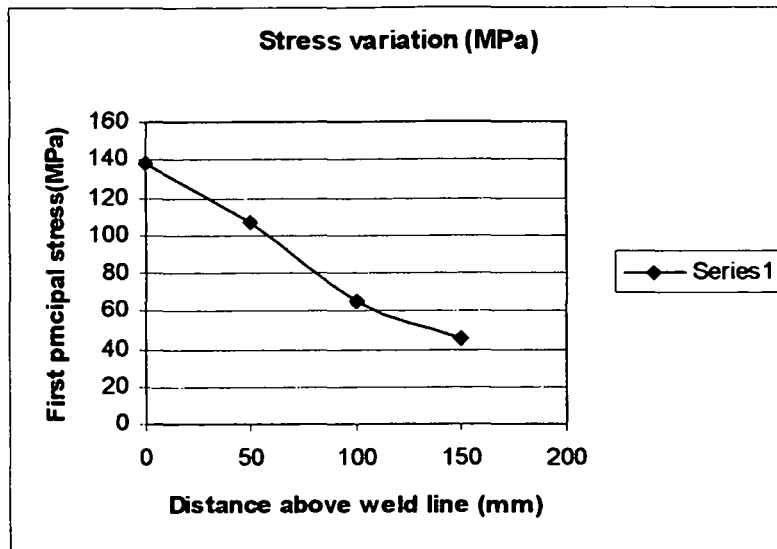


Figure (5.3.4): Load case 1A: Stress variation according to node location for 68075, 70861, 70862, 70863

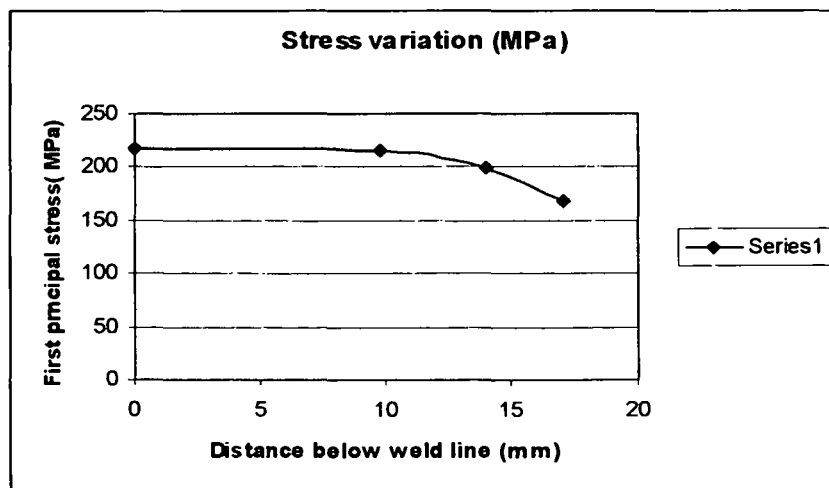


Figure (5.3.5): Load case 1A: Stress variation according to node location for 68069, 68071, 68073 and 68075

Comparing above results it is evident that the principal stresses of load case 1 (LC1) are larger and in this case thermal stresses effect will decrease the principal stresses at the weld location. Therefore, calculations have been continued with principal stresses of load case 1.

Surface paths above and below node number 68075 has been checked for determination of the larger principal stress values. Total stresses at the weld line

have been calculated by interpolation of nodal structural principal stresses from nodes above weld line.

The interpolated values of the principal stresses at the pivot points with distances of 0,4e, 0,9e, and 1,4e, are given in Table (5.3.3).

Table (5.3.3): Principal stresses (MPa) at pivot points (mm)

Distance to weld Stress	34.8 (mm) (.4e)	78.3 (mm) (.9e)	121.8 (mm) (1.4e)
σ_1	157.91	127.885	104.582
σ_2	60.47	50.766	47.567
σ_3	7.75	-4.43	18.031

The equation of the quadratic extrapolation into the hot spot is given in general by

$$Y_0 = 2.52 Y_1 - 2.24 Y_2 + 0.72 Y_3 \quad (5.2.1)$$

and specialized for the first principal stress σ_1 by

$$\sigma_1 = 2.52 (157.91) - 2.24 (127.885) + 0.72 (104.582)$$

$$\sigma_1 = 186.77 \text{ MPa}$$

The extrapolated values of the principal structural stresses coming from shell side are:

$$\sigma_1 = 186.77 \text{ MPa}$$

$$\sigma_2 = 72.92 \text{ MPa}$$

$$\sigma_3 = 42.43 \text{ MPa}$$

Based on figure (5.3.3) and table (5.3.1.1) values of the principal structural stresses coming from tube sheet side govern over the values from shell side, these values are:

$$\sigma_1 = 267.5 \text{ MPa}$$

$$\sigma_2 = 109.65 \text{ MPa}$$

$$\sigma_3 = 64.02 \text{ MPa}$$

Table (5.3.4) gives the value of these principal structural stresses for each load and unload cycle (MPa).

Table (5.3.4): Principal structural stresses

Node	σ_1	σ_2	σ_3	Load cycle
68075	267.5	109.65	64.02	1
68075	0	0	0	2

Based on the values given in table (5.3.4), the structural stress range can be calculated as

$$\begin{aligned}\Delta\sigma_{\text{struct } 1} &= \Delta\sigma_{\text{struct } 1, \text{ max}} - \Delta\sigma_{\text{struct } 1, \text{ min}} \\ \Delta\sigma_{\text{struct } 1} &= 267.5 - 0.0 = 267.5 \text{ MPa} \\ \Delta\sigma_{\text{struct } 2} &= \Delta\sigma_{\text{struct } 2, \text{ max}} - \Delta\sigma_{\text{struct } 2, \text{ min}} \\ \Delta\sigma_{\text{struct } 2} &= 109.65 - 0.0 = 109.65 \text{ MPa} \\ \Delta\sigma_{\text{struct } 3} &= \Delta\sigma_{\text{struct } 3, \text{ max}} - \Delta\sigma_{\text{struct } 3, \text{ min}} \\ \Delta\sigma_{\text{struct } 3} &= 64.02 - 0.0 = 64.02 \text{ MPa}\end{aligned}$$

It should be noted that the directions of principal stresses are constant since the applied actions act simultaneously same in the loading and unloading situations.

The direction of the maximum principal stress is the axial one, and it is normal to the weld joint direction.

$$\begin{aligned}\Delta\sigma_{\text{eq}} &= \max\left(\left|\Delta\sigma_{\text{struct } 1, \text{ max}} - \Delta\sigma_{\text{struct } 1, \text{ min}}\right|, \left|\Delta\sigma_{\text{struct } 2, \text{ max}} - \Delta\sigma_{\text{struct } 2, \text{ min}}\right|, \right. \\ &\quad \left. \left|\Delta\sigma_{\text{struct } 3, \text{ max}} - \Delta\sigma_{\text{struct } 3, \text{ min}}\right| \right) \\ \Delta\sigma_{\text{eq}} &= \max(267.5, 109.65, 64.02) = 267.5 \text{ MPa}\end{aligned}$$

5.3.1.2 Data

In reference to the data sheet values given in section 2, the following parameters are noted, with nomenclatures according to EN 13445-3 Clause 18:

$$\begin{aligned}t_{\text{max}} &= 108 \text{ }^{\circ}\text{C} \\ t_{\text{min}} &= 20 \text{ }^{\circ}\text{C} \\ t^* &= 0.75 t_{\text{max}} + 0.25 t_{\text{min}} \\ t^* &= 0.75(108) + 0.25(20) = 86 \text{ }^{\circ}\text{C} \\ R_m &= 485 \text{ MPa} \\ R_{p \ 0.2/t^*} &= 230 \text{ MPa (see table 2.2.1.A for SA 266 Cl 2 at 86 }^{\circ}\text{C)} \\ 6 \\ e_n &= 87 \text{ mm}\end{aligned}$$

Also, based on detail number 2.2 of Table P.2 of Annex P, the Fatigue Class (FAT) 63, and according to Table 18.7 of EN 13445-3, the endurance limit of 46 MPa results.

The endurance stress is the stress range limit that is given in the code for single-amplitude stress cycles, based on experimental investigation. It is the material allowable stress range value below which no fatigue damage is expected to occur in single-amplitude action cycles.

5.3.1.3 Correction factors

According to sub-clause 18.10.6 of EN 13445-3, the correction factors for temperature, thickness, and plasticity, should be applied. However, since the t^* is below 100 °C the correction factor for temperature is unity. The thickness correction factor is given by

$$f_{ew} = (25/e_n)^{0.25}$$

$$f_{ew} = (25/87)^{0.25} = 0.732$$

Moreover, no plasticity correction factor is required per 18.8 since $\Delta\sigma_{eq,l} < 2R_{p0.2/t^*}$. Herein, $\Delta\sigma_{eq,l}$ is the range of the equivalent linear distribution (over the cross section) corresponding to the actual stress distribution. With $\Delta\sigma_{eq,l} = 267.49$ (see table 5.3.4) and $R_{p0.2/t^*} = 230$ (see table 5.3.1.2), the requirement

$\Delta\sigma_{eq,l} < 2R_{p0.2/t^*}$ is fulfilled:

$267.49 < 2(230)$, i.e. $267.49 < 460$ (no correction for plasticity)

Therefore, the total correction factor is:

$$f_w = f_{ew} f_t^*$$

$$f_w = 0.732(1) = 0.732$$

5.3.1.4 Number of cycles

According to (18.10.7) of EN 13445-3 the Clause 18, the allowable number of load cycles, N , at this stress range (267.49 MPa) and for FAT 63 is 2049 cycles:

$$\Delta\sigma_{eq} / f_w = 267.49 / 0.732 = 365.42 \text{ MPa}, \Delta\sigma_D = 46 \text{ MPa}, \text{ and since } 365.42 > 46:$$

$$N = C_1 / (\Delta\sigma_{eq} / f_w)^{m_1} \text{ with } m_1 = 3 \text{ and } C_1 = 5.0 \times 10^{11}, \text{ and, thus, } N = (5.0 \times 10^{11}) / (365.42)^3 = 2049 \text{ cycle}$$

5.3.2 Groove location (unwelded region)

5.3.2.1 Stresses

The values of the principal stresses extracted from FEA calculation, are given in table (5.3.1.1). Figure (5.3.6) shows node 68073 located in the groove,

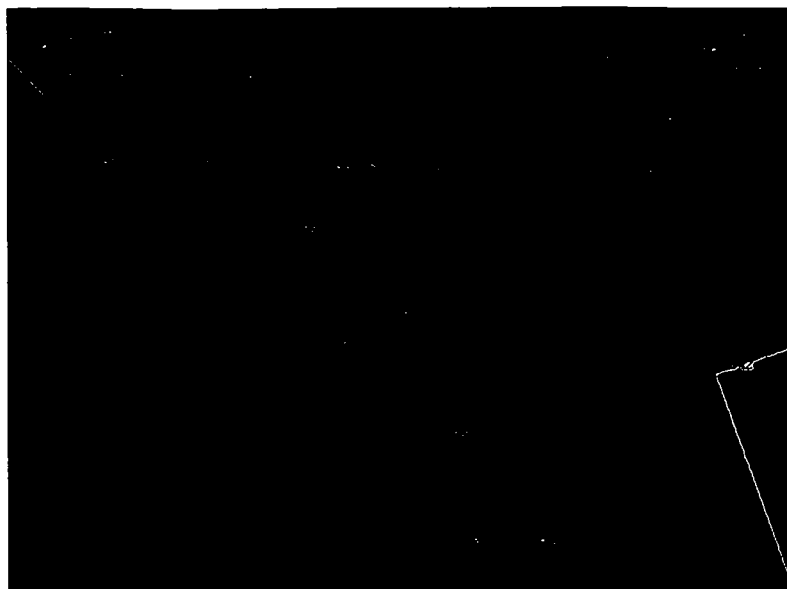


Figure (5.3.6): Location of node 68073 at the radius

Table (5.3.5) gives the values of principal total stresses (MPa) at the end of loading and of unloading.

Table(5.3.5): Principal stresses

Node	σ_1	σ_2	σ_3	σ_{eq}	Load step
68073	265.47	109.16	64.516	182.77	1
68073	0	0	0	0	2

As a first step, the equivalent stress range and the equivalent mean stress, according to requirement (18.7.1.2) of the code, are calculated. The details are:

$$\sigma_1 = \sigma_1(t_1) - \sigma_1(t_2) = 265.47 - 0 = 265.47 \text{ MPa}$$

$$\sigma_2 = \sigma_2(t_1) - \sigma_2(t_2) = 109.16 - 0.0 = 109.16 \text{ MPa}$$

$$\sigma_3 = \sigma_3(t_1) - \sigma_3(t_2) = 64.516 - 0.0 = 64.516 \text{ MPa}$$

$$[S_{1,2}]_{\max} = \sigma_1 - \sigma_2 = 265.516 - 109.16 = 156.31 \text{ MPa}$$

$$[S_{1,3}]_{\max} = \sigma_1 - \sigma_3 = 265.47 - 64.516 = 200.954 \text{ MPa}$$

$$[S_{2,3}]_{\max} = \sigma_2 - \sigma_3 = 109.16 - 64.516 = 44.644 \text{ MPa}$$

$$[S_{1,2}]_{\min} = \sigma_1 - \sigma_2 = 0.0 - 0.0$$

$$[S_{1,3}]_{\min} = \sigma_1 - \sigma_3 = 0.0 - 0.0$$

$$[S_{2,3}]_{\min} = \sigma_2 - \sigma_3 = 0.0 - 0.0$$

$$\Delta\sigma_{eq} = \max (|S_{12\max} - S_{12\min}| ; |S_{23\max} - S_{23\min}| ; |S_{31\max} - S_{31\min}|)$$

$$\Delta\sigma_{eq} = \max (|156.31 - 0.0| ; |200.954 - 0.0| ; |44.644 - 0.0|)$$

$$\Delta\sigma_{eq} = 200.954 \text{ MPa}$$

Also for code item (18.11.1.3), the mean stress correction:

$$\bar{\sigma}_{eq} = 0.5 [(\sigma_{total,i} + \sigma_{total,j})_{\max} + (\sigma_{total,i} + \sigma_{total,j})_{\min}]$$

$$\bar{\sigma}_{eq} = 0.5 [(\sigma_1 + \sigma_3)_{\max} + (\sigma_1 + \sigma_3)_{\min}]$$

where the $\sigma_{total,i} + \sigma_{total,j}$ are maximum and minimum stresses responsible for determination of $\Delta\sigma_{eq}$ i.e. σ_1 and σ_3 .

$$\bar{\sigma}_{eq} = 0.5 [(265,47 + 64,516)_{\max} + (0,0 + 0,0)_{\min}]$$

$$\bar{\sigma}_{eq} = 164,993 \text{ MPa}$$

According to (18.7.1.1) of EN 13445-3, the effective total stress range can be taken to be equal to the equivalent total structural stress range, i.e. the effective stress concentration factor may be used equal to the theoretical elastic stress concentration factor $K_f = 1$. This is a conservative simplification used here, and then

$$\Delta\sigma_f = \Delta\sigma_{eq, struc} = 200,954 \text{ MPa}$$

5.3.2.2 Data

In reference to the data sheet values given in section two of this work, the following parameters are noted, all nomenclatures are according to Clause 18 of EN 13445-3:

$$t_{\max} = 108 \text{ }^{\circ}\text{C}$$

$$t_{\min} = 20 \text{ }^{\circ}\text{C}$$

$$t^* = 0.75 t_{\max} + 0.25 t_{\min}$$

$$t^* = 0.75(108) + 0.25(20) = 86 \text{ }^{\circ}\text{C}$$

$$R_m = 485 \text{ MPa}$$

$$R_{p0.2/t^*} = 230 \text{ MPa (see table 2.2.1.A for SA 266 Cl2 at 86 }^{\circ}\text{C)}$$

$$e_n = 111 \text{ mm (tube sheet thickness under node 68073)}$$

5.3.2.3 Correction factors

The correction factors for the influence of following parameters must be applied per code requirement (18.11.1) of EN-13445-3. These factors are

- Influence of mean stress: (18.11.1.3.1) of EN 13445-3:

Figure 18.16 of the clause 18 of the code gives the plot of the stress range $\Delta\sigma_R$ versus the number of allowed cycles for unwelded ferritic rolled steels with mean stress equal to zero, the corresponding equations are:

$$\Delta\sigma_R = 0.63R_m - 11.5 + 4.6 \times 10^4 / \sqrt{N}$$

For assumed number of cycle of 80000 this results in,

$$\Delta\sigma_R = 0.63(485) - 11.5 + 4.6 \times 10^4 / \sqrt{80000} = 456.7 \text{ MPa}$$

Also, the endurance limit according to table (18.10), or the following equation, is given by

$$\Delta\sigma_D = 21 + 0.63R_m, \text{ i.e. } \Delta\sigma_D = 21 + 0.63(485) = 326.55 \text{ MPa.}$$

Recalling,

$\Delta\sigma_{eq} = 200.954 \text{ MPa}$, the maximum equivalent of total stress

$\sigma_{eq,max} = 182.77 \text{ MPa}$ (see table 5.3.3), and

$R_{p0.2/t} = 230 \text{ MPa}$ (see 5.3.2.2),

one obtains for $\Delta\sigma_{eq} < 2 R_{p0.2/t}$ and $|\sigma_{eq,max}| < R_{p0.2/t}$

$200.954 < 460$ and $182.77 < 230$, and the mean stress correction factor for rolled and forged steel is given by

$M = 0.00035R_m - 0.1 = 0.00035(485) - 0.1 = 0.069$, and

$$f_m = \{1 - [M(2+M)/(1+M)](2\sigma_{eq}/\Delta\sigma_R)\}^{0.5} \\ = \{1 - [0.069(2+0.069)/(1+0.069)](2 \times 164.993 / 456.7)\}^{0.5} = 0.95$$

- Influence of thickness, t : (18.11.1.2) of EN 13445-3:

$$f_c = F_e^{(0.1 \ln N - 0.465)}$$

$$\text{where } F_e = (25 / e_n)^{0.182} = (25/111)^{0.182} = 0.762$$

$$f_c = (0.762)^{(0.1 \ln 80000 - 0.465)}$$

$$f_c = 0.855$$

- Influence of surface finish: (18.11.1.1.1) of EN 13444-3 of EN 13444-3:

$$f_s = F_s^{(0.1 \ln N - 0.465)}$$

$$F_s = 1 - 0.056 (\ln R_z)^{0.64} \ln R_m + 0.289 (\ln R_z)^{0.53}$$

The surface roughness height index of $200 \mu\text{m}$ for the tube sheet has been assumed. There follows

$$F_s = 1 - 0.056(\ln 200)^{0.64} \ln(485) + 0.289 (\ln 200)^{0.53}$$

$$F_s = 0.69$$

$$f_s = (0.69)^{(0.1 \ln 80000 - 0.465)}$$

$$f_s = 0.78$$

- No temperature correction is required since t^* is below 100 °C
- Overall correction factor :

$$f_u = f_s \cdot f_e \cdot f_m \cdot f_t^*$$

$$f_u = (0.78)(0.855)(0.95)(1)$$

$$f_u = 0.63$$

5.3.2.4 Fatigue result for unwelded regions:

The result for $\Delta\sigma_f / f_u$, with the assumed number of 80 000 cycles and corresponding correction factors, is given by

$$\Delta\sigma_f / f_u = 200.9 / 0.63 = 319 \text{ MPa},$$

smaller than $\Delta\sigma_D = 326.6 \text{ MPa}$.

The correction factors depend on the (assumed) number of cycles. Iteration is, therefore, required.

Assuming, as upper limit, 2 000 000 cycles renders

$$f_m = 0.9333; f_e = 0.765; f_s = 0.696;$$

and, thus,

$$\Delta\sigma_f / f_u = 404.2 \text{ MPa},$$

larger than $\Delta\sigma_D = 326.6 \text{ MPa}$ - the correct number of cycles must be smaller than 2 000 000. Further iteration steps result finally, for an assumed number of cycles equal to 425 000, in

$$f_m = 0.937; f_e = 0.798; f_s = 0.737;$$

and, thus,

$$\Delta\sigma_f / f_u = 364.6 \text{ MPa},$$

which renders finally

$$N = 424908 \text{ cycles},$$

close enough to the assumed 425 000 cycles.

This value for the allowed number of cycles for unwelded regions is much larger than the value for welded regions 2049, determined in 5.3.1.4 – the welded region is governing the fatigue design.

6. Inelastic analyses

In the past, up to the turn of the century, the usually used procedures in design by analysis used linear- elastic analyses of stresses and categorization of stresses into primary, secondary, and peak stresses.

The most significant problem in the above procedure is stress categorization and partitioning, which particularly identifies and puts limits on primary stresses to safeguard the component against gross plastic deformation, and on secondary stresses to safeguard against progressive plastic deformation.

This approach is not adequate for locations with structural discontinuity or stress concentrations if an FEA analysis is performed, especially so if in the FEM analysis volume elements are used. It cannot be decided easily which FEA 3D-output stresses can be classified as primary stresses.

The most advanced procedure, bypassing these problems, is the Direct Route given in EN 13445-3 Annex B. There, ideas of inelastic analysis have been used to tackle failure modes directly, and Articles B.4 and B.5 in Annex B of EN 13445-3 provide complete criteria for these failure modes and the limit states. Among various modes, gross plastic deformation and progressive plastic deformation are of major concern for this reactor. Checks for these failure modes are given below. The only additional failure mode to be dealt with – fatigue – has been discussed in detail in section 5 of this work.

6. A Gross Plastic Deformation Design Check

The gross plastic deformation design check requires, in the (load) case under consideration, increase of pressure from zero to its design value in the model with zero initial stress state. As the pressure is continually increased, a region of the vessel becomes plastic and the rate of deformation begins to increase, but deformation of the vessel as a whole is usually still restrained by the surrounding elastic material. Finally, upon further increase in pressure, a limit (plastic) collapse pressure is reached. There the plastic zone has grown sufficiently large so that the deformation begins to increase with little or no additional increase in pressure.

Two types of inelastic analysis method can be used to guard against gross plastic deformation: they are, limit analysis and plastic analysis.

Gerdeen[17] describes the theory of limit analysis as an idealized theory that enables the limit pressure to be found by considering only the limit (analysis) state and by neglecting previous deformation.

Limit analysis, based on small deformation and elastic – perfectly plastic material can be employed to determine the limit resistance of the reactor.

In limit analysis the yield stress S_y the value in the constitutive law of the model to one set of plastic flow, is the basic material property. Limit load is an estimate of plastic load of an actual vessel at which plastic deformation becomes relatively significant as compared to elastic deformation.

As an alternative to calculating limit load, the actual plastic load can be determined by computer analysis, with the results of computer analysis in the form of a deformation parameter as a function of a loading parameter.

EN-13445-3 Annex B sub-clause B.8.2 deviates from this route, provides different rules for checking against gross plastic deformation. In this design check the (plastic) analysis is to be performed with:

- Linear elastic ideal-plastic constitutive law.
- Tresca's yield condition with associated flow rule.
- First- order theory.
- Proportional increase of actions.
- Stress-free initial state.
- Limitations of the maximum value of principal structural strains.

The above has been considered in the ANSYS model by selecting a linear- elastic plastic model with rate- independent plasticity along with isotropic hardening but with zero tangent modulus (no hardening).

Furthermore, plastic flow is specified to be an associated one, i.e. the potential function, which is function of stress and is responsible for identification of direction of plastic strains, is chosen to be identical to the yield function. There follows, that plastic strain rates (infinitesimal increment) occur in a direction normal to the yield surface, i.e. the normality rule applies. The final direction of the total strain is calculated and reported by ANSYS.

It should be noted that the ANSYS routine is not based on the Tresca yield condition, whereas Annex B is. Therefore, since the maximum ratio of the Mises equivalent stress to the Tresca equivalent stress is $2/\sqrt{3}$, a multiplication of the design material strength parameter, the design yield stress, with $\sqrt{3}/2$ always leads to conservative results. Table (2.2.2) gives the values of this yield parameter, which is adjusted by this factor and has been used as input to the software.

It should be emphasized that the radius of the groove on this specific model is all along the circumference at the junction of tube to tubesheet, and its presence indicates that the evaluated strains are not local in nature. Wherever required, total strain is used in following calculations instead of structural strains, although in the strain limiting requirement structural stresses may be used.

Admissibility of the model design to pressure is evaluated by checking both, the carrying capacity of the model with reduced yield strength and the limitation of the maximum absolute value of principal structural stresses by 5%, since either can individually dictate the limitation point.

By examination of the results of series of calculations it became evident that the upper boundary condition (junction to head) specifically and the upper shell itself, in general, are the limiting regions of the model. These parts reach full plasticization before the tubesheet, and before the tubesheet-to-shell junctions.

It should be recalled, that by using Ilyushin's or Ivanov 's generalized yield functions the percentage of plasticization at any arbitrary path for shells and plates can theoretically be evaluated. However, Annex B has no requirement in this regard, but these evaluations can be, and are, used as an additional check of the level of loading vis-à-vis the full plastification.

According to Burgoyne and Brennan [18], Ilyushin's functions are stress functions with capabilities of evaluating shell resultant stresses with regard to the degree of plastification.

Shell stress resultants are quantities of the dimensions force per unit length and moment per unit length, respectively, which are defined on the shell middle surface. These functions can be combined in the form of a generalized yield surface, which then can be used for comparison of the ratio of the plasticization level to the full plasticization based on Mises's yield condition. In this way one can estimate the percentage of plasticization of a cross- section of (thin walled) shells and plates.

To perform a complete check, including possible design improvements, two different designs have been investigated in this step of the work:

Firstly, in a series of the checks, the original data sheet material SA- 516 Gr. 70 have been kept, the results are given in section 6.A.1 below.

Secondly, design checks have been carried out with a stronger material for the upper shell SA – 537 C12. In this way the upper shell is much stronger, and the regions with large plasticization will be shifted from the upper end of the shell into the tubesheet. With this choice of material the tubesheet behavior can be better investigated – the critical regions are now the interesting ones, the tubesheet and the tubesheet-to-shell junction.

It should also be noted, that the shell material is a carbon manganese steel, which can easily be changed to a better quality of steel without much altering the process requirements or the cost criteria in this type of applications with the stronger shell material.

Section 6.2 gives the result of the calculations.

6. A.1 Upper shell material according to original specification (SA 516 Gr. 70)

Results of calculations, which are given below, indicate that for pressure full plasticization is reached first at the upper end of the upper shell section, and, in this case, the tubesheet still remains at the corresponding pressure fully elastic or shows small plasticity.

As an additional check a through-thickness path near the upper boundary condition was selected, and the percentage of the plasticization along this path based on the Ilyushin function was calculated at the evaluated critical pressure.

At 240% of the design pressure load no convergence was achieved. Therefore, the previous ANSYS time step with convergent solution was selected as terminal point for further checks on stress and strain.

At this time step the pressure is 7.932 MPa, which, by considering partial safety factor of 20% according to table B-8.1 of EN 13334-3 Annex B, renders the critical pressure

$$P_{\text{ANSYS}} = 7.932 \text{ MPa}$$

$$P_{\text{critical}} = (7.932)/1.2$$

$$P_{\text{critical}} = 6.61 \text{ MPa}$$

Moreover, as a check, the value for the plastic load of the infinitely long cylinder was calculated [19]. and the result is:

$$P_{\text{plastic}} = (2/\sqrt{3}) R \ln (r_o / r_i)$$

where r_o and r_i are inside and out side radius given in section 2, and the design value of the yield stress. With

$$R = R_{\text{Mises}} = 165 \text{ MPa (table 2.2.2, channel side shell at } 108^\circ\text{C)}$$

there follows

$$P_{\text{plastic}} = (2/\sqrt{3}) (165) (\ln(1.0425)) = 7,9 \text{ MPa}$$

Applying the partial safety factor 1.2, see table B-8.1 of Annex B of EN 13445-3, one obtains $P_{\text{critical}} = 7.9/1.2 = 6.58 \text{ MPa}$, very close to the value obtained by means of the FEA investigation. The difference is caused by the (slight) stiffening effect of the model boundary condition at the upper shell's upper end.

Figures (6.A.1.1) to (6.A.1.4) give details of the above checks.

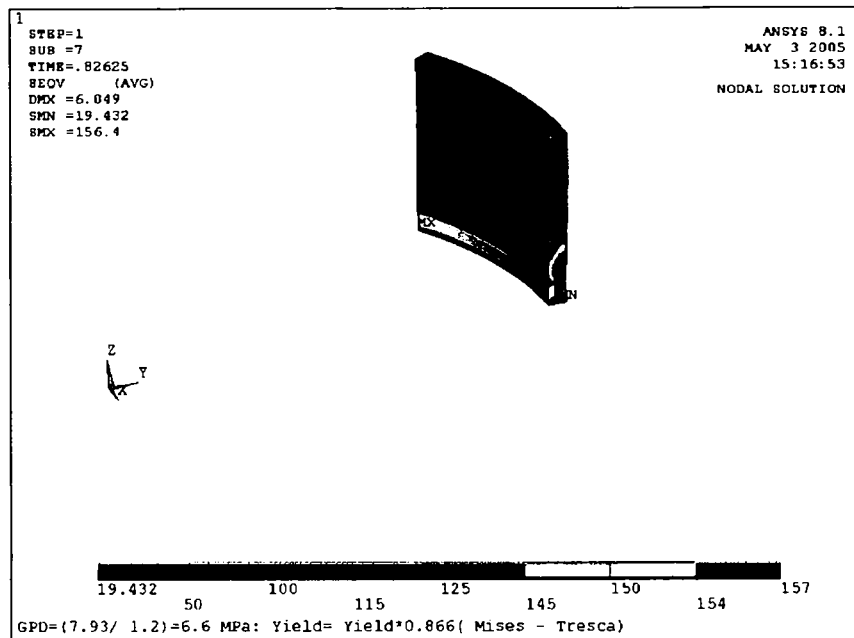


Figure (6.A.1.1): Upper shell: Mises equivalent stress (MPa) for a pressure of 7.93 MPa.

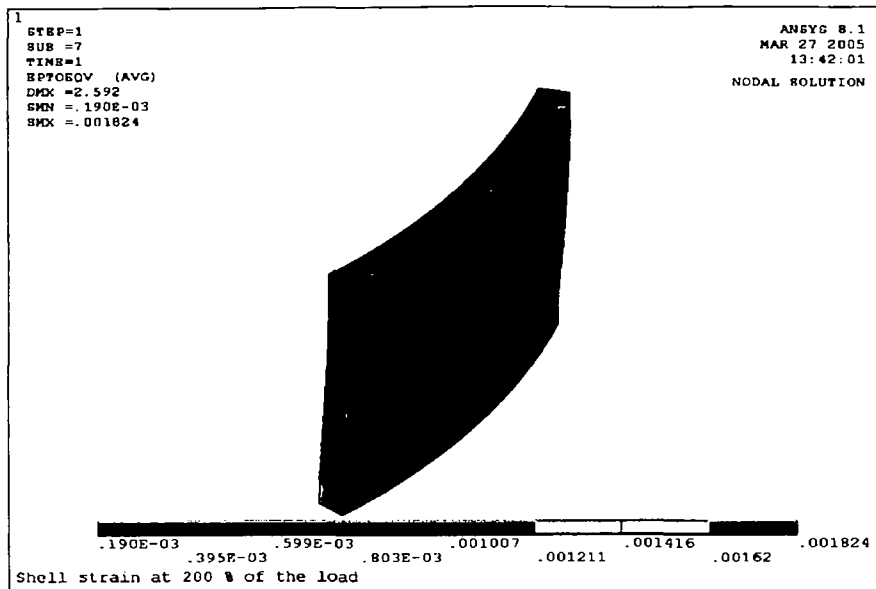


Figure (6.A.1.2): Upper shell: Mises equivalent total strain for a pressure of 7.93 MPa.

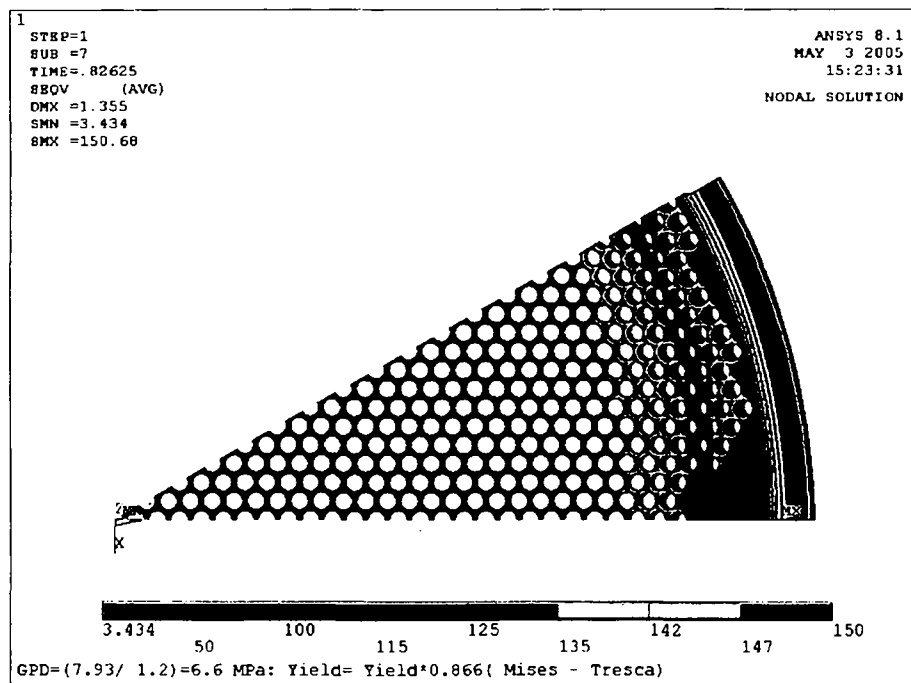


Figure (6.A.1.3): Tubesheet: Mises equivalent stress for a pressure of 7.93 MPa.

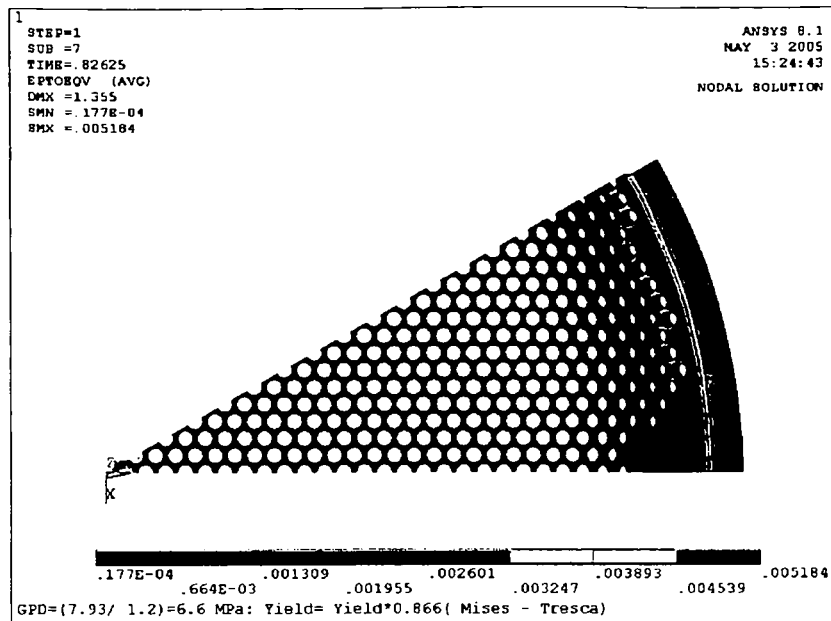


Figure (6.A.1.4): Tubesheet: Mises equivalent strain for a pressure of 7.93 MPa.

At $P_{critical}$ (6.61 MPa) the value of Ilyushin's function is 0.77 at the path defined close to the end of the upper shell, details are given in appendix 1. At this load the upper shell and tubesheet stresses and strains are given in Figures (6.A.1.5 to 6.A.1.8)

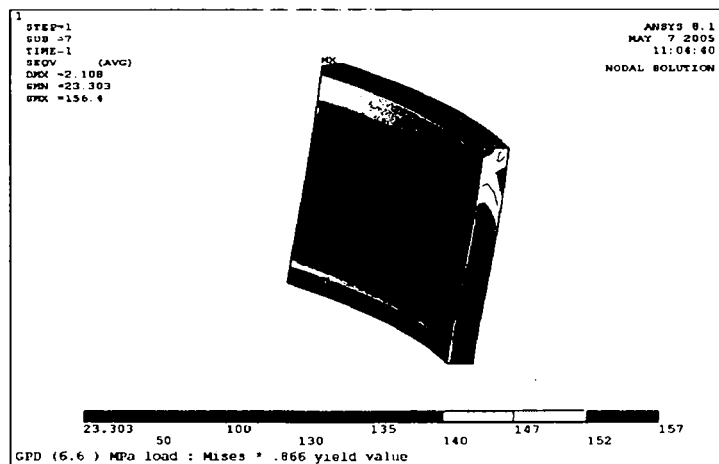


Figure (6.A.1.5): Upper shell: Mises equivalent stress(MPa), inside view, at a pressure of 6.61 MPa

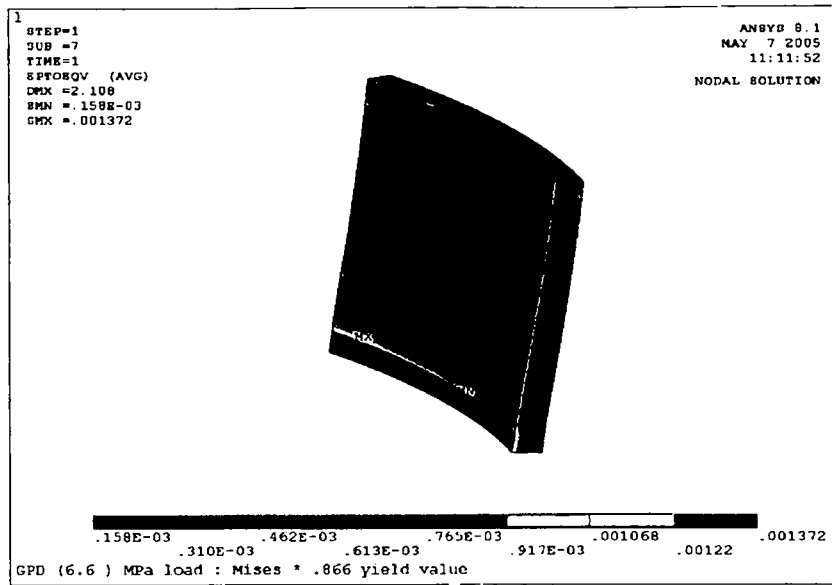


Figure (6.A.1.6): Upper shell: Mises equivalent strain (inside view) at a pressure of 6.61 MPa

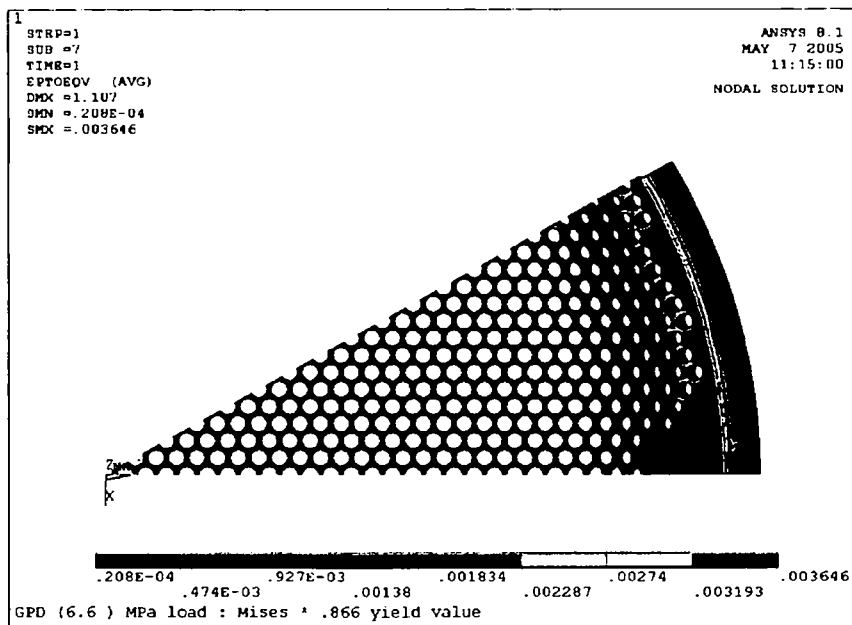


Figure (6.A.1.7): Tubesheet: Mises equivalent strain at a pressure of 6.61 MPa.

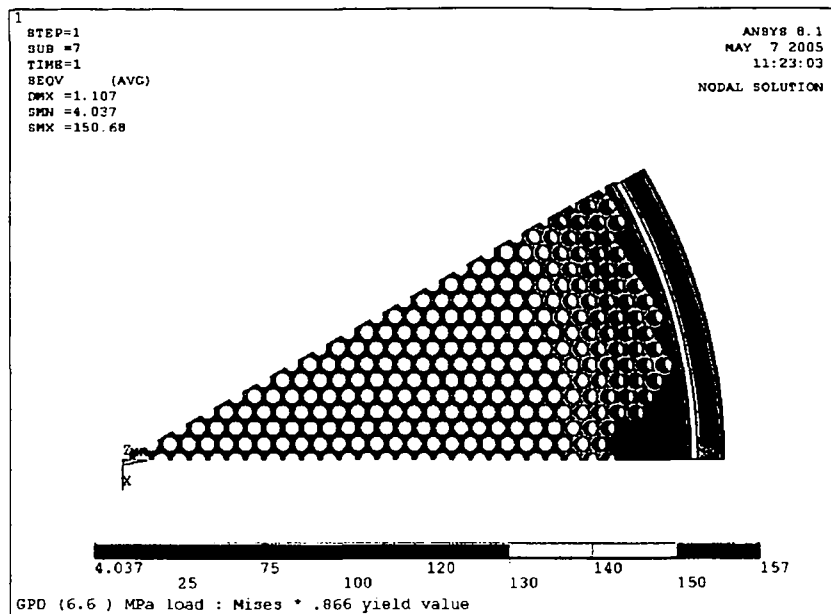


Figure (6.A.1.8): Tubesheet: Mises' equivalent stress at a pressure of 6.61 MPa

6. A.2 Upper shell material – 537 Cl. 2

The calculation for the behavior of the reactor with stronger upper shell material is given below. It should be pointed out that with the stronger upper shell material the critical points will move from the upper boundary of the upper shell to the tubesheet. Both criteria for strain and stress have been checked.

Moreover, it should also be noted that the evaluation of Ilyushin's function is not suitable for a path through the thickness of this tubesheet. This is due to larger stresses along the in- plane (z) direction, shear and torsion bending stresses (that result from stress components acting in the direction of the path and not perpendicular to it. The Ilyushin function is not suitable for cases with large stresses along the path, which are the governing ones in this case.

To bypass this problem, Mises' equivalent stresses have been extracted for a series of the parallel paths next to each other and in the in-plane(z) direction , and by integrating them it is possible to obtain an approximation of the integral over the cross-section considered. To check the reactor performance, simultaneously the upper shell condition has been monitored.

At a pressure of 10.4 MPa the program crashed, indicating no solution at this load, the lower time (load) step for which program converges. corresponds to a value slightly below 8.9 MPa.

Considering the partial safety factor of 1.2 on the action, according to Annex B, the critical load is given by:

$$P_{critical} = 7.4 \text{ MPa}$$

To take into account the correction of the yield stress, required for the usage of Mises yield condition, the reduced, lower material yield value has been used as input to the ANSYS program, a reduced value obtained by multiplication of the design value of the material strength parameter by $\sqrt{3}/2$.

Figures (6.A.2.1) to (6.A.2.4) give information on above value, and other relevant parameters. The results indicate that at a pressure of 8.8 MPa the maximum strain in the tubesheet is 3.2% (at the groove location) which is below the 5% code limitation. Plasticization at the upper end of the tubeside shell is small and is not governing anymore. This can also be seen from the check of the limit analysis pressure of the infinitely long closed cylinder, which is now, for the stronger shell material, given by $R = R_{\text{mises}} = 195 \text{ Mpa}$ (see table (2.2.2)).

$$P_{\text{plastic}} = (2/\sqrt{3}) R \ln (r_o/r_i) = 9.4 \text{ MPa.}$$

Applying partial safety factor 1.2, see table B-8.1 of Annex B of EN 13445-3, one obtains $P_{\text{critical}} = 9.4/1.2 = 7.8 \text{ Mpa}$.

There follows, that the cylindrical shell is not governing any longer.

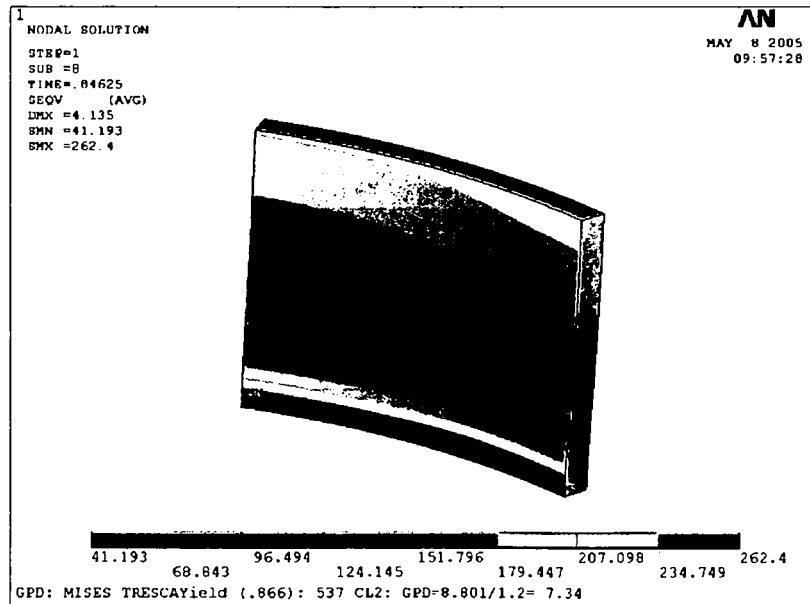


Figure (6.A.2.1): Mises equivalent total stress, inside view of upper shell, for a pressure of 8.8 MPa and SA 537 Cl. 2 material.

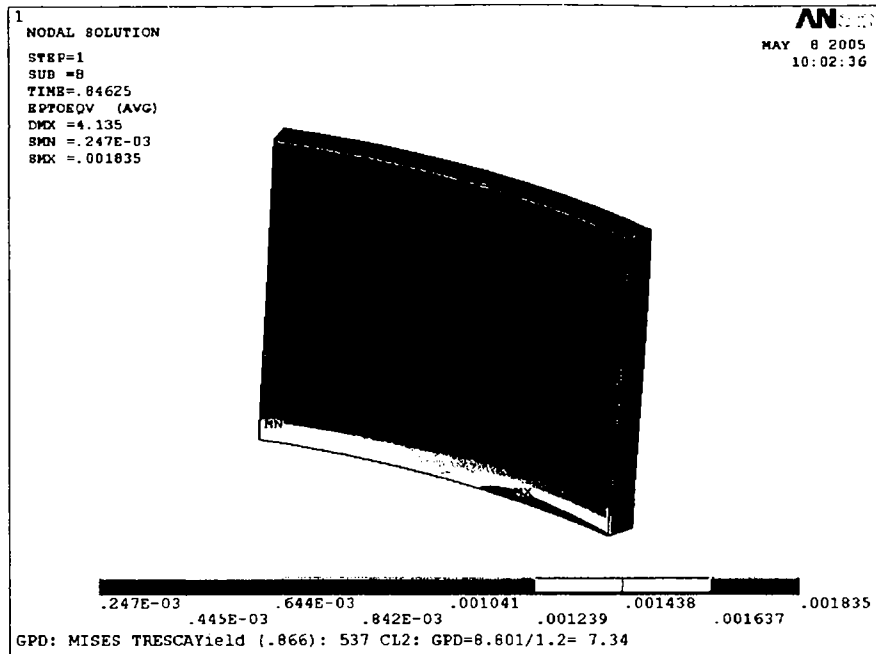


Figure (6.A.2.2): Mises equivalent total strain in upper shell for a pressure of 8.8 (MPa) and SA 537 Cl. 2 materials.

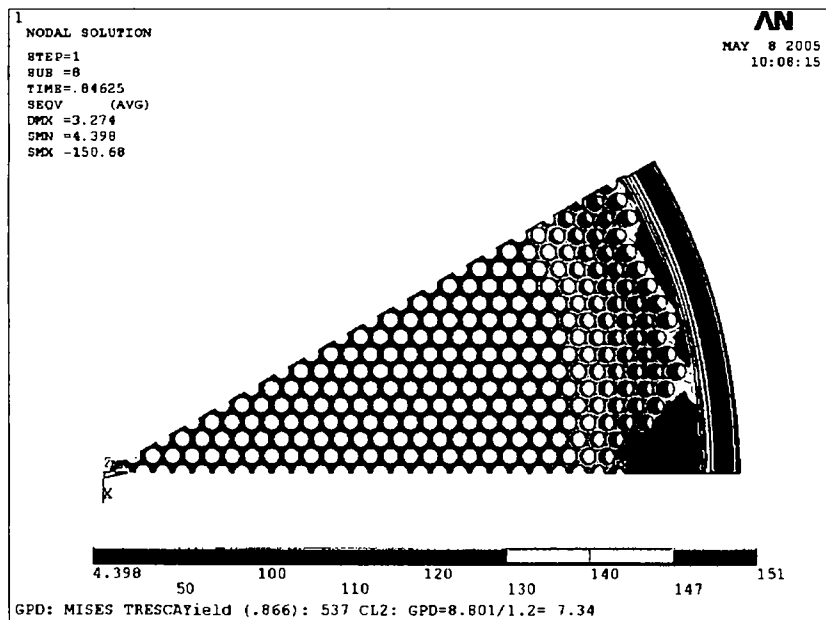


Figure (6.A.2.3): Tubesheet: Mises' equivalent total stress for 8.8 MPa tube side pressure.

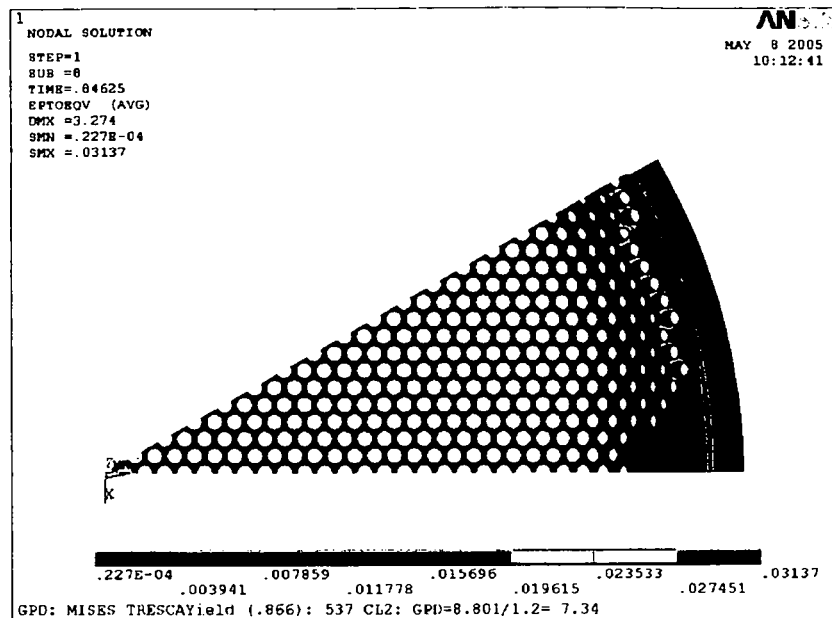


Figure (6.A.2.4): Tubesheet: Mises' equivalent total strain for 8.8 MPa tube side pressure.

B. Progressive Plastic Deformation Design Check

Another important failure mode that needs to be checked is progressive plastic deformation. The reactor operates under base load conditions with just a few cycles coming from startup and shut down as well as process upsets:

The Direct Route in Design by Analysis requires a progressive plastic deformation design check to be performed. Therefore, for the structure with the stronger upper shell material and the reported –GPD- pressure (critical pressure) of 7.4 bar and for the temperature distribution ranging from 50 to 108 °C, the reactor has been examined for shakedown or alternating plasticity. The check performed here is based on EN – 13445 Annex B that states under repeated application of the specified action cycles progressive plastic deformation shall not occur in the model with the following properties:

- First order theory.
- A linear – elastic ideal plastic – constitutive law.
- Mises yield condition (maximum distortion energy hypothesis) and associated flow rule.
- Design strength parameters RM_d .

It should be emphasized that in this design check partial safety factors are equal to 1, i.e. no reduction in material yield strength nor increase in applied actions are necessary.

In the following investigations the actions are pressure and temperature, with variation between zero and maximum (design) values. The maximum value for pressure is 7.4 MPa, which is the critical –GPD- pressure for the case of an upper

shell selected from stronger material (SA 537 Cl.2) instead of shell material (SA 516 Gr.70), which results in GPD- pressure of 6.61 MPa. For this pressure of 7.4 MPa the maximum values for the mean temperatures are the design temperatures of 108 °C for shell side materials and 50 °C for materials in tube side.

Moreover, these temperatures have been used in the model as surface temperatures in thermal boundary conditions, and the temperature distribution has been calculated and incorporated into the model for this design check.

With above parameters the maximum allowable tube side design pressure for shakedown of the structure has been evaluated.

Melan's shakedown theorem states that the structure will shake down for a given cyclic action, if a time-invariant self-equilibrating stress field can be found such that the sum of this stress field and the cyclically varying stress field determined with the unbounded linear –elastic constitutive law for the given cyclic action is compatible with the yield condition. The equivalent stress field (of the superposition of the self-equilibrating stress field and the linear- elastic stress field) should not violate the material yield parameter at any time.

Self-equilibrating stress field can be found by two procedures which, are:

6.B.1 Load-Unload procedure

To obtain a residual stress field, the following procedure has been used:

(A.1) Loading of the model to the action state of GPD- pressure and design temperature, and calculation of the stress field with the elastic-plastic constitutive law (load step 1).

(A.2) Unloading of the model to a condition of above to near zero pressure and zero temperature (load step 2), and calculation of the residual stress field. This stress field, calculated in this way, is self- equilibrating since it is a residual stress field, for zero imposed pressure and zero temperature.

Therefore, this residual stress field can be used in Melan's shakedown theorem by adding it to the stress field obtained with an unbounded linear- elastic constitutive law: With $\sigma_{ij,Res}$ denoting residual stress field, $\sigma_{i,j,limit}$ the elastic-plastic stress field at limit load, $\sigma_{ij,0}$ the elastic-plastic stress field after unloading from load step 2, $\sigma_{ij, limit}$ the unbounded linear elastic stress field, the superposition of the stress fields can be written in the form

$$[\sigma_{i,j}(t)]_{SD} = \sigma_{ij,Res} + \alpha(t) [\sigma_{ij,limit}] \text{ with } 0 \leq \alpha(t) \leq 1$$

6.B.2 Direct subtraction procedure

In this procedure the stress field created in the elastic-plastic model for a specified action will be subtracted from the stress field obtained with the unbounded linear- elastic constitutive law for the same action. For the very same actions this subtraction will result in a self- stress field since by this subtraction all imposed actions become zero. After this step, the calculated self stress field can be added to the linear-elastic solution, as discussed above.

Denoting the self equilibrium stress field by $\sigma_{ij,self}$, one has

$\sigma_{ij, self} = \sigma_{ij, limit} - \sigma_{ij, limit}$
 and, as in 6.B.1, the superposition in the form
 $[\sigma_{ij}(t)]_{SD} = \sigma_{ij, self} + \alpha(t) [\sigma_{ij, limit}]$ with $0 \leq \alpha(t) \leq 1$

It must be indicated again that both extreme stress fields, for $\alpha=0$ and $\alpha=1$, must be compatible with the yield condition, i.e. $\sigma_{eq} \leq R_M$, to fulfill Melan's shakedown theorem.

6.B.3 Upper shell material according to SA 537 Cl.2

The figures below show the results of the calculations for the reactor for an upper shell material according to SA 537 Cl.2. Figure 6.B.3 shows the distribution of Mises equivalent stress for $\alpha=0$, i.e. Mises equivalent stress for the self-stress field. All equivalent stresses are below 121 MPa. Figure 6.B.5 shows the distribution of Mises equivalent stress for the superposition given by $\alpha=1$. This figure shows that after the superposition of the stress fields, in the added stress field, the value of Mises' equivalent stress is slightly above the yield stress given by 226 MPa. This indicates that the created self-stress field is not an optimum one. Since the loading choice for creating self-stress field is arbitrary, the calculations were repeated for a pressure of 8.8 MPa. This 8.8 MPa is the pressure determined in the GPD design check as limit pressure, i.e. before applying partial safety factor.

Figures 6.B.6 and 6.B.7 and 6.B.8 show the results of the repeated calculations. Figure 6. B. 8 shows that the distribution of Mises equivalent stress for the superposition with $\alpha=1$ has no value above the allowable value (for shakedown) given by 226 Mpa, the material yield value.

There follows that Melan's shakedown theorem is fulfilled, the structure shakes down to linear-elastic behavior, plastic deformation does not occur.

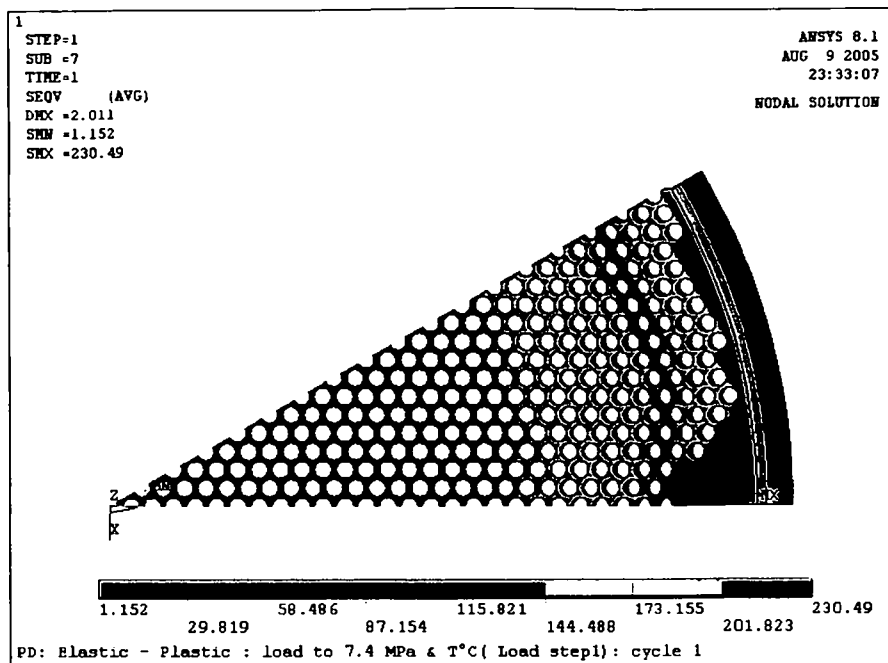


Fig (6.B.1): Mises' equivalent stress for elastic-plastic constitutive law at the limit pressure of 7.4 MPa and temperatures at the surfaces of 108 °C on upper shell, and 50 °C on lower shell. Tubesheet with calculated temperature distribution.

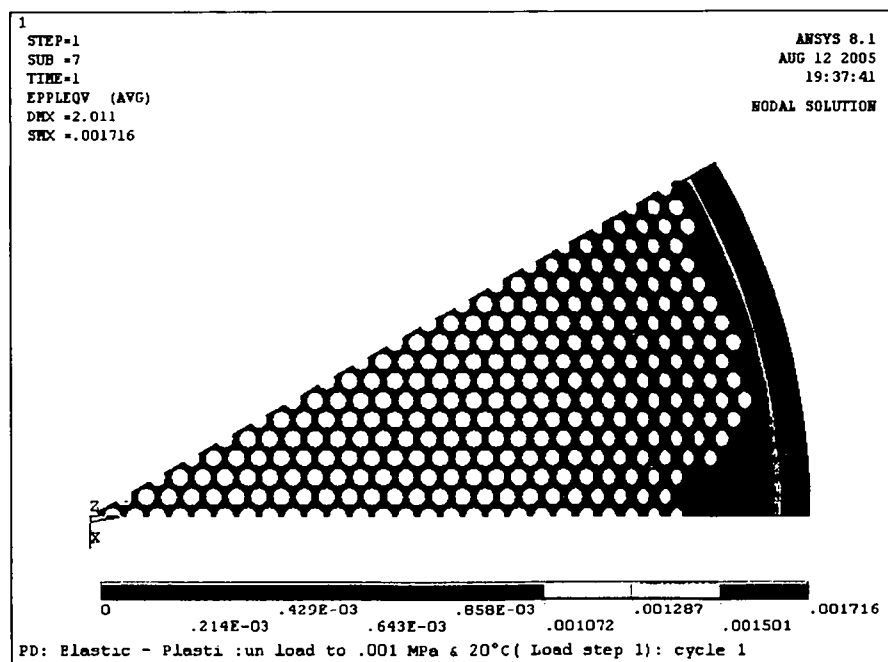


Fig.(6.B.2): Residual Mises' equivalent strain at .001 MPa pressure and temperature T= 20 °C.

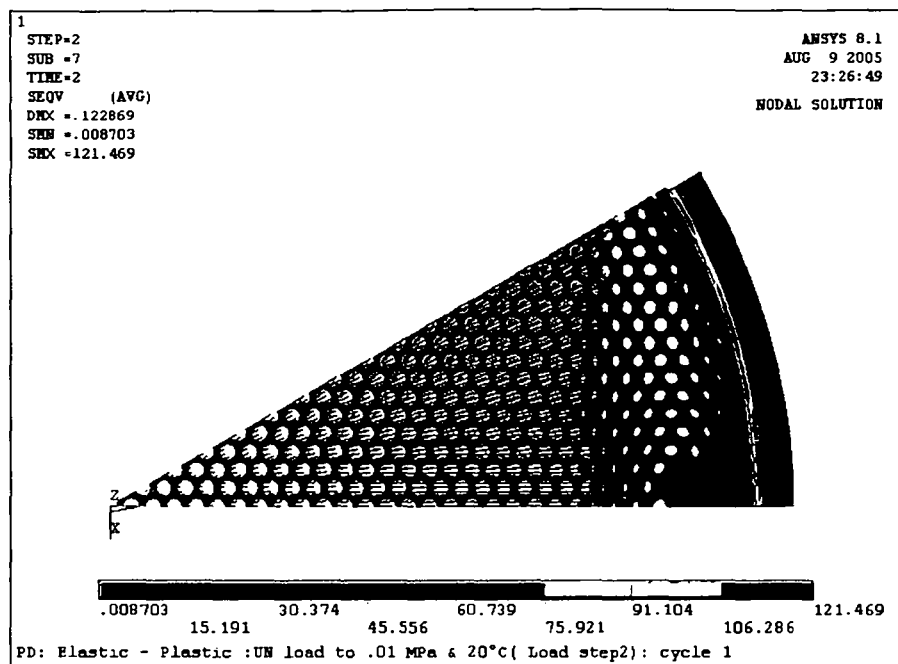


Fig.(6.B.3): Residual Mises' equivalent stress at 0.001 MPa pressure and temperature $T=20^{\circ}\text{C}$.

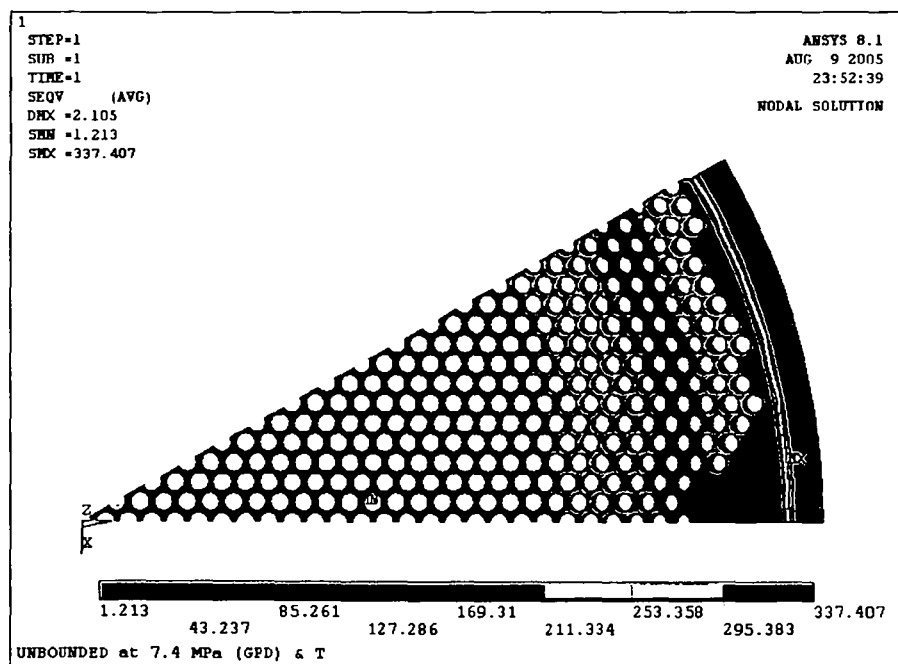


Fig.(6.B.4): Mises' equivalent stress field for linear- elastic constitutive law and limit pressure of 7.4 MPa on tube side and temperatures of 108°C on upper shell and 50°C on the lower shell. Tubesheet with calculated temperature distribution.

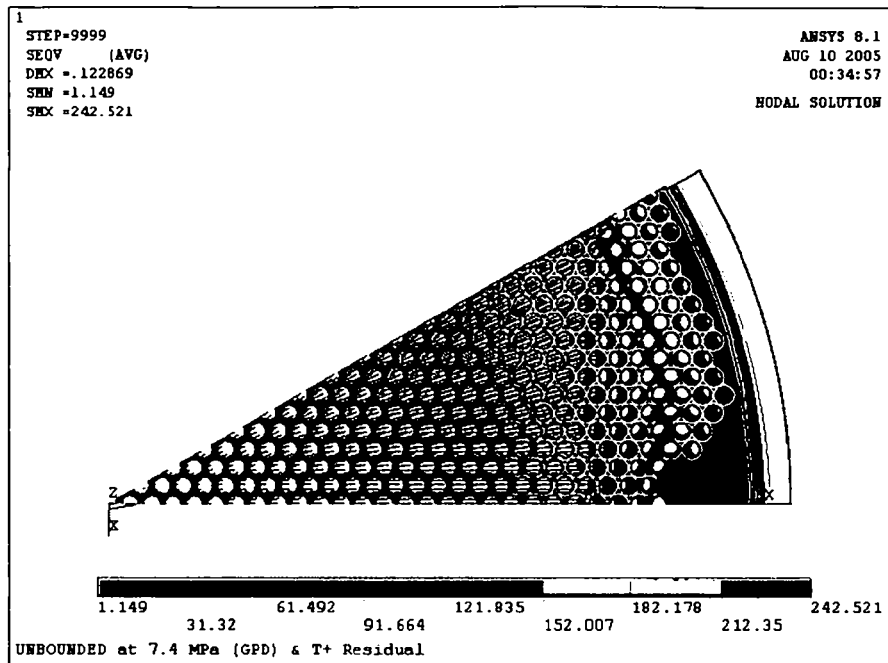


Fig.(6.B.5):Mises' equivalent stress of superposition of stress fields, linear-elastic and residual stress fields.

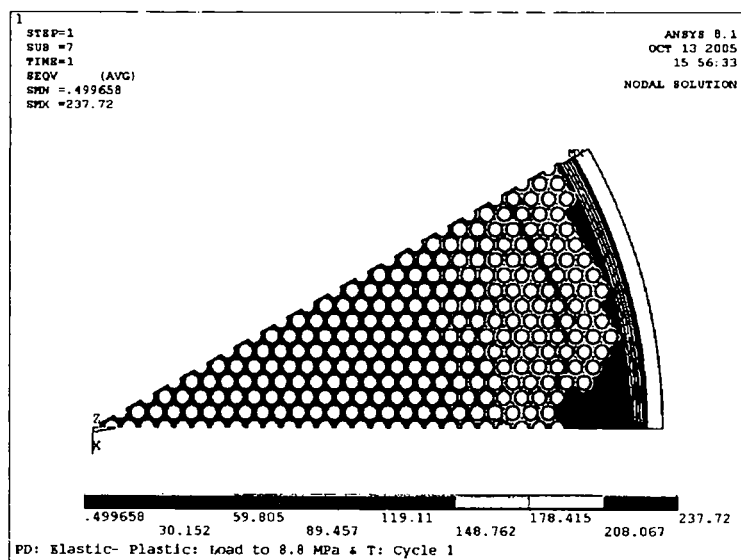


Fig (6.B.6): Mises' equivalent stress for elastic-plastic constitutive law at the limit pressure ad of 8.8 MPa and temperatures at surfaces of 108 °C on upper shell and 50 °C on lower shell. Tubesheet with calculated temperature distribution.

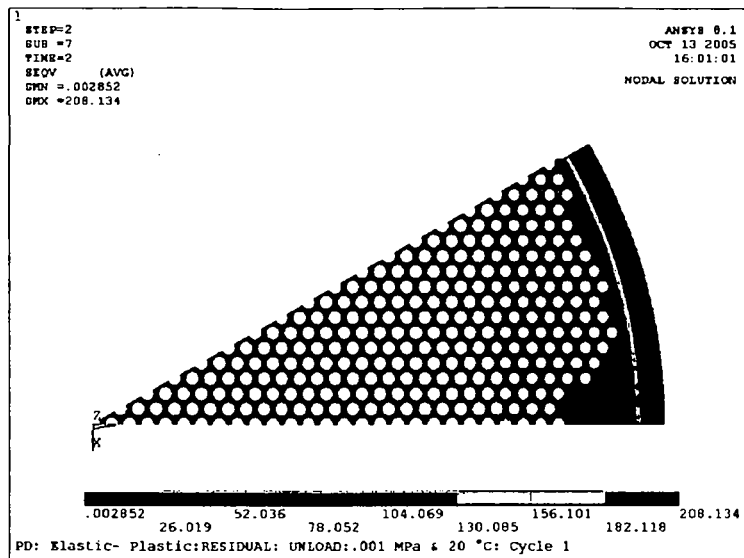


Fig.(6.B.7): Residual Mises' equivalent stress at 0.001 MPa pressure and temperature $T = 20\text{ }^{\circ}\text{C}$ after pressurization of 8.8 MPa.

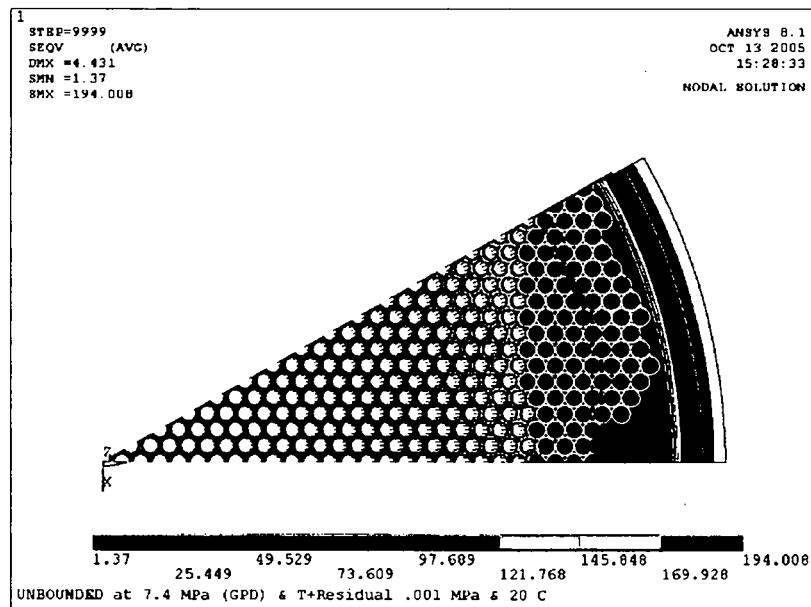
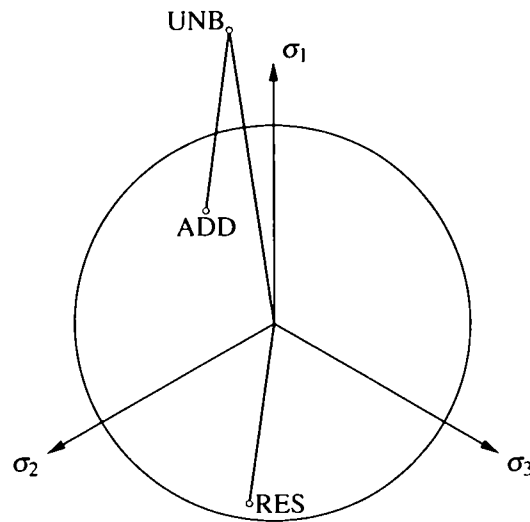


Fig.(6.B.8):Mises' equivalent stress of superposition of stress fields, linear-elastic and residual stress fields.

To plot the state of the stress for the above situation, usage of the deviatoric map is suggested in reference [28]. Figure (6.B.9) shows the plot of Mises equivalent stress as calculated in the figure(6.B.8) in the deviatoric map plane.



Figure(6.B.9): Deviatoric map $\sigma_1 = 260.86$ MPa, $\sigma_2 = 176.93$ MPa, $\sigma_3 = 88.138$ MPa.: $\sigma_{eq} = 149.61$ MPa

The plot is for node number 67921, which has the largest linear-elastic stress value, and the following principal stresses have been used:

Residual stress: $\sigma_1 = 31.02$, $\sigma_2 = -2.25$, $\sigma_3 = -191.75$, all in MPa

Stress for linear- elastic constitutive law and for pressure of 7.7 MPa at prescribed temperature: $\sigma_1 = 452.12$ MPa, $\sigma_2 = 147.11$ MPa , $\sigma_3 = 89.682$ MPa

For an additional check of the possibility of changes in the residual stress and strain fields, the model was run for 6 successive load and unload cycles, with loading and unloading conditions as given above. The result indicates that the small amount of the strain field created after the first unloading cycle will not change in the following cycles.

This further indicates that the structure will shake down to linear-elastic behavior, and there exists no change in the residual strain field. Figure (6.B.10) to (6.B.11) show the constant amount of residual plastic strain after six successive cycle with all load and unload cycles according to the above.

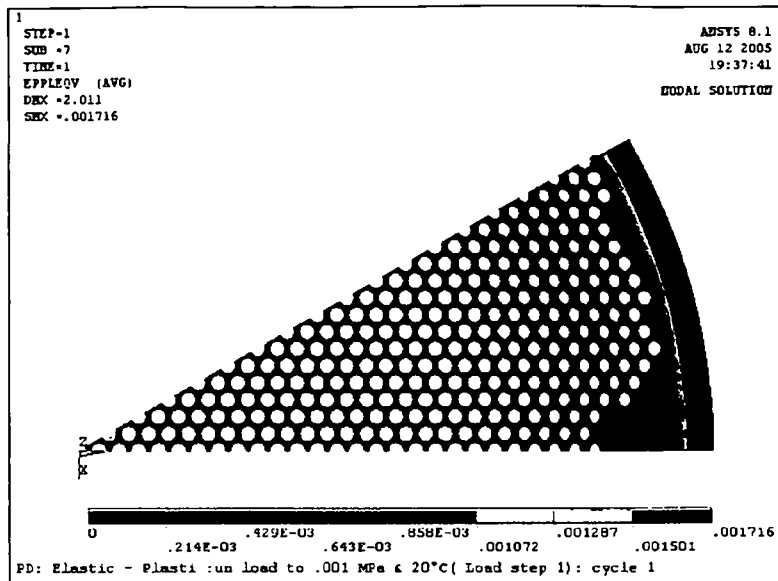


Figure (6.B.10): Residual plastic strain at the end of first cycle

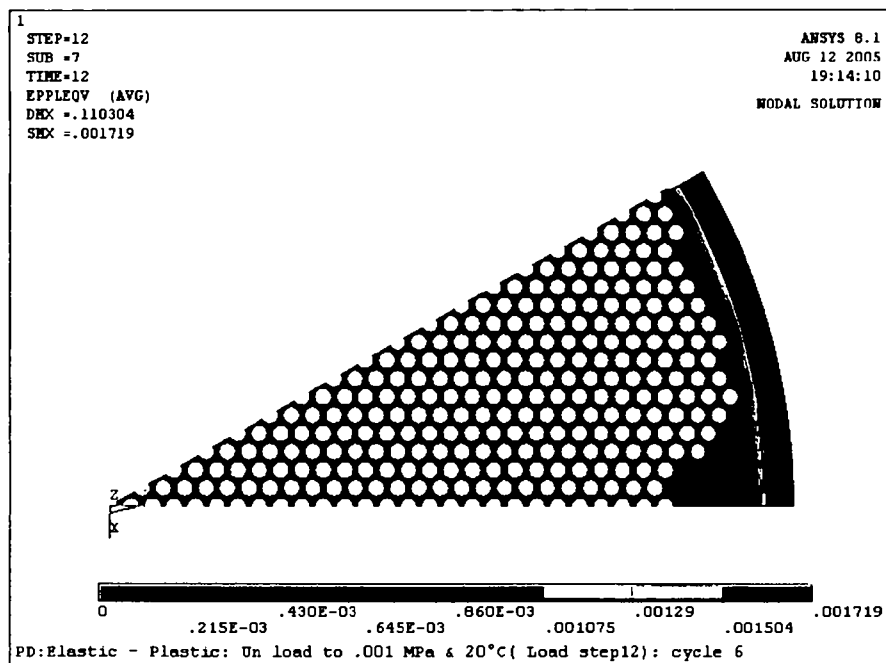


Figure (6.B.11): Residual plastic strain at the end of the sixth cycle

Based on the above results, it can be concluded that for action cycle from zero up to 7.4 MPa, the GPD- pressure and the considered temperature, the progressive plastic deformation design check is fulfilled.

6.B.4 Upper shell material according to original specification (SA 516 Gr. 70)

To investigate the model performance in the progressive deformation design check with upper shell material according to the data sheet original material (SA 516 Gr. 70) the relevant calculations have been performed. In these calculations the maximum value for pressure is 7.9 MPa, which is the last valid solution before applying safety factor, and the GPD- pressure is 6.61 MPa.

The maximum values for the mean temperatures are design temperatures of 108 °C for shell side materials and 50 °C for materials in tube side.

Figures (6.B.12) to (6.B.15) show the result of these calculations.

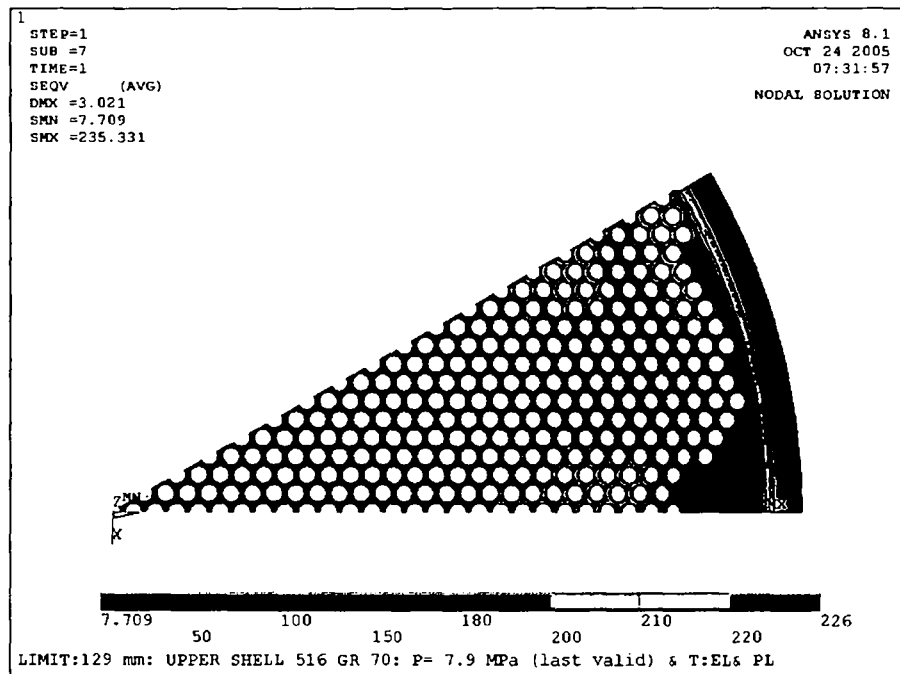


Fig (6.B.12): Mises' equivalent stress for elastic-plastic constitutive law at the limit pressure of 7.9 MPa and temperatures at surfaces of 108 °C on upper shell and 50 °C on lower shell. Tube sheet with calculated temperature distribution.

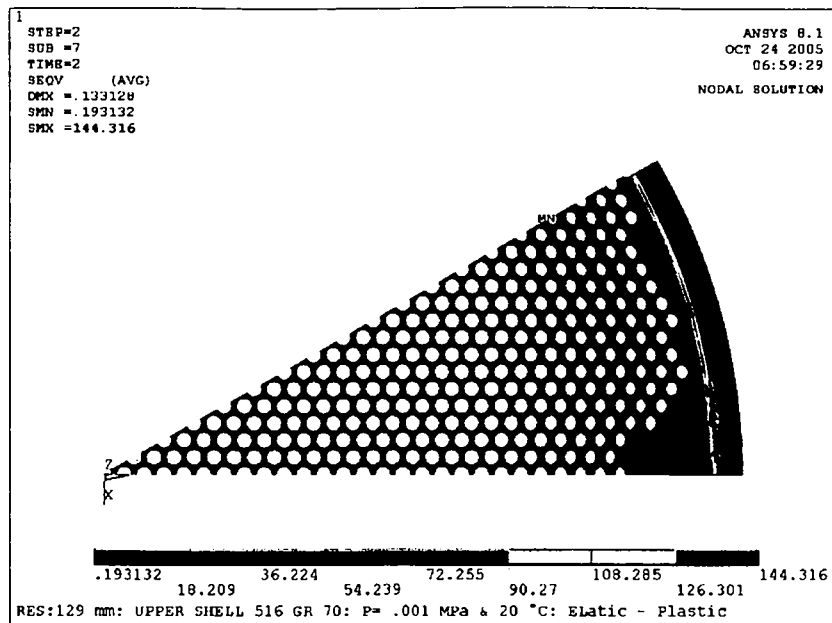


Fig.(6.B.13): Residual Mises' equivalent stress field at .001 MPa pressure and temperature $T=20\text{ }^{\circ}\text{C}$.

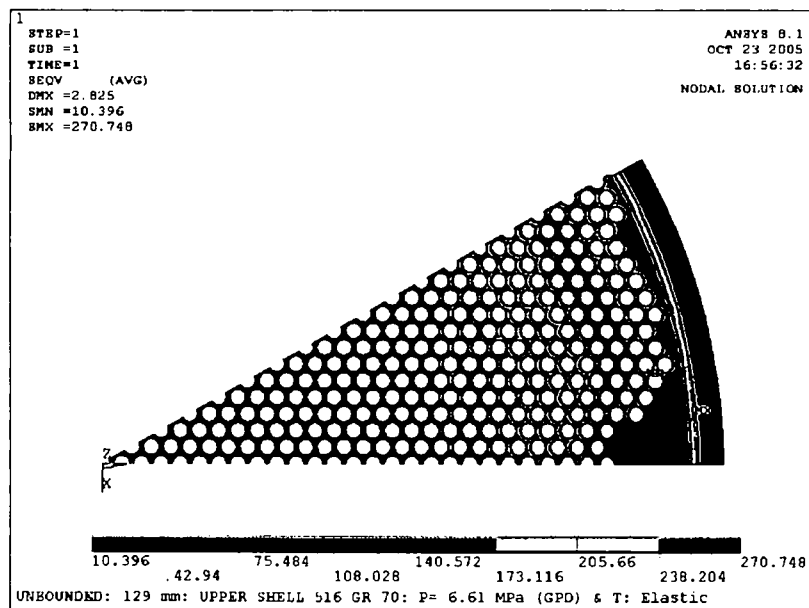


Fig.(6.B.14): Mises' equivalent stress field for the linear- elastic constitutive law and limit pressure of 6.61 MPa on tube side and surface temperatures of $108\text{ }^{\circ}\text{C}$ on upper shell and $50\text{ }^{\circ}\text{C}$ on the lower shell. Tubesheet with calculated temperature distribution.

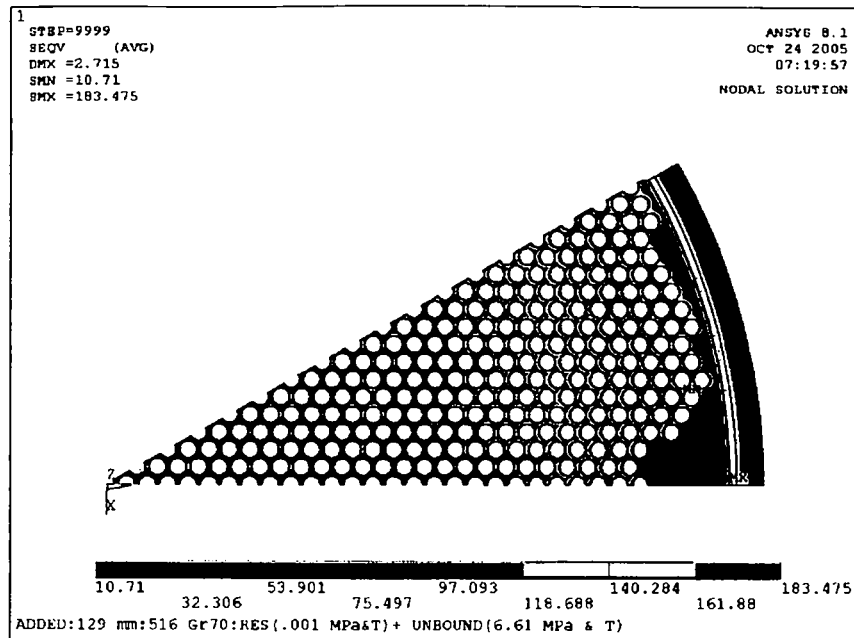


Fig.(6.B.15):Mises' equivalent stress of superposition of stress fields, the linear-elastic and the residual stress fields.

The figures show that in the residual stress field and the superposition stress field no value of Mises equivalent stress is larger than the yield stress, i.e. Melan's shakedown theorem is fulfilled, the structure will shakedown to linear-elastic behaviour under the investigated action cycle.

7. Discussion of the results

In reference to chapter five and six of this work, which use elastic and inelastic analyses of the reactor, the following conclusions and results apply:

- The results of the elastic analyses of the reactor, as shown in tables 5.1 and 5.4 for two load cases, indicate that the values of Mises' equivalent stress are reduced by the temperature effect. Comparison of these results with values given in table 3.3.1 indicates that the result of calculations according to design by formula also confirms such an effect of temperature.
- Incorporation of complete perforation on the tubesheet with real elastic constants brings much more realistic results to the analyses.
- It is not possible to categorize the type of stresses at the junction, where quite a complex situation exists. Any attempt in this regard gives an unrealistic base for any comparison. Such an attempt has been made in the past, and has resulted in unrealistic conclusions [15].
- Categorization of the stresses away from the junction can be performed but this brings no improvement to the work.
- To produce the optimum design with realistic bases for comparisons, the investigations in chapter six of this work have been performed. According to the results given there, this reactor can withstand safely much larger pressure as given in the data sheet.
- Temperature and cyclic loading provides no specific problem, and the reactor is safe with regard to progressive plastic deformation.
- Fatigue analyses of this work indicated that the reactor is safe with regard to anticipated load cycles. It should be also noted that the circumferential weld between tubesheet and shell is the critical region with regard to cyclic fatigue.
- The material selection for the upper shell is not optimal since with stronger material the high stress region will shift to the tubesheet. The analyses indicate that this tubesheet is thick enough to withstand such a shift to the high stress region.
- It also can be stated that the classical plate and shell theory approach, which is specified in the design by formula approach, is incapable of determining the stress in regions at or near the junction, with strong non-linearities along evaluation lines and large shear stresses, whereas design by analysis, as indicated, provides detail information for these parts. Therefore, the results obtained by such analysis, which was the practice in the past is not optimal. The Direct Route with FEM calculations render much improved results and insight into the behaviour.

8. Groove radii effect

In fixed tubesheet exchangers grooves are normally placed at the junction of the tubesheet to the adjoining shells for two main objectives. One objective is from a computational point of view and the other one is from structural point a view. By introducing grooves one can bypass the singularities, which will be created at the intersection point. In this way the transition from one geometry to the other one (tubesheet to shell) will be smooth and sharp corners will be avoided, sharp corners produces high stresses, possibly even singularities, and more realistic stresses can be captured by modelling the radii.

The other objective of grooves is to reduce the high surface stresses; by the introduction of grooves, the allowable number of cycle loads will be increased at the weld toe and at the base materials.

To investigate the effect of various groove radii on the principal and equivalent stresses, different radii sizes were incorporated in the model. All calculations have been performed for the same pressure and temperature loadings on the models with different radii.

The pressure was selected to be 6.6 MPa, which is the GPD- limit pressure, and the temperature was taken from tabulated values in the process data sheet(LC8). For detail in limit load and metal temperatures see section 6 and 2 of this work.

Investigation of the computed values of relevant stresses at nodes at the top and bottom of the grooves resulted in two conclusions:

(1) Top of the grooves

In this welded region, principal stresses are the relevant ones. At 5 mm radii size this point has very large principal stress values and these large values do decrease to smaller ones by increasing the radii. For radii of 21 to 27 mm the stresses drop considerably from the previous high values and the changes are in these radii region small. For larger radii the stresses continue to decrease.

(2) At the bottom of the grooves

In this unwelded region equivalent stresses are the relevant ones. Equivalent stresses are approximately the same up to radii of 24 mm, and they increase for increasing radii due to the decrease in tubesheet thickness under this point.

Figure (8.1.A.1) shows the node locations and table (8.1.A.1) is extracted from program outputs and shows the relevant stress values. Figures (8.1.B.1 to 8.1.B.2) show quite clearly how the stresses change for change in radii.

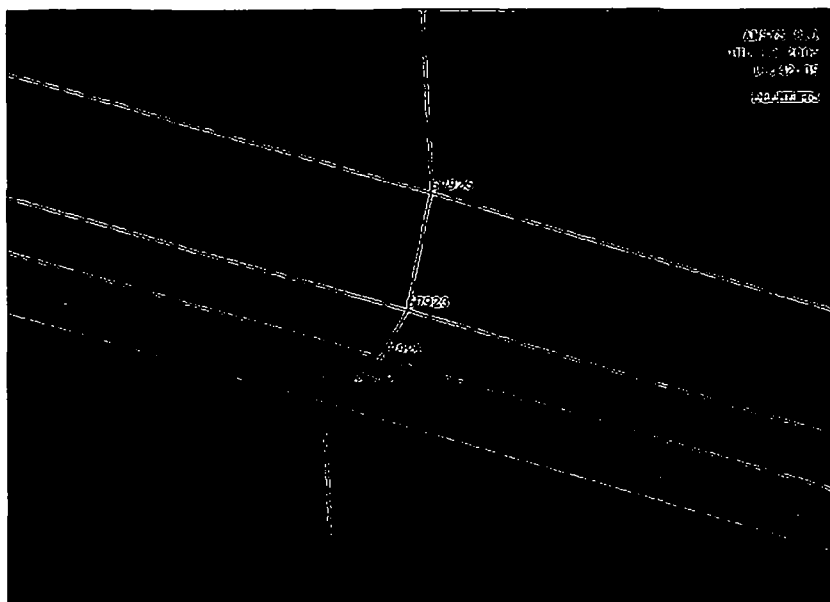


Figure (8.1.A.1): Location of nodes 67919 and 67925 locations.

Table (8.1.A.1): Stresses (MPa) for various radii (mm), nodes 67919, 67925

Diameter	node number	σ_1	σ_2	σ_3	σ_{equ}
8	67919	358.17	107.04	57.3	279.31
	67925	447.67	133.28	92.26	336.75
15	67919	328.7	76.37	36.2	274.66
	67925	421.37	122.07	94.18	314.17
18	67919	331.4	83.99	54.17	263.55
	67925	416.38	120.92	97.02	308.1
24	67919	332.5	79.63	54.8	266.14
	67925	399.19	112.68	93.48	297.3
27	67919	334.8	78.4	54.1	269.4
	67925	394.8	109.55	90.159	295.46
30	67919	334.74	77.15	52.78	270.6
	67925	381.77	104.37	85.133	287.5

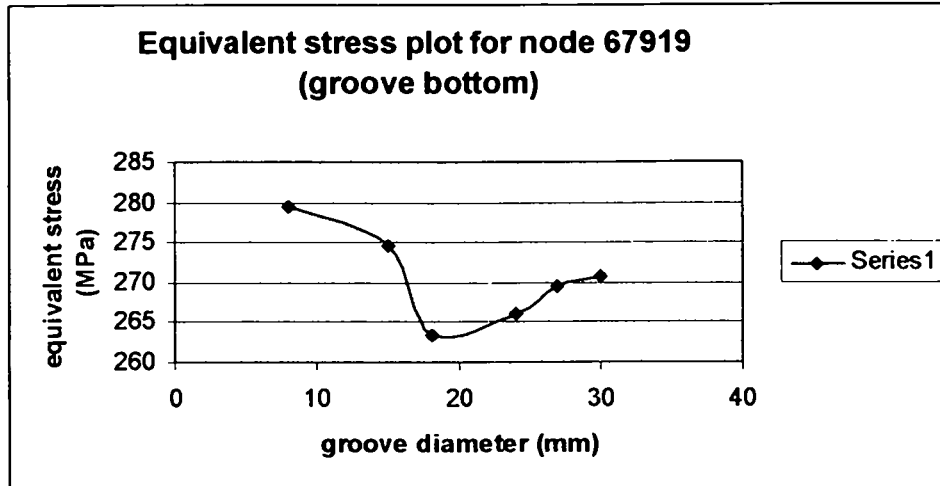


Figure (8.1.B.1): Equivalent Stress Plot for grooves of various size

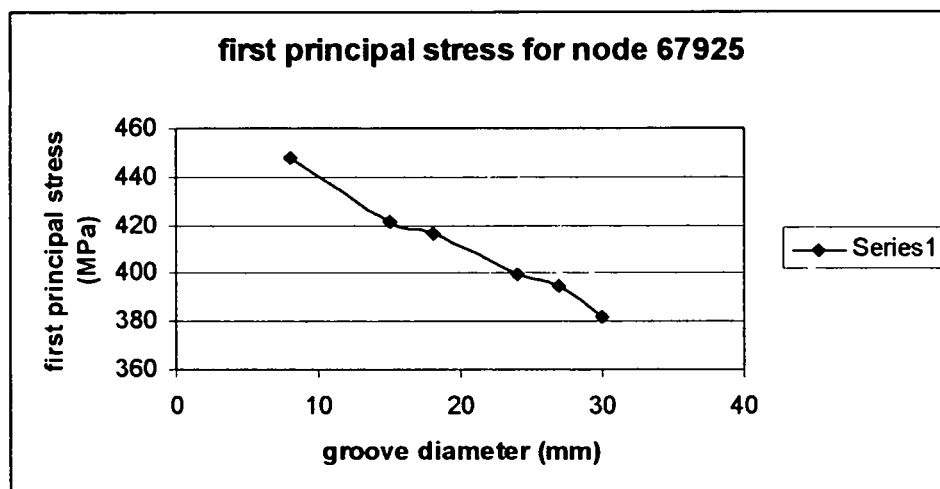


Figure (8.1.B.2) First principal stress plot for grooves of various size

Reviewing above results one can conclude that in this heat exchanger thermal stresses reduce the stressess, load case with out thermal stresses are governing.

9. Reduced shell thickness

One important result that has been noted in the preceding sections is the value of the pressure that the tubesheet can carry safely. It has been shown that with 129 mm (corroded) thickness a pressure of as high as 6.6 MPa is permissible. This thickness is the datasheet stated tubesheet thickness, obtained by FEA elastic analysis with the method specified in ASME Section VIII, Div. 2, Appendix 4, which uses the stress categorization technique.

With employing the direct route in design by analysis a reduction of this thickness seems to be permissible. The tables and figures given below depict results of calculations for a tubesheet thickness of 100 mm and the usage of the Direct Route of Design by Analysis approach. The shell thickness at the junction has also been reduced to the uniform value of 60 mm down from the data sheet values of 90 and 70 mm.

A. Elastic analysis

Tables (9.1) and (9.2) give the Mises' equivalent stress and displacement of 100 mm tubesheet thickness for two load cases.

Load case 1(in section 5 this is load case 4) is for the normal operating case given by 3 MPa in tubes and on channel side of the tubesheet; 4 MPa in the upper shell, and 1 MPa on the lower shell. All parts are considered with temperature distribution according to the data sheet.

The second load case (pressure only), in section 5 this is load case 1), covers the case with no pressure on the shell side, 4 MPa in the tubes and on the channel side of the tubesheet and on the upper shell, and no pressure on the lower shell and the whole structure at ambient temperature.

Tables (9.1) and (9.2) give displacements and Mises's equivalent stresses calculated for above load cases.

Table (9.1): Result of FEA – pressure and temperature (load case 1)

[^]	tubesheet	tubes	upper Shell	lower shell
Displacement (mm)	2.366	2.365	4.465	2.077
Mises' equivalent stress (MPa)	182.33	91.63	149.8	90.8

Table (9.2): Result of FEA –pressure only (load case 2)

[^]	tubesheet	tubes	upper shell	lower shell
Displacement (mm)	.4956	2.698	1.581	.492
Mises' equivalent stress (MPa)	230.48	128.18	148.22	64.643

Comparing the results in above tables with the results of tables (5.1) and (5.4), it is evident that stresses rise due to lower tubesheet thickness. Whether or not the design is admissible is investigated in the section following this one.

For a complete comparison of these results with results given in other part of this report see section 10: Discussion of results.

B. Inelastic analysis

In this analysis, with the exception of tubesheet and shell thickness, all parameters are the same as given in chapter 7.

- **Upper shell material SA 516 Gr. 70, tubesheet thickness 100 mm, upper and lower shell thickness 60 mm**

With this material due to its low strength value the critical section will be at the upper end of the upper shell. At 6.0 MPa the program crashes, indicating no solution for this pressure. The last valid solution is at load step 0.895, which corresponds to a pressure of 5.37 MPa. Application of the partial safety factor of 1.2 gives an allowable pressure of 4.475 MPa

$$P_{\text{critical}} = 4.45 \text{ MPa}$$

This pressure is still larger than 4.0 MPa, the values of the data sheet. Under 4.475 MPa, although tubesheet stresses are reasonably below yield point, the upper shell still is undergoing yielding through a considerable portion of the thickness. This is shown in figures (9.3) and (9.4).

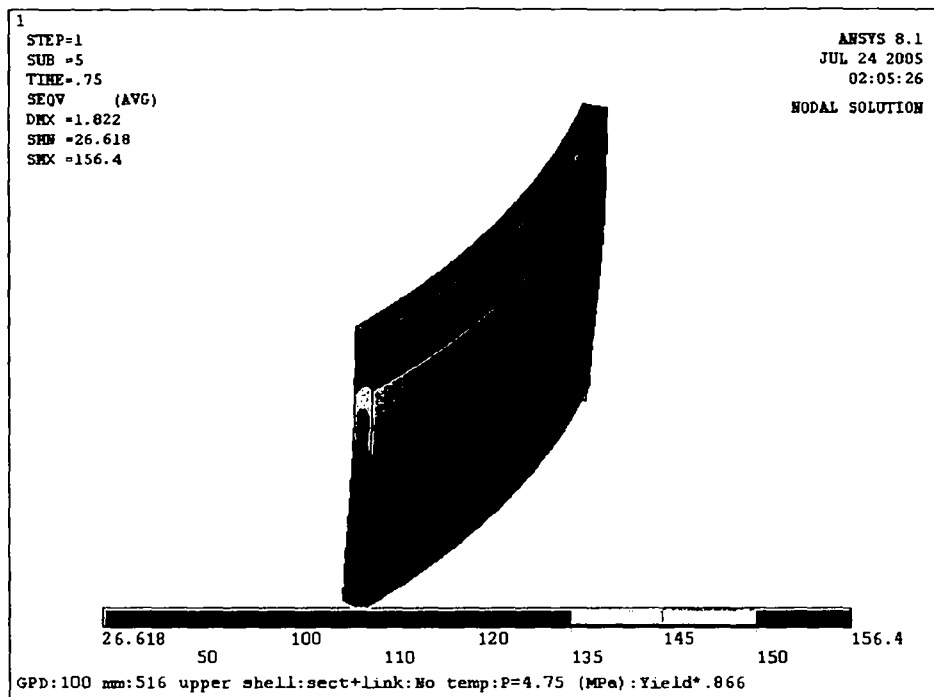


Figure (9.3): Mises' equivalent stress at upper shell (MPa)

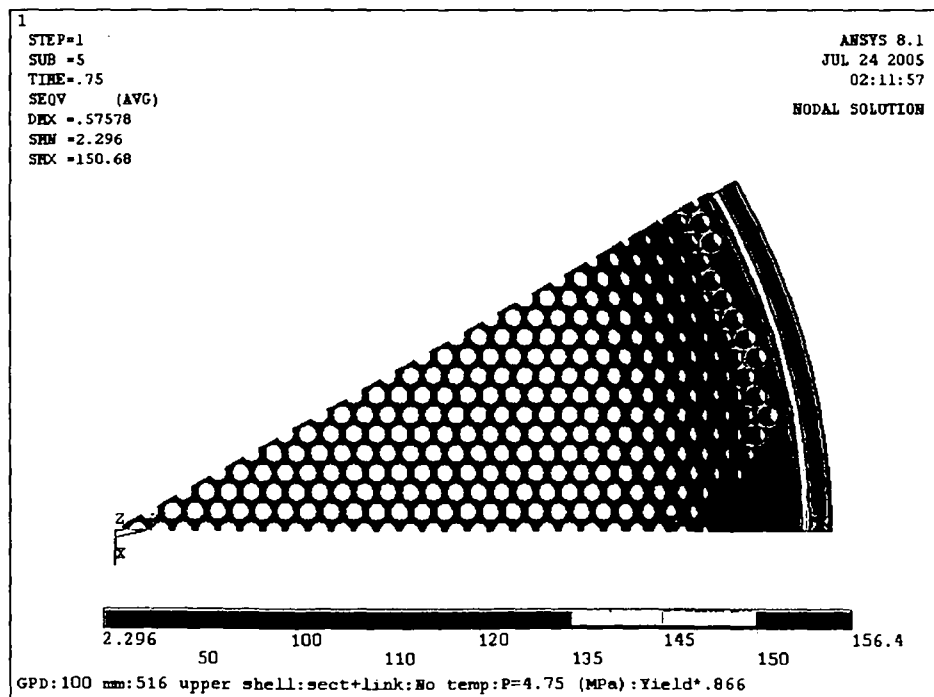


Figure (9.4): Mises's equivalent stress at tubesheet (MPa)

To reduce the stresses at the upper shell without changing the material or increasing the 60 mm shell thickness, the amount of stress and strain at a pressure of 4.0 MPa, which is the same as the one given on the data sheet, is given in figures (9.5 to 9.8) below.

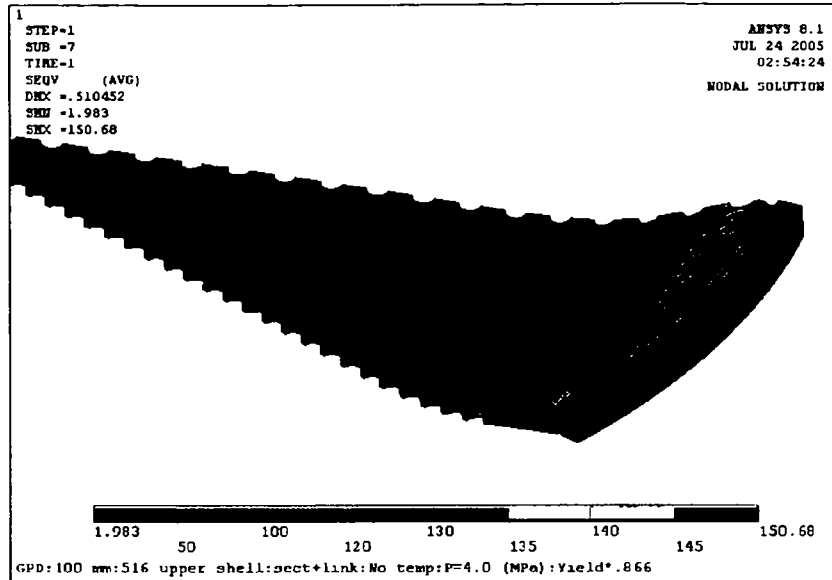


Figure (9.5): Mises' equivalent stress at tubesheet (MPa)

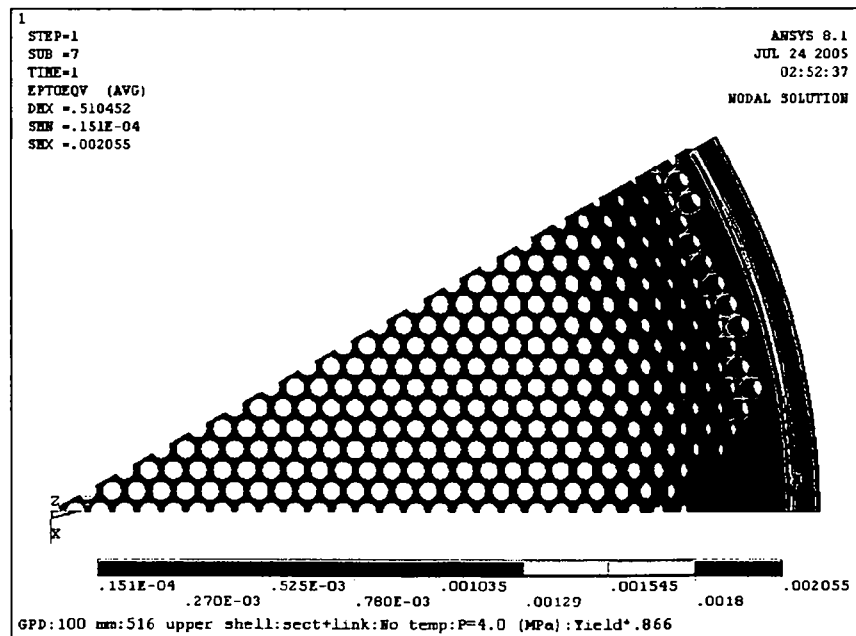


Figure (9.6): Mises' equivalent strain at tubesheet.

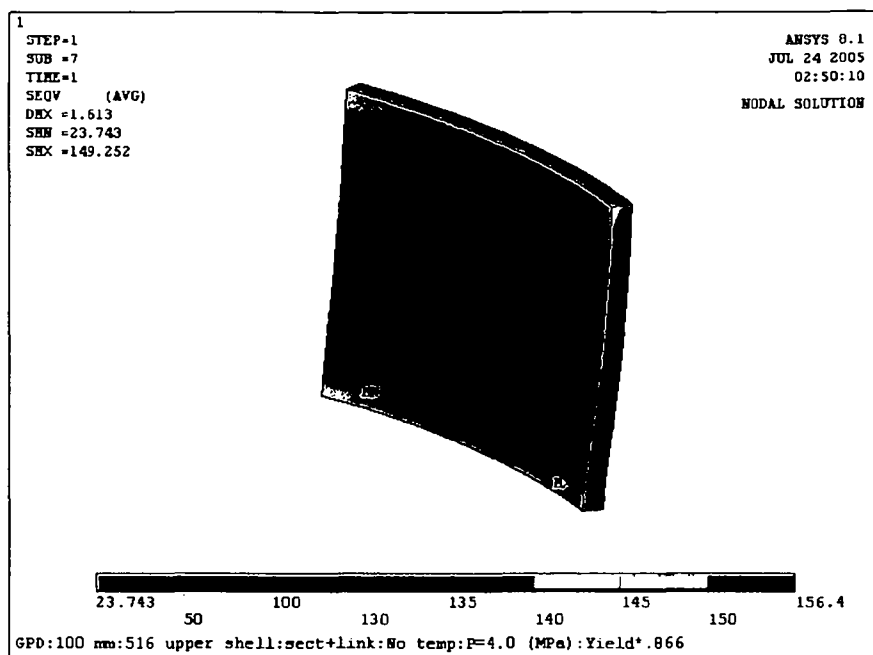


Figure (9.7): Mises' equivalent stress at upper shell (MPa).

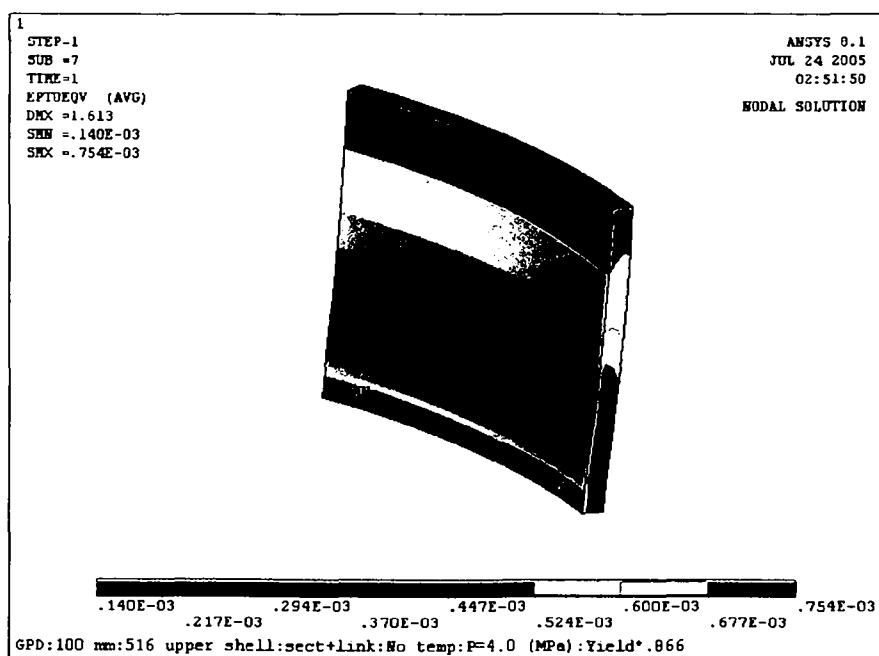


Figure (9.8): Mises' equivalent strain at upper shell.

The next step considered is the progressive deformation design check. Figures (9.8.A) to (9.8.D) show the result of this check for upper shell material with 516 Gr 70 material. According to this check the model shakes down to full elastic behaviour under 4.45 MPa pressure.

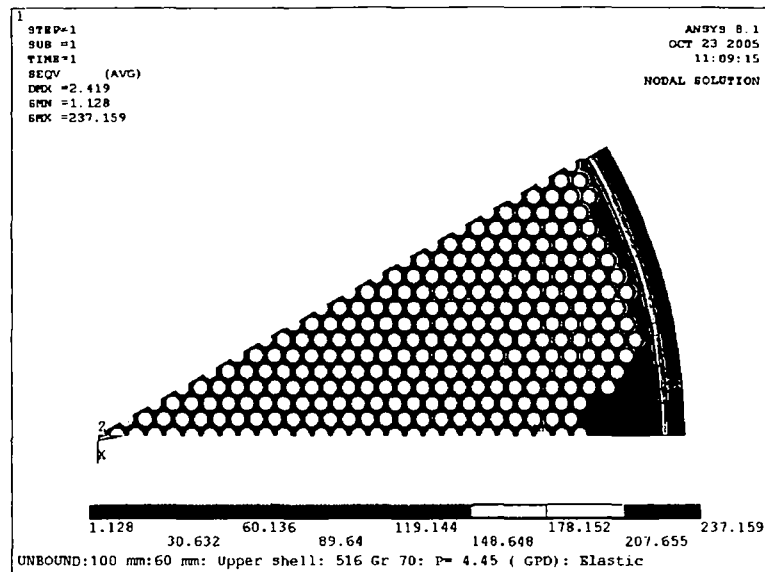


Fig.(9.8.A): Mises' equivalent stress field for linear- elastic constitutive law and limit pressure of 4.45 MPa on tube side and temperatures of 108 °C on upper shell and 50 °C on the lower shell. Tubesheet with calculated temperature distribution.

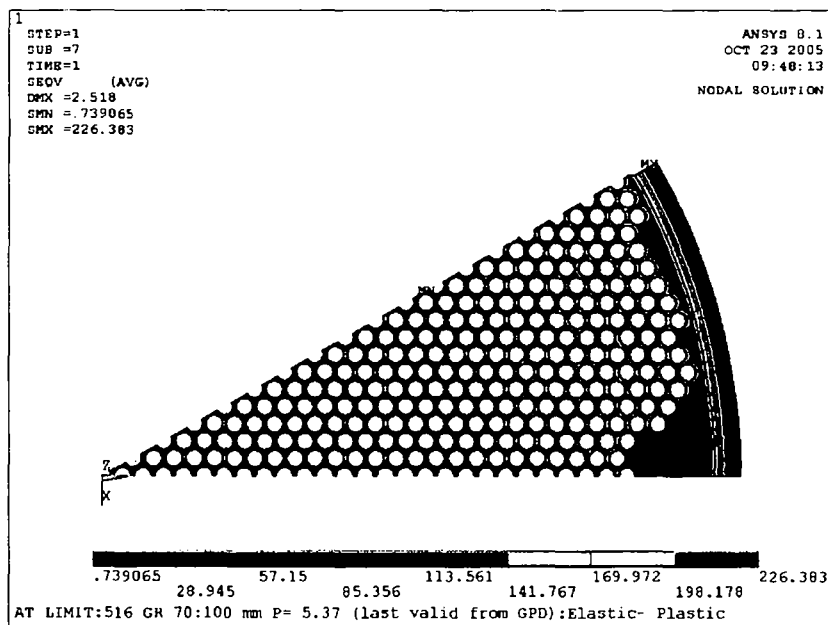


Fig (9.8.B): Mises' equivalent stress for elastic-plastic constitutive law at the limit pressure ad of 4.45 MPa and temperatures boundary of 108 °C on upper shell and 50 °C on lower shell. Tubesheet with calculated temperature distribution.

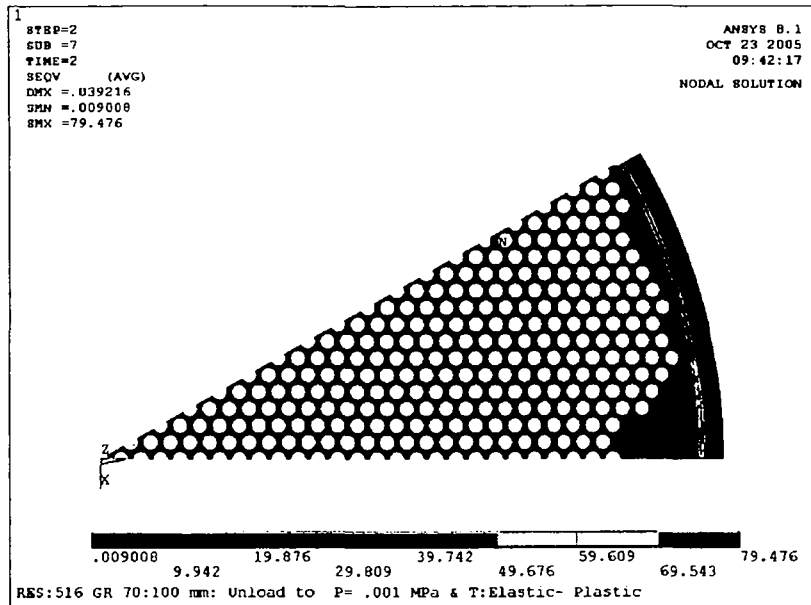


Fig.(9.8.C): Residual Mises' equivalent stress field at 0.001 MPa pressure and temperature $T=20^{\circ}\text{C}$ after pressure loading of 5.37 MPa.

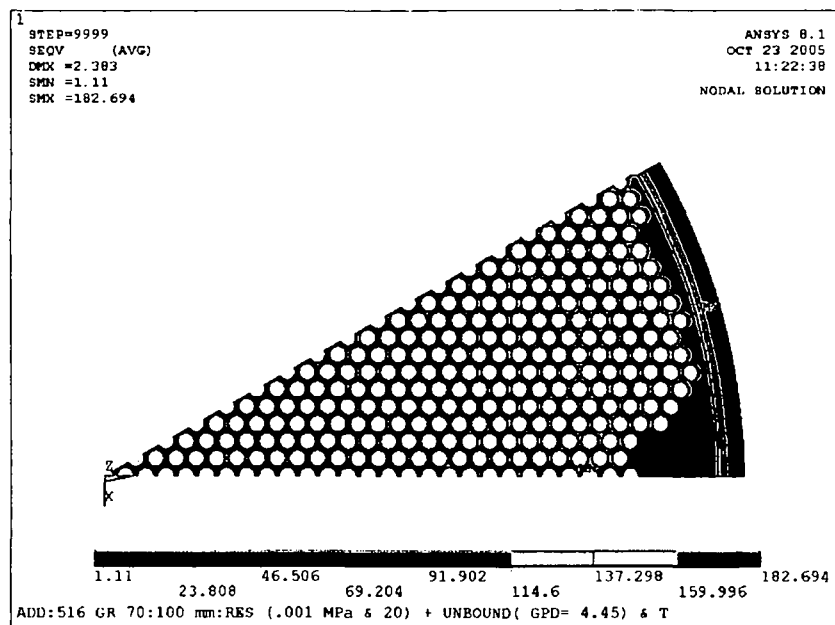


Fig.(9.8.D):Mises' equivalent stress of superposition of stress fields, linear-elastic and residual stress fields.

- Upper shell material SA-537 Cl. 2 , tubesheet thickness 100 mm, upper and lower shell thickness 60 mm

In order to investigate the tubesheet performance for large pressures, with 100 mm thickness of the tubesheet, the upper shell material was changed to the stronger type SA 537 Cl.2. With this material for gross plastic deformation design check the program crashes at 9.03 MPa indicating no solution for this pressure.

The last valid solution occurs at load step 0.721, which, after applying the partial safety factor on action, results in a permissible pressure of 5.5 MPa.

$$P_{critical} = 5.42 \text{ MPa}$$

Figure (9.9 to 9.12) indicates the plot of Mises' equivalent stress and strain.

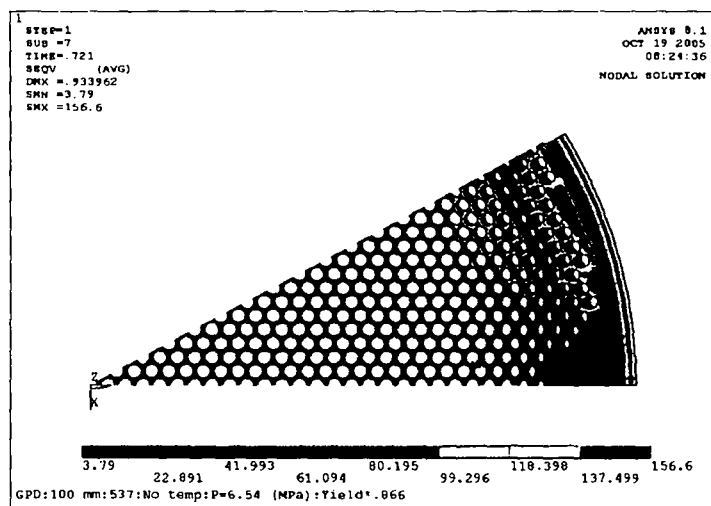


Figure (9.9): Mises' equivalent stress in tubesheet (MPa)

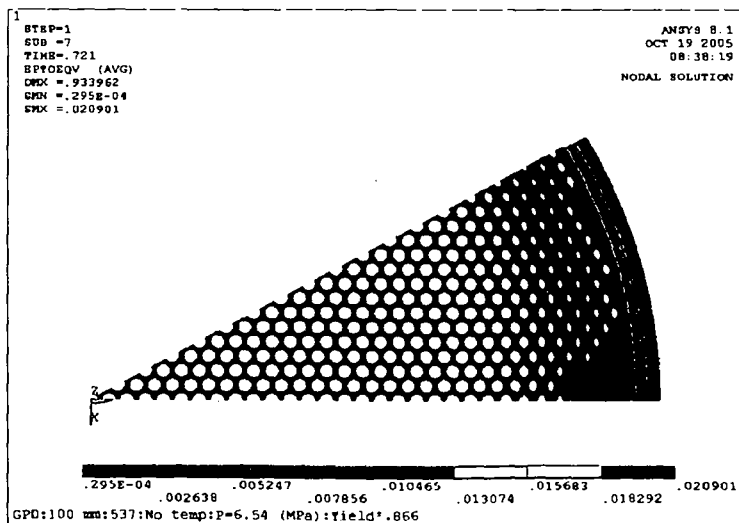


Figure (9.10): Mises' equivalent strain in tubesheet.

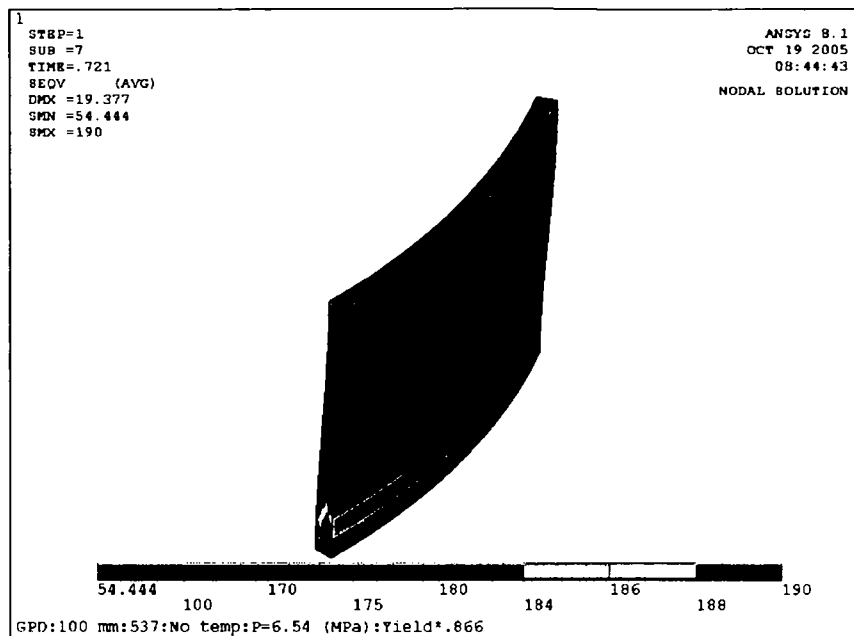


Figure (9.11): Mises' equivalent stress in upper shell (MPa)

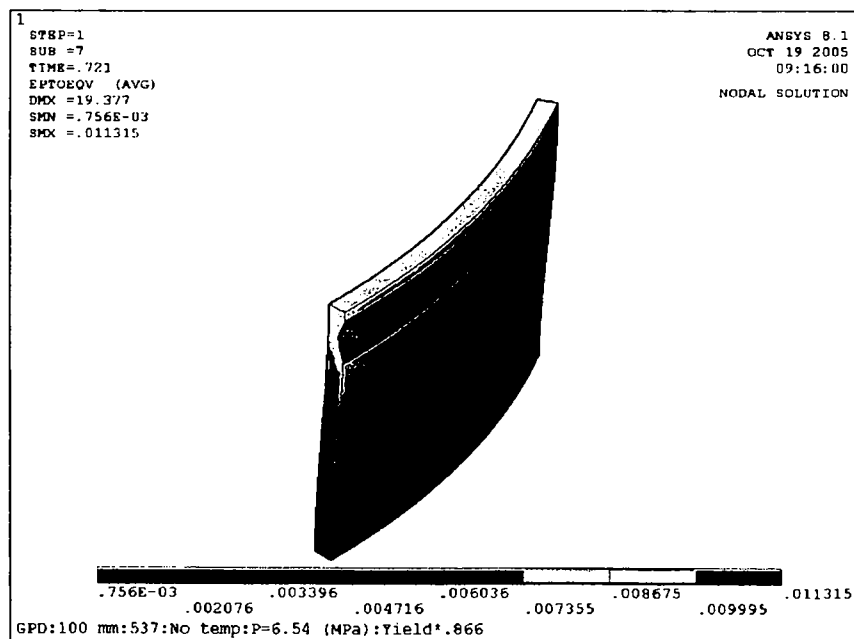


Figure (9.12): Mises' equivalent strain in upper shell.

Based on the above figures, it is evident that the tubesheet can withstand the pressure of 5.42 MPa with thickness of 100 mm provided that for the upper shell SA 537 Cl.2 material, which has higher yield strength is used. This pressure is larger than the data sheet pressure.

Furthermore, the case with a material possessing a higher yield strength value of 380 MPa has also been checked. With this yield strength, the program crashes at 9.0 MPa indicating no solution for this pressure. The last valid solution occurs at load step .98, which, after application of the partial safety factor on action, results in a permissible pressure of 7.3 MPa.

Figure (9.9A to 9.12A) show the plots of Mises' equivalent stress and strain.

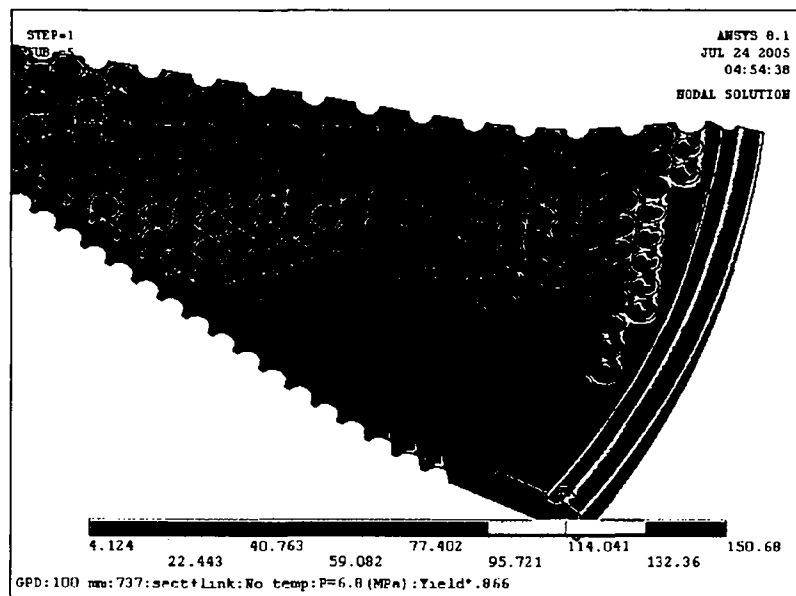


Figure (9.9A): Mises' equivalent stress at tubesheet (MPa)

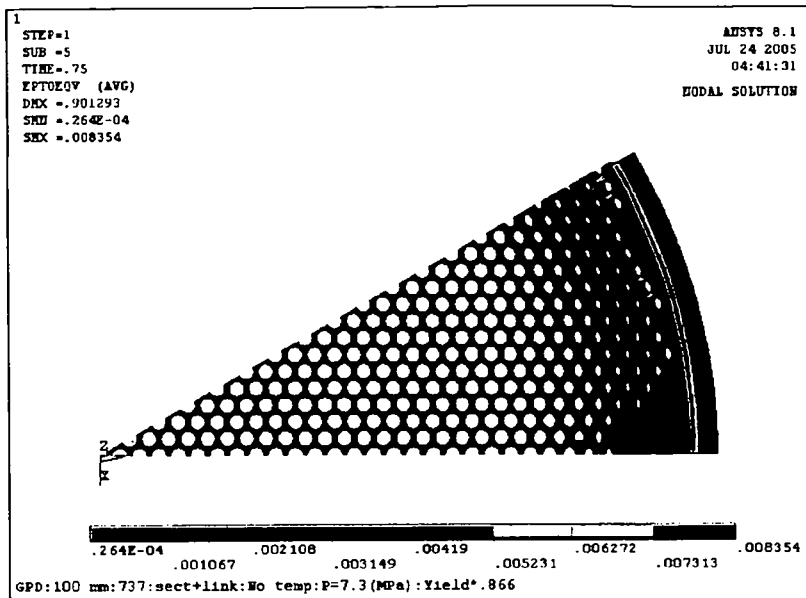


Figure (9.10A): Mises' equivalent strain at tubesheet.

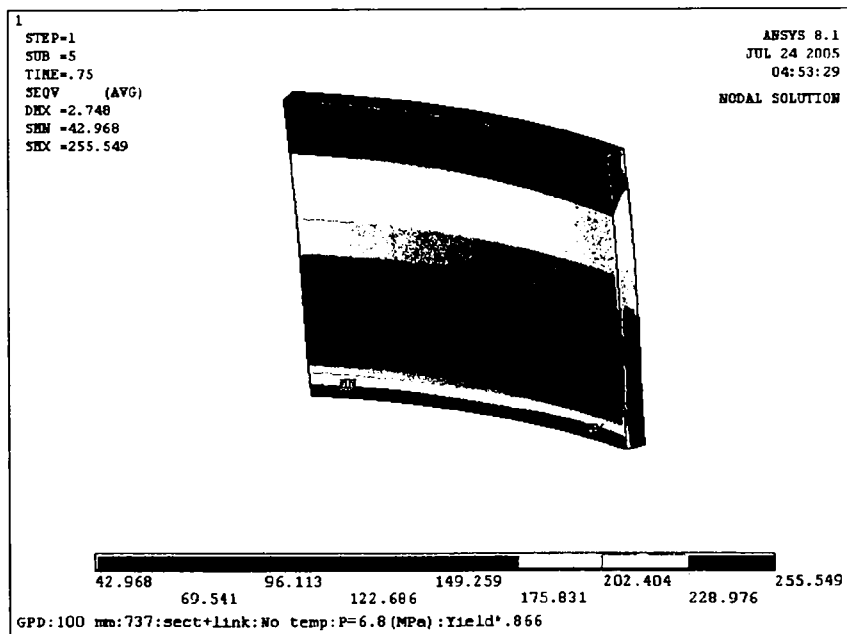


Figure (9.11A): Mises' equivalent stress at upper shell (MPa)

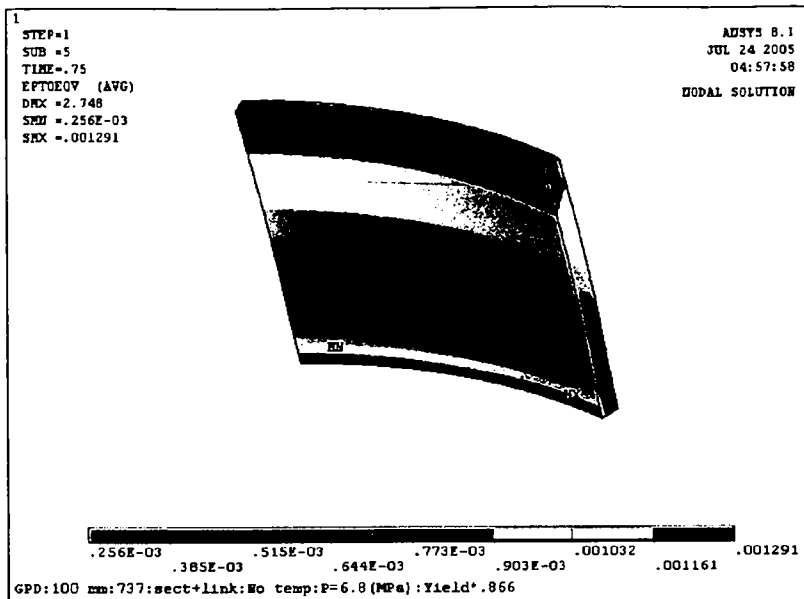


Figure (9.12A): Mises' equivalent strain at upper shell.

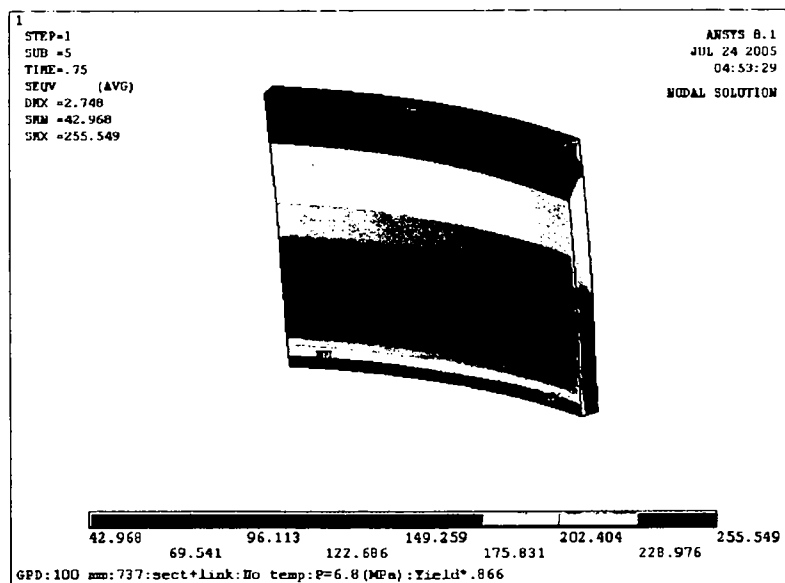


Figure (9.11): Mises's equivalent stress at upper shell (MPa)

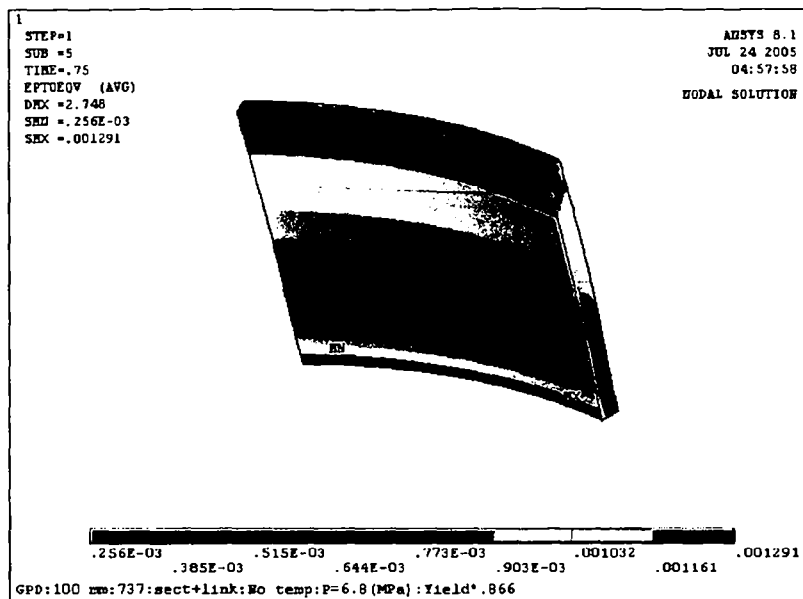


Figure (9.12): Mises' equivalent strain at upper shell.

Based on the results shown in above figures, it is evident that the tubesheet can withstand the pressure of 7.4 MPa with thickness of 100 mm, provided that upper shell material with the 380 MPa yield strength value is used. This pressure is larger than the data sheet pressure.

The next step is the progressive deformation design check. For both of the above material cases this check has been performed.

Figures (9.13) to (9.15) show the results of this check for the upper shell material SA 537 Cl2, and figures (9.13A) to (9.15A) show the result of this check for the material with 380 MPa yield strength value.

According to these checks, the model shakes down to fully elastic behaviour for pressure cycles from zero to 5.42 MPa for the SA 537 Cl.2 material, and upto 7.4 MPa for the material with 380 MPa yield strength value.

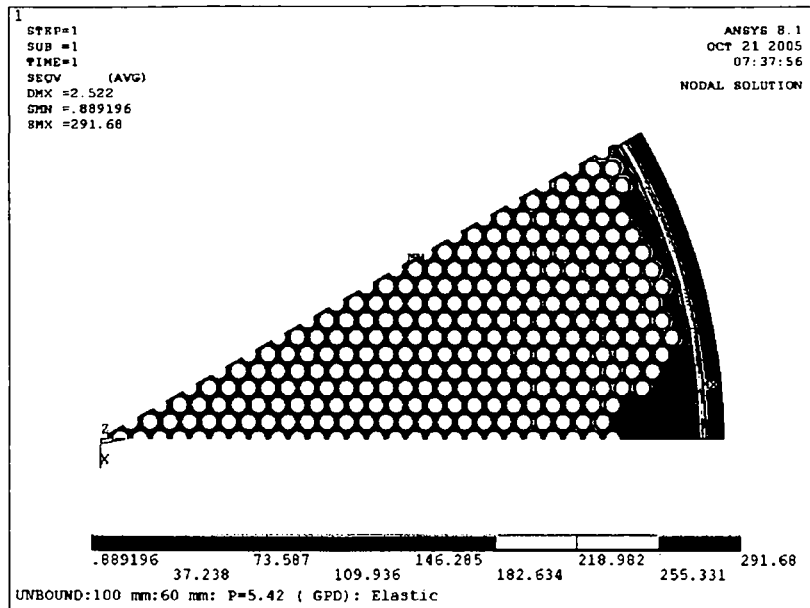


Fig. (9.13): Mises' equivalent stress (MPa) for the linear- elastic constitutive law and the limit pressure of 5.42 MPa on tube side and temperatures of 108 °C on upper shell and 50 °C on the lower shell. Tubesheet with the calculated temperature distribution

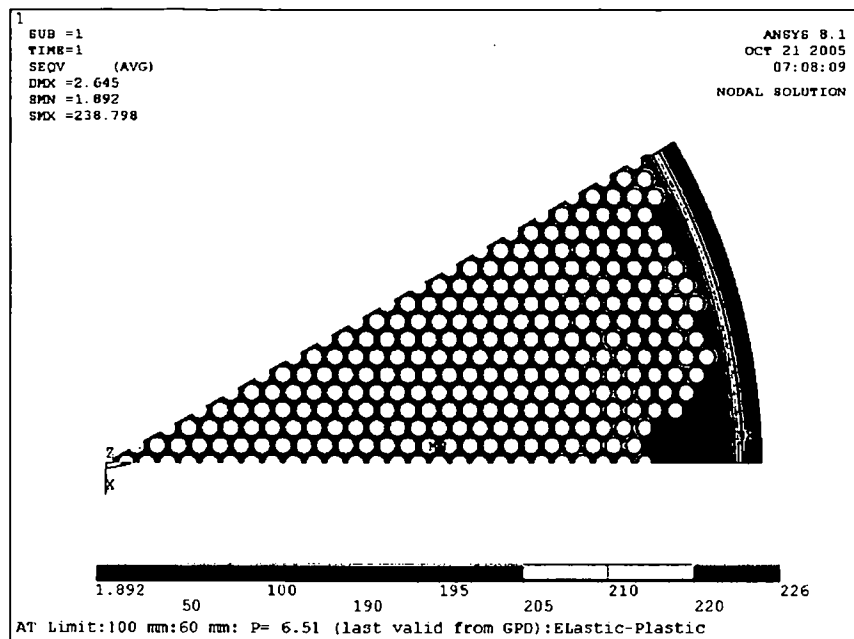


Fig. (9.14): Mises' equivalent stress(MPa) for the elastic-plastic constitutive law at the limit pressure of 5.42 MPa and temperatures boundary of 108 °C on upper shell and 50 °C on lower shell. Tubesheet with calculated temperature distribution.

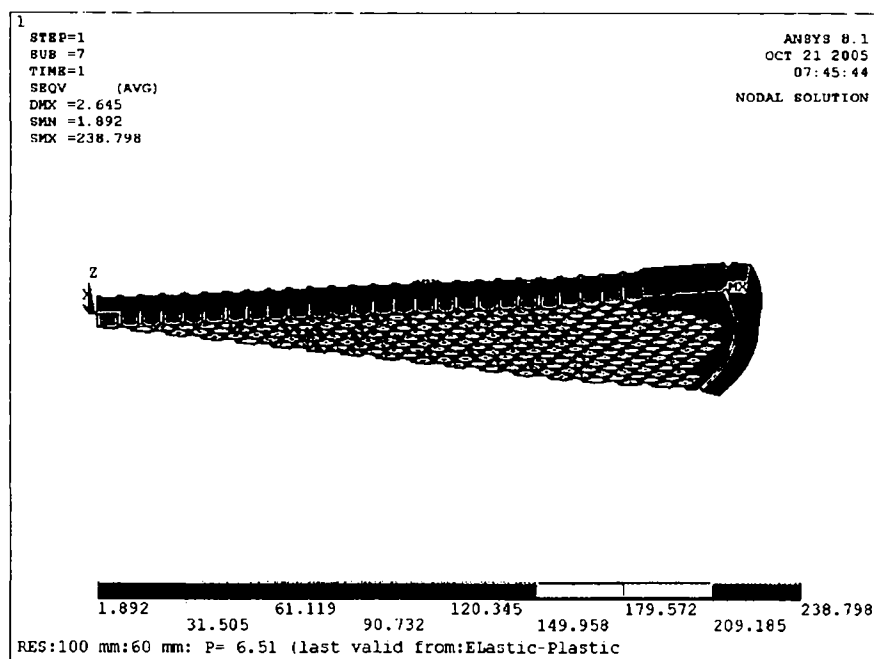


Fig. (9.14.1): Mises' equivalent stress (MPa) for the elastic-plastic constitutive law at the limit pressure of 5.42 MPa and temperatures of 108 °C on upper shell and 50 °C on lower shell. Tubesheet with the calculated temperature distribution.

It should be noted that, by comparing figures (9.14) and (9.14.1), it can be observed the plasticization has already occurred at the channel side of the tubesheet, which possesses a lower yield stress there due to the higher temperature in comparison to the shell side of the tubesheet which is at 50 °C and, therefore, has a higher yield stress value. The amount of stress at lower side is quite high and very close to the yield stress value at this location. See table (2.2.1.A) for material hot yield properties.

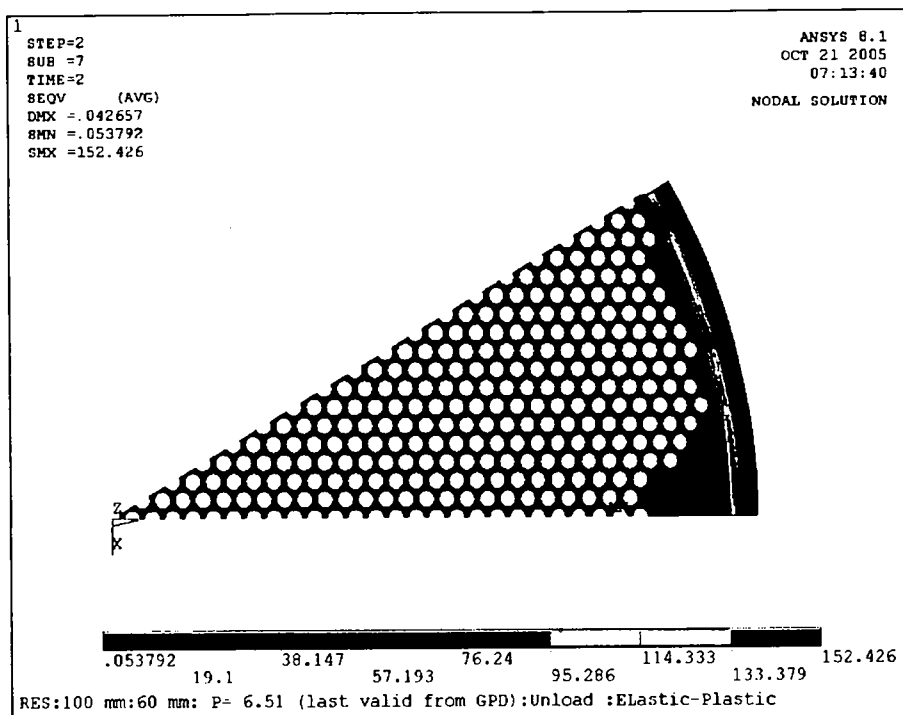


Fig. (9.15): Residual Mises' equivalent stress field at 0.001 MPa pressure and temperature $T= 20\text{ }^{\circ}\text{C}$ under pressure loading of 5.42 MPa.

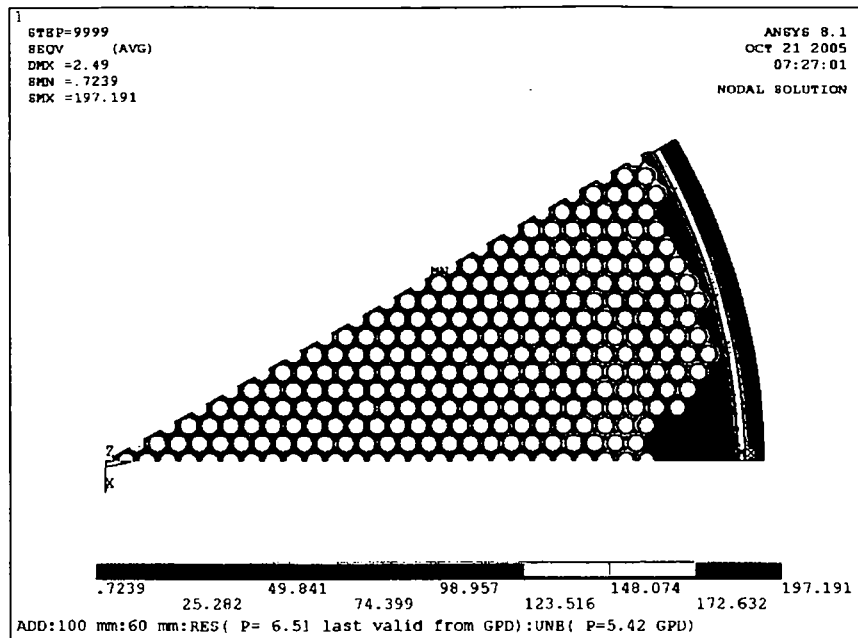


Fig (9.16):Mises' equivalent stress (MPa) of superposition of stress fields, linear-elastic and residual stress fields.

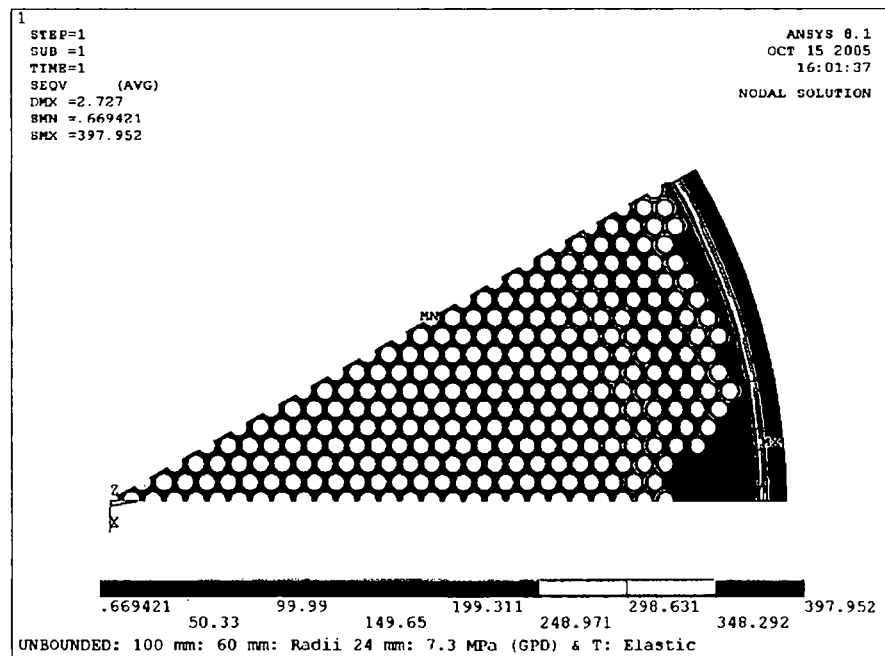


Fig (9.13A): Mises' equivalent stress (MPa) for linear- elastic constitutive law and limit pressure of 7.3 MPa on tube side and temperatures of 108 °C on upper shell and 50 °C on the lower shell. Tubesheet with the calculated temperature distribution.

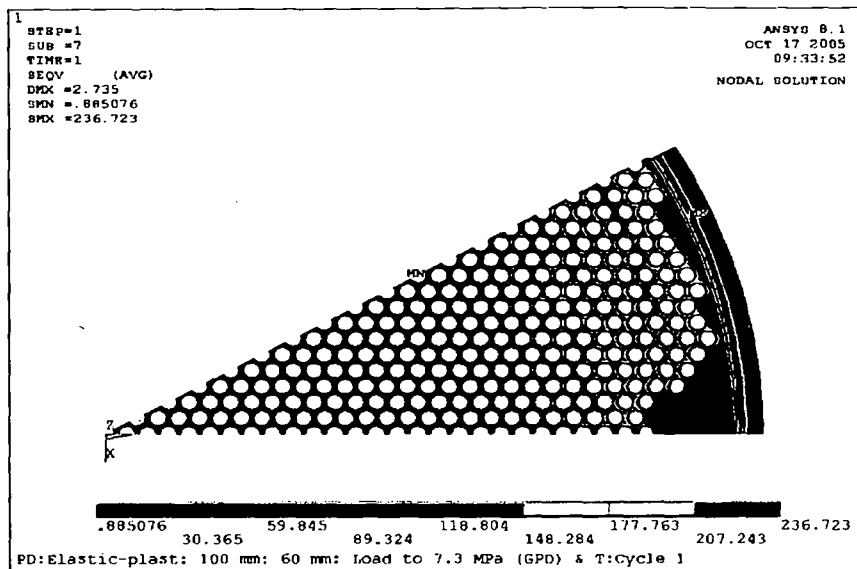


Fig. (9.14A): Mises' equivalent stress (MPa) for the elastic-plastic constitutive law at the limit pressure of 7.3 MPa and temperatures of 108 °C on upper shell and 50 °C on lower shell. Tubesheet with the calculated temperature distribution.

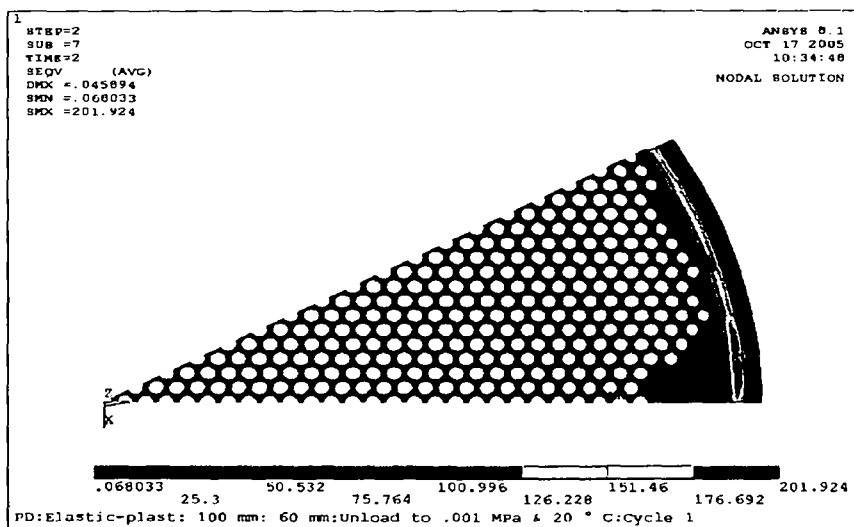


Fig.(9.15A): Residual Mises' equivalent stress (MPa) at 0.001 MPa pressure and temperature T= 20 °C under original loading of 7.3 MPa.

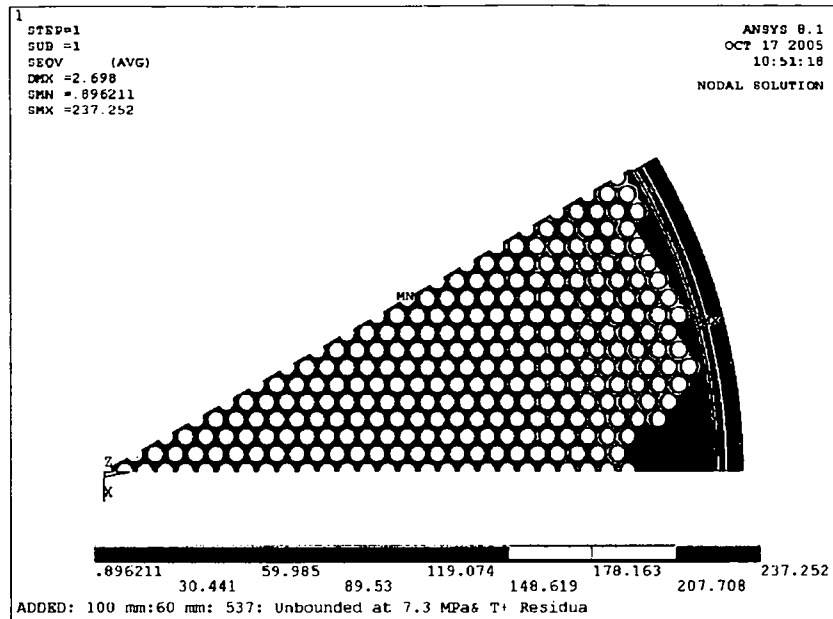


Fig. (9.16A): Mises' equivalent stress (MPa) of superposition of stress fields, linear-elastic and residual stress field.

To plot the stress states for the above situation, in [28] it is suggested to use the deviatoric map.

Figure (9.17) and (9.17A) shows the plot of Mises' equivalent stress, as calculated, in the deviatoric map plane.

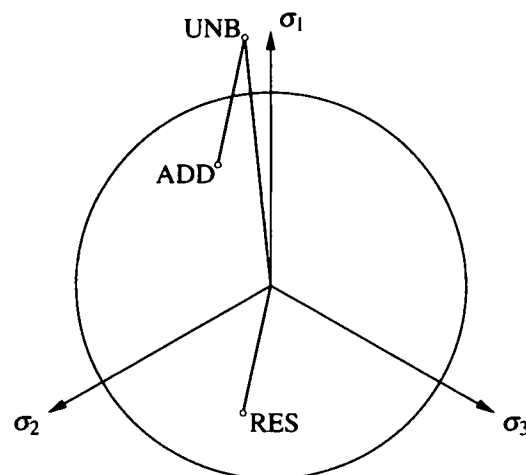


Figure (9.17.A): Deviatoric map $\sigma_1 = 246.5$ MPa, $\sigma_2 = 141$ MPa, $\sigma_3 = 69.3$ MPa:

$\sigma_{eq} = 154.3$ MPa: Upper shell 537 C12

The plot is for node number 67921, which has highest value for the linear- elastic model, and following principal stresses have been used:

Residual stress: $\sigma_1 = -128.6$ MPa, $\sigma_2 = 39.2$ MPa, $\sigma_3 = 1.19$ MPa

Stress for the linear- elastic constitutive law and for the pressure of 5.42 MPa at the prescribed temperature: $\sigma_1 = 375$ MPa, $\sigma_2 = 102.7$ MPa, $\sigma_3 = 67.3$ MPa

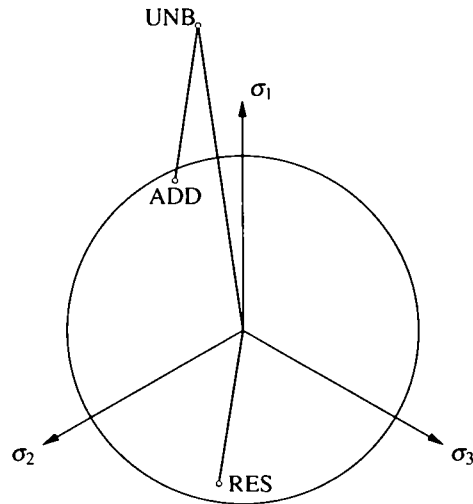


Fig.(9.17.A): Deviatoric map $\sigma_1 = 339.9$ MPa, $\sigma_2 = 195.4$ MPa, $\sigma_3 = 95.324$ MPa:
 $\sigma_{eq} = 212.97$ MPa: Upper shell yield strength 380 MPa

The plot is for node number 67921, which shows the largest value for the linear-elastic model, and the following principal stresses had been used:

Residual stress: $\sigma_1 = -180.54$ MPa, $\sigma_2 = 37.15$ MPa, $\sigma_3 = 0.62$ MPa

Stress for the linear- elastic constitutive law and for the pressure of 7.4 MPa at the prescribed temperature: $\sigma_1 = 520.41$ MPa, $\sigma_2 = 159.09$ MPa, $\sigma_3 = 93.88$ MPa

10. Discussion and comparison of the results

Based on various calculations performed for a variety of load cases, geometry variants, different approaches, the following results can be reported.

a. Code calculations

In reference to table (3.3.1), which is given below as table (10.1), the EN 13445 Clause 13 calculations in comparison with ASME Sec. VIII Div 1 code result in bending stresses that are identical in both codes, and that there are only slight differences in shear stresses.

In fact, since both codes are based on similar approaches (shell and plate theory with effective elastic constants), the close results have been anticipated to be obtained with similar material properties.

The basic difference between the results for these two codes as far as the comparison within the frame work of this study is concerned, results from differences in the values of the equivalent elastic constants. In the ASME code the elastic constants are out of range for this reactor with its specific geometry, whereas Clause 13 of EN 13445-3 provides comprehensive data in regard to these values.

ASME Sec VIII, Div 2, Article 4-900(c) and (b) indicate that the method contained in (4-9) does not account for the staying action from tubes, and recommends that the stiffening effect resulting from the staying action of the tubes should be obtained by an analysis and incorporated. It also suggests that such stiffening may either increase or decrease the stresses in the tubesheet itself and in the attached shells. For this reason this division was not considered.

With regard to results of calculation based on Annex J it should be noted that Annex J is not explicit with regard to the required length of thickened portion of the shell on the head side. Usage of the corresponding requirements for the shell side is obvious but not stated.

Comparing EN 13445-3 Annex J results with Clause 13 results indicate that Annex J gives larger values for the maximum allowable pressure. The values in Table (3.3.1) are not the optimal ones as far as the calculations per EN 13445-3 Annex J are concerned – based on a limit analysis approach, the large margin for bending stresses can be used, according to this Annex J approach, to increase the small margin for shear stresses, resulting in an increase in the maximum permissible pressure.

Table (10.1) Results of calculations according to codes (A)

	Load Cases	$\sigma_{b,max}$ (MPa)	τ_{max} (MPa)	τ_a (MPa)	$\sigma_{b,a}$ (MPa)	τ_{max} / τ_a	$\sigma_{b,max} / \sigma_{b,a}$	Notes
EN 13445-3 Clause 13	Pressure	266.64	63	116	290	0.44	0.92	(F)
	Press & Temp.	130.33	30.8	116	435	0.27	0.30	$f_{allow} = 3f$ (E)
Annex J	Pressure	-	-	-		0.88	0.51	(B) 0.39
ASME Sec. VIII Div I	Pressure	265.53	56	110	275.86	0.51	0.96	(C), (D)
	Press & Temp.	115	40.2	110	552	0.68	0.36	

Notes:

(A) $\sigma_{b,max}$ is maximum calculated bending stress (MPa).

τ_{max} is maximum calculated shear stress (MPa).

τ_a is allowable stress in shear (MPa).

$\sigma_{b,a}$ is allowable stress in bending (MPa).

(B) Uniform wall thickness is assumed. Annex J deals not with equivalent stress to allowable stress ratios, but with action to allowable action ratios. The method does not incorporate effect of thermal stresses, being a strict limit analysis approach. The 0.39 is the optimum value of $\sigma_{b,max} / \sigma_{b,a}$, optimal for the whole structure.

(C) Curve for E^*, ν^* are out of range also E^*, ν^* are not function of thickness.

(D) ASME Sec. VIII, Div 2 has not been considered since the staying action of tubes is not directly covered. Furthermore, curves for the equivalent elastic properties are out of limit.

(E) f is the allowable stress in tension see table (2.2.4).

(F) The allowable stress in shear is $.8f$, the allowable stress in bending is $2f$.

b. Elastic calculations

Table 10.2 shows the results of elastic analyses.

Table (10.2): Result of elastic analyses at the tube sheet

Thickness (mm)	Load case	Displacement (mm)	Maximum σ_{eq} (MPa)
129	pressure	.725	197.27
129	Pressure + temp.	2.39	149.02
100	pressure	.49	230.5
100	Pressure + temperature	2.36	182.33

c. Inelastic analysis

Table (10.6) shows the results for the permissible pressure in accordance with the GPD design check.

Table(10.6): Results of inelastic calculations

Check type	Tube Sheet Thickness(mm)	Upper Shell Material	Pressure
GPD	129	SA 516 Gr 70	6.61 ^a
PD	129	SA 516 Gr 70	6.61 ^b : O.K.
GPD	129	SA 537 Cl.2	7.4 ^a
PD	129	SA 537 Cl.2	7.4 ^b : O.K.
GPD	100	SA 516 Gr 70	4.5 ^a
PD	100	SA 516 Gr 70	4.5 ^b : O.K.
GPD	100	SA 537 Cl.2	5.42 ^a
PD	100	SA 537 Cl.2	5.42 ^b : O.K.

^a Critical pressure according to gross plastic deformation design check.

^b The requirements of the PD design check are fulfilled for this pressure, the maximum permissible pressure according to the GPD design check.

11. Conclusions

The following conclusions result from this work:

A) Code calculations

- Calculations according to EN 13445-3 clause 13 and ASME Sec VIII, Div 1 produce precisely the same results in the case of this reactor. The same value of the bending stresses and close values for the shear stresses have been obtained with similar approximations for these cases.

This comes from the fact that both codes are based on the shell and plate theories with effective elastic constants. EN 13445-3 Clause 13 gives tabulated values for the equivalent elastic constants as a function of thickness, still not included in ASME Sec. VIII, Div 1 code.

- Calculations according to EN 13445-3 Appendix J indicate that the maximum allowable pressure on the tube sheet can be doubled as far as bending is concerned, and some increase can be achieved as far as shear is concerned. With further iterations an optimum between shear and bending could be achieved. This is a clear indication of the overly conservative design of the tubesheet as per data sheet.
- ASME Sec. VIII, Div 2 has the limitation of not considering the staying effect from tubes, and some parameters must be obtained by procedures not tabulated in the code. In this regard, calculations according to this code are not recommended.
- ASME Sec. VIII, Div. 1 and EN 13445-3 Clause 13 and Annex J differ from each other considerably in the allowable stress values. Usage of the different allowable stresses in above calculations would result in additional differences between these codes.
- Incorporation of thermal stresses in the calculations according to both ASME Sec. VIII, Div1 and EN 13445-3, show in the considered load cases a reduction in bending and shear stresses. Being based on limit analysis ideas, EN 13445-3 Annex J does not include thermal stress effects.

B) Elastic Analysis

- The base for obtaining tubesheet thickness in the data sheet has been an approach based on stress categorization. This stress categorization cannot be performed realistically for the junction of tubesheet to shell.
- According to the calculations performed in this work, the tubesheet shows larger Mises' equivalent stress in the case of pressure action only in comparison with the case of the combination of pressure and temperature. In this case thermal stresses reduce the overall stresses. This is in line with the results obtained by code calculations.

- The calculation of the displacements of the tubesheet are larger in the case with inclusion of the temperature effect. For the case of pressure only the tubesheet moves up and rotates slightly, due to the influence of the upper shell. This behavior is the same for the case calculated with temperature, but with much larger values and almost no rotations.
- Reduction in the tubesheet thickness shows small amount of increase on Mises' equivalent stress with some changes in displacements for the same pressure and temperature.
- Checking fatigue indicates that the circumferential weld between channel shell and tubesheet can safely withstand a number of full pressure cycles far above the shutdown and startup cycle anticipated for this reactor to occur during its useful life.
- Check for various radii sizes have indicated that the data sheet design is not optimal.

C) Inelastic Analysis

- Based on calculation results performed with data sheet thickness and according to EN 13445-3, Annex B, the maximum allowable pressure on the tubesheet could be greatly increased.
- Usage of stronger material for the channel side shell results in an increase of 85%. This means that the datasheet thickness is not an optimum one and can be reduced to lower values.
- With above increase in maximum allowable pressure it has been shown that the model shakes down to elastic behavior. Thermal stresses have been included in these investigations.
- On repeated cyclic actions it has been shown that there is no progressive plastic deformation. The small amount of plastic strains determined as residual strain field after first unloading will not grow.
- Calculations with reduced tubesheet thickness indicate that even with the weaker data sheet material for the channel side shell the tubesheet can carry safely the imposed actions.
- With stronger channel side shell material and reduced tubesheet thickness and reduced shell thicknesses at the the junction, it has been shown that the requirements of the GPD design check are fulfilled and the tubesheet shakes down to linear-elastic behaviour. The reduction in thicknesses of tubesheet and shells at the either side of the tubesheet renders a safe design, and can be adopted for this reactor.
- All calculations could be repeated to obtain an optimal tubesheet thickness. Above calculations have been performed for a 22% reduction in tubesheet thickness, and these show that a further (small) reduction is possible.

12. Appendices

- 1. Evaluation of yield surfaces**
- 2. Code calculations**

1. Evaluation of yield surfaces

To evaluate the degree of plasticization of a cross-section along lines in thickness direction of plates and shells, two approaches have been employed. These approaches are: Evaluation of the Ilyushin generalized yield function for portion of the model located at a shell region, and averaging of Mises' equivalent stress for paths located in tubesheet area.

It should be noted that the actual stresses at the path of interest have non-linear distribution, and via integration along the paths an equivalent linear stress distribution can be obtained automatically by the software program.

A.1 Evaluation of Ilyushin's yield function

Ilyushin's yield function is a function of standardized stress resultants. Standardized stress- resultants are quantities obtained by dividing the stress resultants by their fully plastic values.

Stress- resultants are quantities based on (thin) shell and plate theories, and, therefore, can be determined directly only for cases treated with shell or plate elements. For stresses obtained by usage of volume elements an appropriate integration along evaluation lines in thickness direction is required. The selected path is indicated below. It is located at the upper end of the upper shell, the percentage of plasticization has been determined to be 93 %. Figures (A.1.1 to A.1.4) give the relevant information.

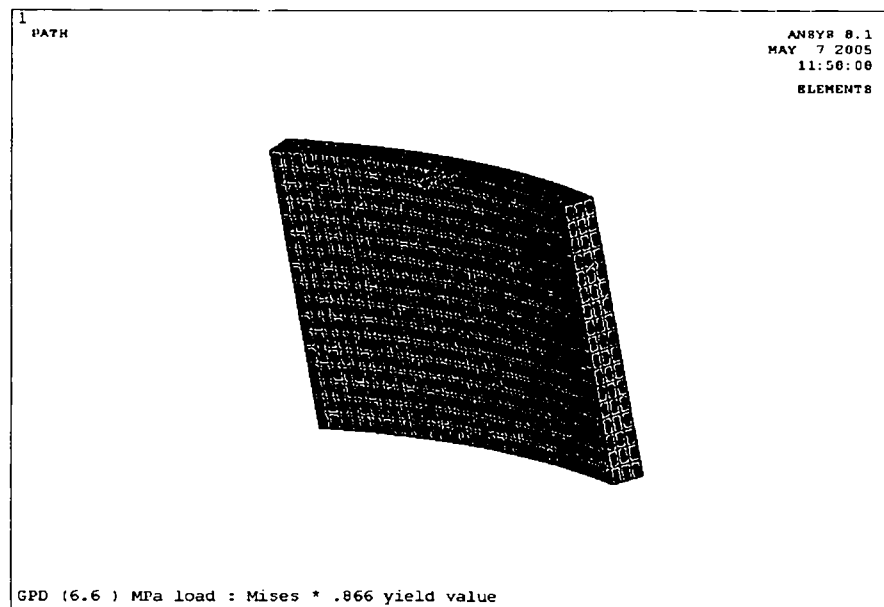


Figure (A.1.1): Path location at upper shell, close to top boundary of upper shell.

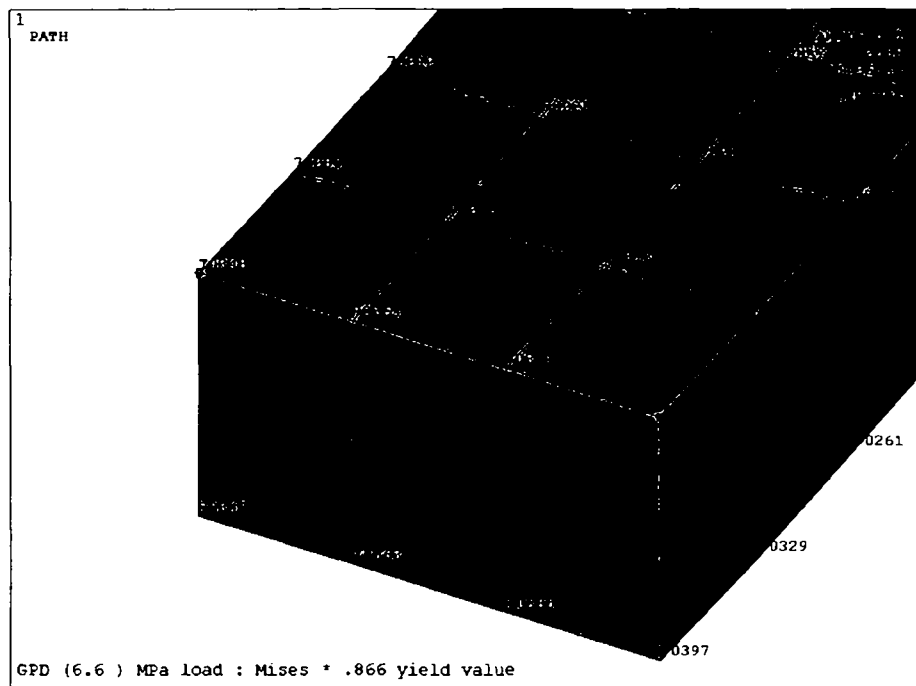


Figure (A.1.2): Path location from node 70398 to 70348 at upper shell close to end.

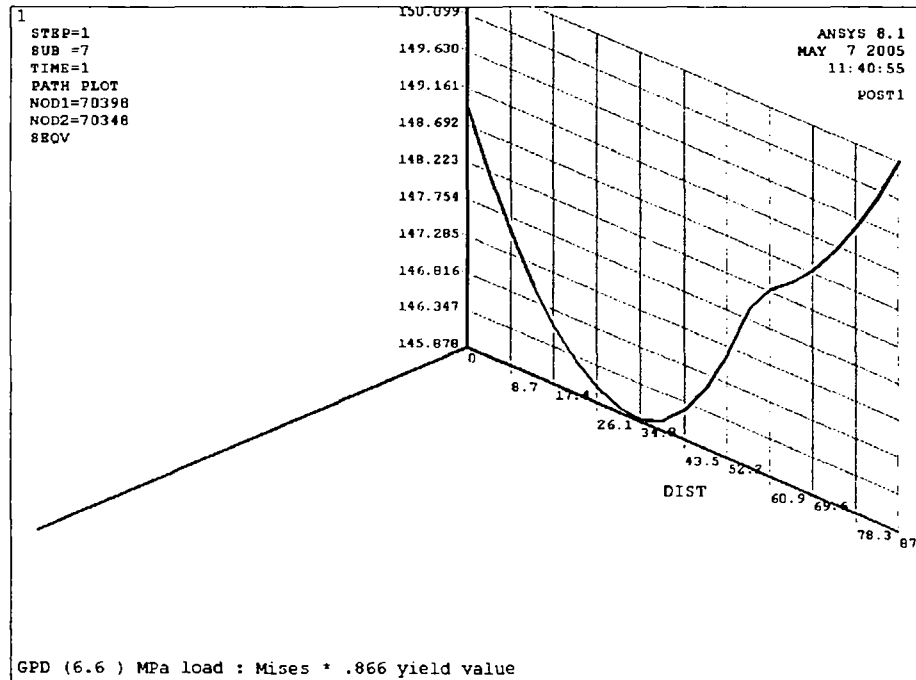


Figure (A.1.3): Mises' equivalent stress(MPa) for through-thickness path, at a pressure of 6.61 MPa applied to the upper shell.

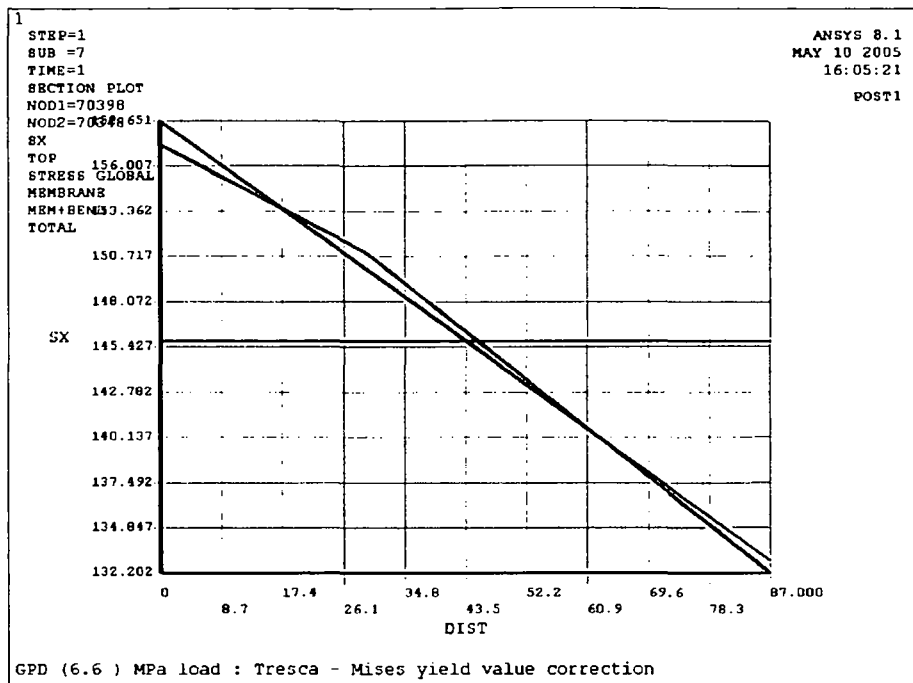


Figure (A.1.4): Equivalent linear stress distribution for a pressure of 6.61 MPa

It should be recalled that Ilyushin yield surface has been derived for Mises yield condition. If Tresca's yield condition is required, the yield stress has to be corrected, the reduced value used.

A.2 Evaluation of average Mises' equivalent stress in the tubesheet

Figures (A.2.1 to A.2.) indicate the path locations and the values of Mises' equivalent stress through the thickness of the tubesheet.

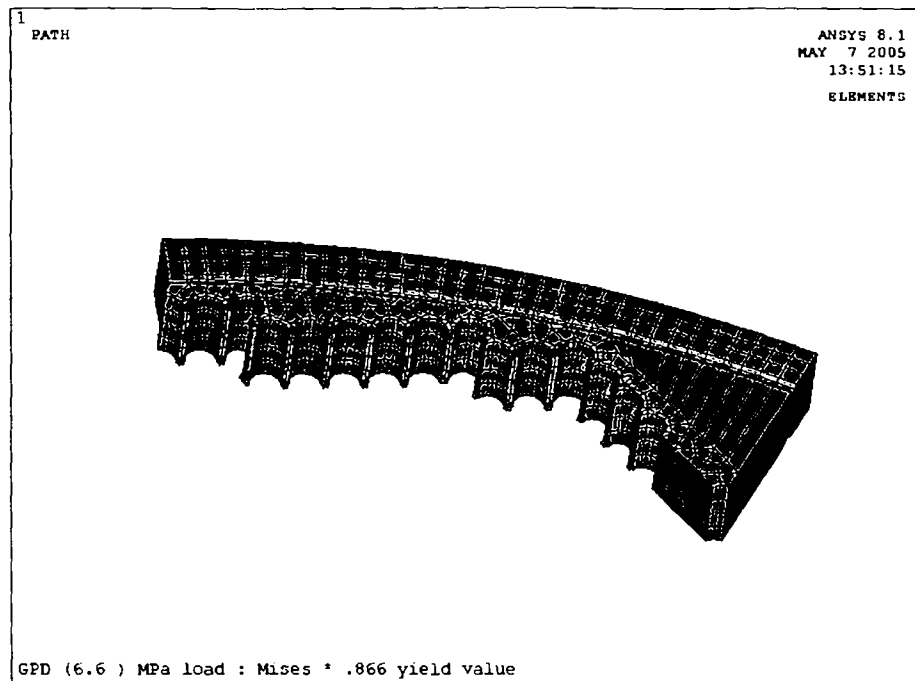


Figure (A.2.1): Location of paths at the tubesheet

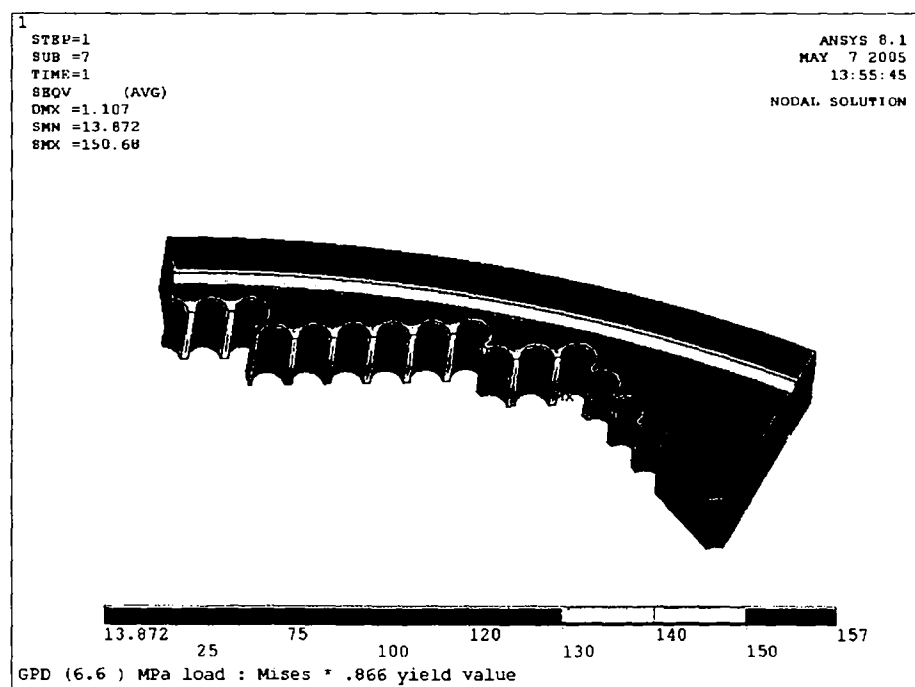


Figure (A.2.2): Mises' equivalent stresses for 6.61 MPa pressure at the paths.

Figures (A.2.3) to (A.2.4) show the location of path A and path B, used in the averaging Mises' equivalent stresses.

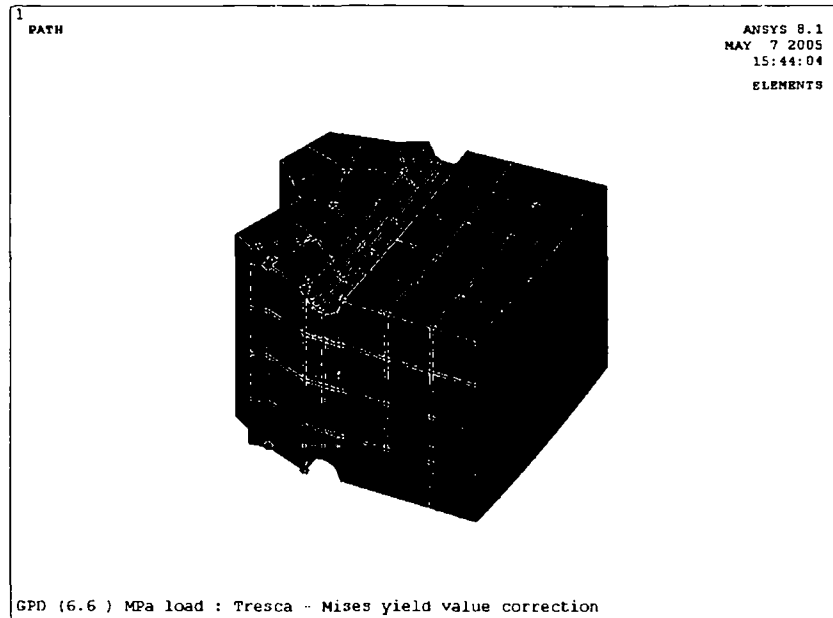


Figure (A.2.3) Path A and B locations.

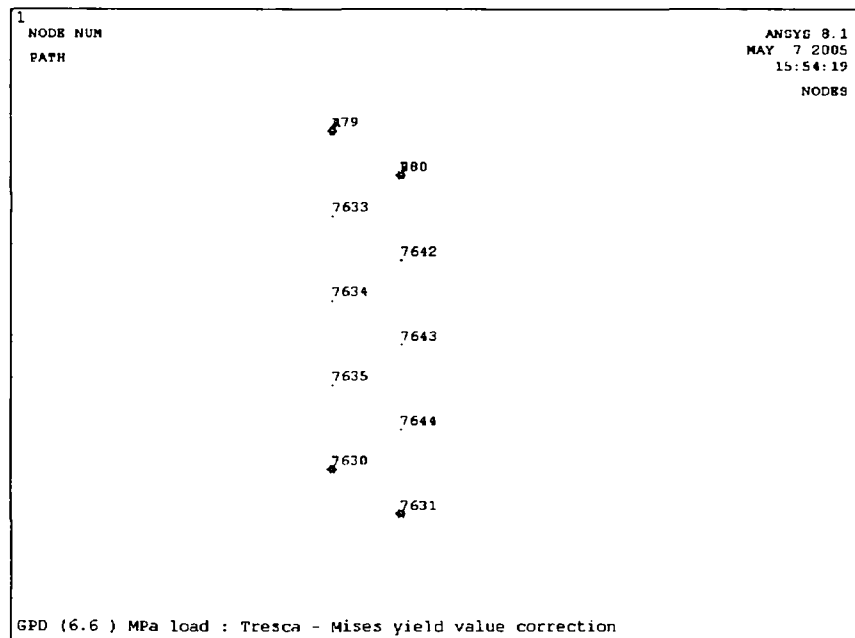


Figure (A.2.4): Number of nodes attached to path A and B, see fig.(A.2.3)

Table (A.2.1): Mises' equivalent stress at path A and B at 6.61 MPa pressure

Node	σ_1	σ_2	σ_3	σ_{eq}	Path
779	69.5	26.4	-17.128	75.023	A
7633	46.573	21.373	-21.998	60.075	A
7634	37.103	14.932	-29.02	58.296	A
7635	23.85	5.8026	-34.835	52.062	A
7630	16.751	3.49	-58.888	69.956	A
780	105	60.75	13.192	79.6	B
7642	70.601	43.114	-6.3432	67.535	B
7643	46.634	30.893	-24.617	64.83	B
7644	17.911	13.348	-52.839	68.583	B
7631	10.316	9.988	-58.775	68.928	B

Path series A

Mises' equivalent stresses at the paths are extracted from the program output:

$$\sigma_{A1} = 75 \text{ MPa}$$

$$\sigma_{A2} = 60 \text{ MPa}$$

$$\sigma_{A3} = 58 \text{ MPa}$$

$$\sigma_{A4} = 52 \text{ MPa}$$

$$\sigma_{A5} = 70 \text{ MPa}$$

There follows the average value

$$\begin{aligned} \sigma &= (\sigma_{A1} + 2\sigma_{A2} + 2\sigma_{A3} + 2\sigma_{A4} + \sigma_{A5}) / (2n - 2) \\ &= [75 + 2(60) + 2(58) + 2(52) + 70] / 8 = 60.6 \text{ MPa} \end{aligned}$$

The material design yield stress, after application of the partial safety factor, see section 2, is given by

$$\sigma_{\text{material}} = 156.6 \text{ MPa}$$

and the degree of plasticization thus given by $60.6 / 156.6 = 39 \%$

Path series B

Mises' equivalent stresses at the paths are extracted from the program output as:

$$\sigma_{B1} = 79.6 \text{ MPa}$$

$$\sigma_{B2} = 64.83 \text{ MPa}$$

$$\sigma_{B3} = 68.58 \text{ MPa}$$

$$\sigma_{B4} = 68.9 \text{ MPa}$$

$$\sigma = [79.6 + 2(67.5) + 2(64.83) + 2(68.58) + 68.9] / (2(5) - 2) = 68.79 \text{ MPa}$$

The material design yield stress, after application of the partial safety factor, see section 2, is given by

$$\sigma_{\text{material}} = 156.6 \text{ MPa}$$

and the degree of plasticization thus given by $68.79/156.6 = 44 \%$

App.2 : Code Calculations

This appendix gives the detail calculations according to the code procedures with results tabulated in table (3.3.1). Two load cases have been considered: normal operating condition, and condition for tube side pressure only, see section 3.3 for details.

A. EN – 13445 –3 Clause 13

The rules provided in above clause are based on the classical elasticity theory of thin plates and shells, effective elastic constants, and assuming that the tubesheet rests on elastic foundation created by the tubes. The results of the calculations according to this code have been tabulated below for the three major parts and for the corroded condition.

For the purpose of comparison, the allowable stresses are taken from EN13445- 3, details are provided in chapter 2. These parts deal with the evaluation of geometry data, effective elastic constants, rigidities, and their conversion in the effective pressure, as well as the stress calculation and the comparison with allowable limits.

For fixed tubesheet exchangers this clause permits a local reduction of thickness at the periphery of the tubesheet in the form of a relief groove. For details in this regard see section on groove analysis.

In the following, all nomenclature is accordance with the EN 13445, part 3.

(A.I) Effective geometry and constants

a) Effective constants:

Diameter of the perforated tube sheet area, $D_0 = \text{OTL} = 4136 \text{ mm}$

Basic ligament efficiency:

$$\mu = (p - d_i)/p = (69-57)/69 = 0.174$$

$$\mu^* = (p^*-d^*)/p^*$$

where

$p^* = p = 69$ (no unperforated diameter row, $S=0$)

$d^* =$ effective tube hole diameter

$$d^* = \max \{ [d_i - 2e_t (E_t/E) \cdot (f_t/f) \cdot \rho]; [d_i - 2e_t] \},$$

with outside tube diameter $d_i = 57 \text{ mm}$, and tube thickness $e_t = 2.9 \text{ mm}$, there follows

$$E_t = 193875 \text{ MPa}$$

$$E = 193875 \text{ MPa}$$

$$f_t = 121 \text{ MPa (see chapter 2)}$$

$$f = 145 \text{ MPa (see chapter 2)}$$

$$d^* = \max \{ [57 - 2(2.9)(193875/193875)(121/145)\rho], [57 - 2(2.9)] \}$$

where $\rho = l_{t,x}/e$.

Since tubes are not expanded, $l_{t,x}=0.0$, $\rho=0.0$, and

$$d^* = 57 \text{ mm}$$

$$\mu^* = (69-57)/69=0.174$$

Fig. 13.7.8.1, render, with $\mu^* = 0.174$ and $(e/p) = (129/69) = 1.87$,

$$\alpha_0 = -2.1218 \cdot 10^{-3}, \alpha_1 = 0.24215, \alpha_2 = 3.961, \alpha_3 = -6.0035, \alpha_4 = 3.29124, (E^*/E) = 0.1313,$$

$$E^* = 0.1313(193875) = 25455.8 \text{ MPa}$$

Further more,

$$\beta_0 = 0.99605, \beta_1 = -4.2825, \beta_2 = 9.2546, \beta_3 = -8.1112, \beta_4 = 2.680187, \nu^* = 0.49$$

b) Effective tube sheet diameter (Corroded)

$$De = (Ds + Dc)/2, De = (4256 + 4236)/2 = 4246 \text{ mm}$$

c) Effective tube length

$$L = L_t - 2e, L_t = 4396 + 2(135 - 6), e = 135 - 6 = 126 \text{ mm}, L = 4396 \text{ mm}$$

d) Tube sheet perforation coefficients

$$X_s = 1 - N_t (d_t/D_e)^2, X_t = 1 - N_t [(d_t - 2e_t)/D_e]^2,$$

With N_t = number of tubes = 3100, $d_t = 57 \text{ mm}$, $e_t = 2.9 \text{ mm}$, one has

$$X_s = 1 - 3100(57/4246)^2, X_s = 0.4413$$

$$X_t = 1 - 3100[(57 - 2 \cdot 2.9)/4246]^2, X_t = 0.5492$$

e) Axial rigidities

Tube:

$$K_t = [\pi \cdot e_t (d_t - e_t) \cdot E_t / L]$$

With $e_t = 2.9 \text{ mm}$, $d_t = 57 \text{ mm}$, $L = 4396 \text{ mm}$, $E_t = 193875 \text{ N/mm}$, one has

$$K_t = [\pi \cdot (2.9)(57 - 2.9)(193875)] / 4396 = 21727.25$$

Shell:

$$K_s = [\pi \cdot e_s \cdot (D_s + e_s) E_s] / L$$

With $e_s = 70 - 3 = 67$ mm, $(D_s)_{corr.} = 4250 + 6 = 4256$ mm,

$E_s = 195000$ Mpa, $L = 4396$ mm, one has

$$K_s = [\pi \cdot 67 \cdot (4256 + 67) \cdot 195000] / 4396 = 40363316.05, \text{ and}$$

$$K_{s,t} = K_s / (N_t \cdot K_t)$$

$$K_{s,t} = 40363316.05 / (3100)(21727.25) = 0.599$$

Elastic foundation:

$K_w = (8K_t N_t) / (\pi \cdot D_e^2)$, K_w is the modulus of the assumed elastic foundation equivalent to the tube bundle:

$$K_w = [8(21727.25)(3100)] / (\pi(4246)^2) = 9.513$$

$$J = 1.0 \quad (\text{no expansion joint})$$

f) Tube bundle to tube sheet rigidity ratio

$$X = (K_w / D^*)^{0.25} (D_e / 2)$$

D^* is the equivalent bending rigidity of the tube sheet (effective bending rigidity) given by

$$D^* = (E^* \cdot e^3) / [12(1 - \nu^{*2})].$$

With $e = 129$ mm, $E^* = 25455.8$ MPa, one obtains

$$D^* = [25455.8 \cdot (129)^3] / [12(1 - 0.49^2)] = 5992640023$$

$$X = (9.518 / 599264002309)^{0.25} (4246 / 2) = 13.4$$

g) Bending rigidity of the shell away from thickened portion

$$K_s = [2E_s(e_s)^{2.5}] / \{ [12(1 - \nu_s^2)]^{0.75} (D_s + e_s)^{0.5} \}$$

$E_s = 195000$ N/mm², modulus of elasticity of the shell side shell at the calculated temperature, with the shell inside diameter below the thickened portion, D_s , and with $e_s = 31$ mm, one obtains

$$E_{s,l} = E_s = 195000 \text{ N/mm}^2$$

$$K_s = \{ (2)(195000)(31^{2.5}) \} / \{ [12(1 - 0.3^2)]^{0.75} \cdot (4292 + 31)^{0.5} \} = 42317008.7 \text{ N/mm}^2$$

Note: Due to shell thickening at the junction the axial rigidity already calculated should be corrected as indicated below,

$$K_s^* = [\pi(D_s + e_s)] / \{ [(L - l_1 - l'_1) / (e_s E_s)] + [(l_1 + l'_1) / (e_{s,1} E_{s,1})] \}$$

$$D_s = 4292 \text{ mm}, e_s = 31 \text{ mm}, e_{s,1} = 67 \text{ mm}, l = 4396 \text{ mm}, l_1 = 1146 \text{ mm}, l'_1 = 745 \text{ mm}$$

$$E_s = E_{s,1} = 195000 \text{ N/mm}^2$$

$$K_s^* = [\pi(4292 + 31)] /$$

$$\{ [(4396 - 1146 - 745) / (31)(195000)] + [(1146 + 745) / (67)(195000)] \}$$

$$K_s^* = 24289713.05$$

$$(K_{st})_{\text{corrected for end thickening}} = K_s^* / N_t K_t$$

$$(K_{st})_{\text{corrected for end thickening}} = 24289713.05 / (3100) (21727.25) = 0.36$$

Bending rigidities of shell and channel corrected for thickened portion,

$$K_s = [2E_{s1}(e_{s1})^{2.5}] / \{ [12(1 - \nu_s^2)]^{0.75} (D_s + e_{s1})^{0.5} \}$$

$$= [2(195000) (67)^{2.5}] / \{ [12(1 - 0.3^2)]^{0.75} (4250 + 67)^{0.5} \} = 36307271.3$$

Channel Shell

$$K_c = [2E_c (e_c)^{2.5}] / \{ [12(1 - \nu_c^2)]^{0.75} (D_c + e_c)^{0.5} \}$$

$$E_c = 192000 \text{ MPa}, E_c = 90 - 3 = 87 \text{ mm}, \nu_c = 0.3, (D_c)_{\text{corr}} = 4236 \text{ mm}$$

Note: e_c at the thickened portion has been used in the determination of K_c since the head starts immediately after this portion.

$$K_c = [2(192000) (87)^{2.5}] / \{ [12(1 - 0.3^2)]^{0.75} (4236 + 87)^{0.5} \} = 68638812.21$$

h) Tube sheet edge restraint factor due to both shelles

$$Z = (K_s + K_c) / [(K_w)^{0.25} (D^*)^{0.75}]$$

$$Z = (36307271.3 + 68638812.21) / [(9.513)^{0.25} (5992640023)^{0.75}] = 2.78$$

A. II Effective Pressure

$$P_e = [(J \cdot K_{st}) / (1 + JK_{st} F_q)] \{ X_s + 2\nu_t (1 - X_s) + (2\nu_s / K_{st}) - [(1 - J)((D_j + 2W_j)^2 - D_s^2) / (2JK_{st} D_s^2)] \} P_s - (JK_{st} / (1 + JK_{st} F_q)) [X_t + 2\nu_t (1 - X_t) + (1 / JK_{st})] P_t + [JK_{st} / (1 + JK_{st} F_q)] (Kw/2) \gamma$$

$$J = 1.0, K_{st} = 0.36, F_q = \text{Fig 13.5.4-1}, X = 13.4 \text{ and } Z = 2.78, F_q = 5.983$$

$$X_s = 0.4413, v_t = 0.3, v_s = 0.3, X_t = 0.5492, K_w = 9.513$$

$$\gamma = \gamma^* = (T_{t,m} - 20)\alpha_{t,m}L - (t_{s,m} - 20)[\alpha_{s,m}(L - l_1 - l'_1) + \alpha_{s,m,1}(l_1 + l'_1)]$$

$$\gamma^* = (167.5 - 20)(12.51)(10^{-6})(4396) - (145 - 20)[(12.42)(10^{-6})(4396 - 1146 - 745) + (12.42)(10^{-6})(1146 + 745)]$$

$$\gamma^* = 1.286$$

$$P_e = [0.36 / (1 + (0.36)(5.983))] [0.4413 + 2(0.3)(1 - 0.4413) + (2(0.3)/0.36) - 0] P_s - [0.36 / (1 + (0.36)(5.983))] [0.5492 + 2(0.3)(1 - 0.5492) + (1/0.36)] P_t + [0.36 / (1 + 0.36(5.983))] [9.513/2] \gamma^*$$

$$P_e = 0.278 P_s - 0.411 P_t + 0.543 \gamma^*$$

$$\text{For } P_s = 10 \text{ bar} = 1.0 \text{ MPa}, P_t = 40 \text{ bar} = 4.0 \text{ MPa}$$

$$P_e = 0.278(1.0) - 0.411(4.0) + 0.543\gamma^* = -1.366 + 0.543\gamma^*$$

A. III Load Cases

With regard to operating modes of the reactor, the following load cases are considered in the following. Generally possible modes are:

- A. Load case 1: Design pressures and ambient temperatures.
- B. Load case 2: Design pressure and design temperature on both sides.
- C. Load case 3: Tubeside design pressure and temperature, no pressure or no temperature shellside.
- D. Load case 4: Shellside design pressure and temperature, no pressure or no temperature tube side.

Due to plant operation requirements, these load cases are all also possible for the purpose of this work, but the cases, with the largest effect on stresses have been considered only. These considered load cases are: Normal operating condition on shell and tube side, and design pressure on both sides but no temperature.

A.IV Stresses

a). Maximum radial bending stresses

$$\sigma_b = (1.5 F_m / \mu^*) (D_e / (e - h'_g))^2 P_e$$

$$F_m = 1 / (6H)$$

H, Fig 13.5.5.1 ($0 \leq X \leq 20$) for $X = 13.4$, $Z = 2.78$, $H = 7.97568$

$F_m = 1 / [(7.975)(6)] = 0.0209$, $h'_g = 0.0$, no groove

$$\sigma_b = [(1.5)(.0209)/0.174] [(4246/129)^2] P_e = (195.195) P_e \text{ MPa}$$

Allowable stress for pressure only is $|\sigma| \leq 2f$, where f is the allowable stress, according to table (2.2.4) given by 145 MPa.

For $\gamma = 0.0$ (load case with pressure but no temperature), there follows:

$$P_e = -1.34 \text{ MPa}$$

$$\sigma_b = (195.195) (-1.366) = -266.64 \text{ MPa}$$

Therefore,

$$266.64 < 2(145) = 290, \text{ and } \sigma_b / \sigma_{\text{allow}} = 266.64 / 290 = 0.92.$$

The allowable stresses for the load case considered, P_t and P_s with thermal expansion effect γ (normal operating condition), are given by 3f:

$$|\sigma| \leq 3f$$

For the load case with normal operating condition pressure and

temperatures, $\gamma = \gamma^* = 1.286$, and

$$P_e = -1.366 + 0.543\gamma^*$$

$$P_e = -1.366 + 0.543(1.286)$$

There follows: $P_e = -0.6677$, and $\sigma_b = -130.33 \text{ MPa}$

Therefore,

$$130.33 < 435, \text{ and } \sigma_b / \sigma_{\text{allow}} = 130.33 / 435 = 0.30.$$

b) Shear stresses

$$\tau = (1/4\mu) (D_0/e) P_e$$

$$P_e = -1.34 + 0.53 \gamma^* = -1.366 + 0.543(1.286)$$

For load case with thermal load

$$P_e = -0.6677, \text{ and}$$

$$\tau = [1/(4(0.174))](4136/129)P_e$$

$$\tau = 46.07 P_e = 46.07(-0.6677) = 30.76 \text{ MPa.}$$

The allowable shear stress is given by 0.8f:

$$|\tau| \leq 0.8 f = 0.8 (145) = 116 \text{ MPa, and}$$

$$\tau / \tau_{\text{allow}} = 30.76 / 116 = 0.265$$

For case without thermal load

$$P_e = -1.366, \text{ and}$$

$$\tau = 46.07 P_e$$

$$\tau = 46.07(-1.366) = 63 \text{ MPa, and}$$

$$\tau / \tau_{\text{allow}} = 63 / 145 = 0.44$$

B. Calculation according to EN-13445 – Annex J

Annex J provides alternative rules and has been created on the basis of limit analysis theory.

(J.5) Parameters

$$d_1 = \text{OTL} = 4136 \text{ mm}$$

$$d_2 = \min \{ \max (d_C, d_{GC}; \max(d_S, d_{GS})) \}$$

no gasket, and, therefore, $d_{GC} = d_{GS} = 0$

$$d_2 = \min \{ (4230, 4250) \} = 4230 \text{ mm, where } d_C = 4230 \text{ mm and } d_S = 4250 \text{ mm.}$$

Furthermore,

$$b_R = (d_2 - d_1) / 2 = (4230 - 4136) / 2 = 47 \text{ mm}$$

$$\lambda_R = (2 b_R) / d_1 = (2)(47) / 4136 = .0227$$

$$b_s = \{ \max (d_c; d_{GC}) - \max(d_s; d_{GS}) \} / 2 = (4230 - 4250) / 2 = -10$$

$$\lambda_s = 2b_s / d_2 = (2)(-10) / 4230 = -0.00473$$

The signs of b_s and λ_s must be strictly observed.

(J.5.2) Tube sheet perforation

$$d_{0,e} = \max \{ d_0 - (2\delta_X A_X / e_p); d_T - 2e_T \}$$

$$A_X = (l_X + \sqrt{d_T} e_T) e_T$$

According to manufacturing detail on tubesheet groove and tube weld,

$$l_X = h_t = 4.0 \text{ mm}$$

$$A_X = (4 + \sqrt{(57)(2.9)}) (2.9) = 48.885 \text{ mm}^2$$

$$\delta_X = \min \{ (1, 0); (f_t / f_p) \}$$

f_t and f_p are the nominal design stresses for tubes and tubesheet, see table 2.2.2:

$$f_t = 121 \text{ MPa}, f_p = 145 \text{ MPa}.$$

Furthermore, one has

$$\delta_X = \min \{ (1, 0); (121 / 145) \} = \min \{ (1, 0); 0.834 \} = 0.834, \text{ and}$$

$$\begin{aligned} d_{0,e} &= \max \{ 58 - [(2)(0.834)(48.885) / 129]; 57 - 2(2.9) \} \\ &= \max \{ (58 - 0.63); 51.2 \} = \max (57.36; 51.2) = 57.36, \text{ the effective tube hole di} \\ &\quad \text{diameter} \end{aligned}$$

(J.5.2.2) Parameters of the equivalent (effective) weakened plate

$$\Phi_P = 1 - d_{0,e} / P$$

$$\Phi_P = 1 - 57.36 / 69 = 0.1686 < 0.5$$

For $\Phi_P < 0.5$, one has

$$\kappa_P = \sqrt{\Phi_P (1 - \Phi_P)} = \sqrt{0.1686 (1 - 0.1686)} = 0.374$$

(J.6.2) Active pressure

(J.6.2.1) Direct fluid pressure difference at the whole tubesheet

$$P_D = P_T - P_S = 4.0 - 1.0 = 3.0 \text{ MPa.}$$

(J.6.2.2) Resultant shear force pressure at the outer boundary of the tube region

$$P_R = P_D = 3.0 \text{ MPa}$$

(J.7) Tube sheet supported by straight tubes**(J.7.1.2) Relative area in the tubed region**

For the relative fluid pressure loaded area in the tube region one has:

$$X_T = 1 - N_T \cdot \{(d_T - 2e_T) / d_i\}^2 = 1 - 3100 \{(57 - 2(2.9)) / 4136\}^2 = 0.5249,$$

$$X_S = 1 - N_T (d_T / d_i)^2 = 1 - 3100 (57 / 4136)^2 = 0.412, \text{ and}$$

$$v = X_T - X_S = 0.5249 - 0.412 = 0.1129$$

(J.7.1.3) Buckling length of tubes

$$N_{Be} = 3, I_A = I_B = I_C = 1165 \text{ mm}$$

$$I_{T,K} = \max \{0.70 I_A ; Y I_B; 0.70 I_C\} = \max \{ 0.70(1165); Y(1165); 0.70(1165)\}, \\ \text{for } I_C = I_B$$

Furthermore,

$$\lambda_A = I_A / I_B = 1.0, \text{ and } \lambda_C = 1.0.$$

$$Y = \sqrt{(0.4888 + 0.102(1) + 0.11(1) + 0.091(1) + 0 + 0.01(1))} = 0.895$$

$$I_{T,K} = \max \{0.7(1165); 0.905(1165); 0.70(1165)\}$$

$$K = \max \{815.5; 1054.3; 815.5\} K = 1054.3 \text{ mm}$$

(J.7.1.4) Effective throat thickness of tube end welds

According to the weld layout, as given in the data sheet:

$$h_t = 4.0, h_p = 4.0, w_p = 4.0, h_R = 4.0, w_R = 2.0 \text{ and } w_T = 0.0$$

$$a_{T,P} = (0.6(h_p^2 + w_p^2) / \sqrt{h_p^2 + w_p^2}) = (0.6(4^2 + 4^2) / \sqrt{4^2 + 4^2}) = 4.525$$

$$a_{T,R} = (0.6(h_R^2 + w_R^2) / \sqrt{h_R^2 + w_R^2}) = (0.6(4^2 + 2^2) / \sqrt{16 + 2^2}) = 3.04$$

$$a_{T,T} = [(0.6)h_t^2 + w_T^2] / \sqrt{(h_t^2 + w_T^2)} = (0.6(16)) / \sqrt{16} = 2.4$$

(J.7.2) Active Direct Pressures

$$P_D = P_T - P_S = 584 - 146 = 438 \text{ Psig} = 3.02 \text{ MPa}$$

$$P_E = P_T X_T - P_S X_S = 4.0(0.525) - (1.0)(0.412) = 1.6876$$

(J.7.3) Tube Support

The allowable longitudinal stress for the tubes in tension MPa $f_{T,t}$ is given by

$$f_{T,t} = f_T - (|P_S| d_T) / (2e_T), \text{ with the}$$

nominal design stress for the tubes $f_T = 121 \text{ MPa}$ one obtains

$$f_{T,t} = 121 - [(1)(57) / ((2)(2.9))] = 111.17 \text{ MPa}$$

(5.7.3.1.2) Allowable longitudinal compressive stress in tubes

$$f_{T,C} = \sigma_{T(P)} + (f_T - |\sigma_{T(P)}|) / \sqrt{1 + \{(1216/E_T)(130f_T - |\sigma_{T(P)}|)((d_{T,K}/(d_T - e_T))^2\}^2}$$

where

$$\sigma_{T(P)} = [P_S d_T^2 - P_T (d_T - 2e_T)^2] / (6(d_T - e_T)e_T)$$

$$\sigma_{T(P)} = [(1)(57)^2 - 4(57 - 2(2.9))^2] / [6(57 - 2.9)(2.9)] = -7.68, \text{ and}$$

$$f_{T,C} = -7.68 + (121 - 7.68) / \sqrt{1 + \{(1.216/193875)(1.30(121) - 7.681)(1054.3/(57 - 2.9))^2\}^2} = 99.06$$

This calculation of the allowable longitudinal compressive stress in the tubes includes a higher safety and, therefore, is more conservative than that in 13.9.3, because here limit analysis is being applied.

(J.7.3.2) Calculation of the design stress for the tube to tube sheet connection

(J.7.3.2.1) for welded only:

With $f_R = (f_p + f_T) / 2 = (145 + 121) / 2 = 133 \text{ MPa}$ one obtains for

$$f_X = f_{XW} = \min((f_p a_{T,R}); (f_R a_{T,R}); (f_T a_{T,T})) / e_T$$

$$f_X = f_{XW} = \min [145(4.425); 133(3.04); 121(2.4)] / 2.9$$

$$w = \min (641.625; 404.32; 290.4) / 2.9 \quad w = 100.13$$

(J.7.3.3) Allowable axial forces per area unit of the tube bundle

$$v = 0.1129 \text{ (see J.7.1.2)}$$

$$[Q_t] = v \min \{ f_{T,t} ; f_X \}$$

$$[Q_t] = (0.1129) \min(111.17; 100.13)$$

$$[Q_t] = 11.30 \text{ Mpa}$$

$$[Q_c] = v \min(f_{T,c} ; f_X)$$

$$[Q_c] = 0.1129 \min(99.06; 100.13)$$

$$[Q_c] = 11.18$$

$$-[Q_c] < [Q_t]$$

$$-11.18 < 11.30$$

Note: Normally $-[Q_c] < [Q_t]$. If these condition in not met, the tubebundle is overloaded and should be redesigned, in this case this was not required.

(J.7.4) Reactive pressures

The expected reactive axial forces per area unit of the tubebundle in the tubed region are Q_t in the inner zone and Q_A in the outer zone. They are to be determined as follows:

Recalling $P_E = 1.6876$ (see J.7.2):

$$\text{For } -[Q_t] \leq P_E \leq [Q_c], -11.79 < 1.6876 < 11.448:$$

$$Q_t = -P_E = -1.6876, P_R = P_D = 3.021 \text{ MPa} > 0.0 \text{ (See J.6.2.1), and } Q_A = +[Q_t] = 11.30$$

(J.7.5) Active resultant pressure

The resultant active axial shear force at the outer boundary of the tubed region is expressed by a corresponding pressure P_R . For heat exchangers with fixed tubesheet and without expansion bellows, as in the present case, reactive forces are included in P_R .

(J.7.5.6) Fixed tube sheet without expansion bellows

Here P_R is statically undetermined, and, therefore, and in consequence of the limit analysis approach, only the extreme possible and allowable values are given. Later, calculations may be made using any value P_R between the given extreme values, and the most favourable final result be used.

$$P_{R,max} = \min\{P_E + [Q_i]; (F_R + [F_C])/A_R\}$$

With $P_E = 1.6876$, $[Q_i] = 11.30$, and

$$F_R = P_D \cdot A_R + P_S d_S^2 (\pi/4) = \{P_T d_I^2 + P_S (d_S^2 - d_I^2)\} (\pi/4).$$

Furthermore

$$P_T = 4, d_I = OTL = 4136, P_S = 1, d_S = 4250.$$

There follows

$$F_R = [4.0 (4136)^2 + 1.0(4250^2 - 4136^2)](\pi/4) = 54492485.95 \text{ N}$$

$[F_i]$ and $[F_C]$ are allowable axial tensile and compressive force in the shell and have been calculated with

$$[F_C] = \pi \cdot d_s \cdot e_s \cdot [\sigma_{sxt}] \cdot \min\{[\sigma_{sxc}]/[\sigma_{sxt}]; 1 - P_S/[P_{Si}]; 1 + P_S/[P_{Se}] - P_S/(2 \cdot [P_{Si}])\}$$

With $d_s = 4250$ mm, $e_s = 67$ mm (shell is thickened), and the allowable longitudinal tensile stress for the shell $[\sigma_{sxt}]$, $f_s = 154.66$ MPa (see table 2.2.4).

$[\sigma_{sxc}]$ is the allowable longitudinal compressive stress of the shell, equal to $\sigma_{c,all}$, where $\sigma_{c,all}$ is to be determined in accordance with subclause 16.14.8.1 and limit as 8.4.2. Details are:

- according to 8.4.2

$$\sigma_c = R p \ 0.2/t = 232 \text{ MPa (see also table 2.2.1)}$$

- according to 16.14.8.1

$$K = 1.21 E e_a / \sigma_c D:$$

With $E = 195000$ MPa, $E_a = 67$ mm, the mean shell diameter D is given by $(4256 + 4390)/2 = 4323$ mm.

There follows

$$K = 1.21(195000)(67) / (232)(4323) = 15.76$$

$$\text{With } D/e_a = 4323/67 = 64.522 < 424$$

$$\alpha = 0.83 / \sqrt{1.0 + 0.005D/e_a} = 0.83 / \sqrt{1.0 + 0.005(64.522)} = 0.7217, \text{ and}$$

$$\Delta = [1 - 0.4123 / (0.7217(15.76)^{0.6})] / 1.5 = 0.603$$

one obtains

$$\sigma_{c,all} = 232(0.6) = 140 \text{ MPa}, [\sigma_{Sxc}] = 140 \text{ MPa}$$

P_{Si} is the allowable internal fluid pressure for the shell, equal to P_{max} (Subcluse 7.4)

Note: Since the shell is thickened locally this pressure has been calculated

for 67 mm corroded thickness.

Furthermore,

$$P_{max} = (2f.z.e_a)/D_m, F = 154.66, Z = 1.0, e_a = 67 \text{ mm}, \text{ and } D_m = 4323 \text{ mm},$$

resulting in

$$P_{max} = (2(154.66) (1.0)(67))/ 4323 = 4.8 \text{ MPa}$$

$$P_{Si} = 2.218 \text{ MPa}$$

$[P_{se}]$ is the allowable external fluid pressure for the shell; $[P_{Sc}] = P_{e,max}$ (subclause 16.14)

- 16.14.7 item 4, $P_{e,max}$ the maximum permissible external pressure in the absence of other loadings, from clause 8 is calculated as
- Clause 8 (8.5.2.2)

$$L/2R = 1165 / 2(2161.5) = 0.3$$

where 1165 mm is the maximum length between stiffeners (baffel grids).

$$2R/ e_a = 4323 / 31 = 140, \epsilon = .0025.$$

$$P_m = E.e_a. \epsilon / R_m = 195000(31) (.0027) / 2161.5 = 7.55$$

There follows,

$$[P_{Se}] = P_{e, max} = 7.55$$

Furthermore,

$$F_c = \pi.(4250)(67)(154.66)$$

$$\min \{ (140/ 154.66); (1 - 1/ 4.8); [1 + 1/7.55 - 1/(2(4.8))] \}$$

$$= 138353965.5 \min. \{0.905; 0.8; 1.0282\} = 110683172.4 \text{ N}$$

$$P_{R,\max} = \min \{ P_E + [Q_I]; (F_R + [F_C]) / A_R \}$$

With $A_R = (\pi/4)(d_I)^2 = \pi/4 (4136)^2 = 13435410.54 \text{ mm}^2$ one obtains

$$\begin{aligned} P_{R,\max} &= \min \{ (1.6876 + 11.3); (54492485.95 + 110683172.4) / 13435410.5 \} \\ &= \min \{ 12.9876; 12.294 \} \end{aligned}$$

$$P_{R,\max} = 12.3 \text{ MPa}$$

Similarly:

$$P_{R,\min} = \max \{ P_E - [Q_C]; (F_R - [F_I]) / A_R \}, F_t = \pi (d_S)(e_S)[\sigma_{Sxt}] \min \{ 1; 1 + P_S/[P_{Si}] \}$$

With

$$d_S = 4250 \text{ mm}, e_S = 67 \text{ mm},$$

the allowable longitudinal tensile stress in shell $[\sigma_{Sxt}] = f_S = 154.66 \text{ MPa}$,

$$P_S = 1.0,$$

$$[P_{Si}] = P_{\max} = \text{allowable internal fluid pressure for the shell}, P_{\max} = 2.218 \text{ MPa},$$

one obtains

$$F_t = \pi (4250)(67)(154.66) \min \{ 1; 1 + (1.0/2.218) \} = 138353965.5 \text{ N}$$

Furthermore,

$$\begin{aligned} P_{R,\min} &= \max \{ P_E - [Q_C]; (F_R - [F_I]) / A_R \} \\ &= \max \{ 1.6876 - 11.18; (54492485.95 - 138353965.5) / 13435410.54 \} \\ &= \max \{ -9.4924; -6.241 \} = -6.241 \text{ MPa}. \end{aligned}$$

$$P_{R,\min} = -6.241 \text{ MPa}$$

(J.7.6) Governing pressure representing the resultant effective axial force

Resultants of active and reactive axial force per area unit in the tube bundle:

$$P_I = P_E + Q_I$$

$$P_E = 1.6876$$

$$Q_I = -P_E = -1.6876 \text{ (see J.7.4)}$$

$$P_I = 1.6876 - 1.6876$$

$$P_I = 0.0$$

$$\begin{aligned}
P_A &= P_E + Q_A \\
P_E &= 1.6876 \\
Q_A &= 11.3 \\
P_A &= 1.6876 + 11.30 = 12.98 \text{ MPa}
\end{aligned}$$

Note: If the strength of the tube is large enough to give the optimum support for the tube sheet, then $P_I = 0.0$. But, if this optimum is not realized, the tube bundle may still have an acceptable good design.

(J.7.6.2) Force distribution parameter

$$\zeta^2 = (P_A - P_R) / (P_A - P_I)$$

A necessary minimum requirement for the tube bundle strength is $0 \leq \zeta^2 \leq 1$. If this requirement is not met the tube bundle is unable to bear the active loadings and must be redesigned.

For $P_R = 0.0$ and $P_I = 0.0$, there follows $\zeta^2 = 1.0$

For $P_R < 0.0$ and $P_I = 0$, there follows, $\zeta^2 = 1 - P_R / P_A$, $\zeta > 0$, not acceptable

For $P_R > 0.0$ and $P_I = 0$, there follows, $\zeta^2 = 1 - P_R / P_A$

Various values of ζ corresponding to P_R are possible.

(J.7.6.3) Governing pressure

P_Q represents the governing resultant axial force. It depends on η and ζ , where ζ is the force distribution parameter, and η is the moment distribution parameter.

$P_R = 1.35$

P_R should be assumed, and the ratio of Φ_s and Φ_b to be checked to be less than unity. Other values of P_R fail the check or are not optimal. There follows:

$$\eta_{\min}^2 = (12 \kappa_P \Phi_P f_p e_p^2) / (P_A d_1^2)$$

κ_P is the shear strength of tube sheet given by 0.374 (see J.5.2.2),

Φ_P is the relative bending strength of the tube sheet, given by 0.1683 (see J.5.2.2),

f_p is the tube sheet strength, given by 145 MPa,

$e_p = 129 \text{ mm}$, $P_A = 12.98 \text{ MPa}$, $d_1^2 = (4136)^2 \text{ mm}^2$

There follows

$$\eta_{\min}^2 = [12(0.374)(0.1683)(145)(129)^2] / (12.98)(4136)^2 = .008208$$

$$\eta_{\min} = 0.0906$$

Calculation of the following auxiliary parameters (J.7.6.3.3)

$$u = \zeta^2 \left| P_I / P_A \right|, P_I = 0.0 \text{ (see J.7.6)}$$

$$u = 0.0$$

$$v = \eta_{\min}^2 - u = .0082$$

$$\zeta^2 = 1 - P_R / P_A$$

$$P_A = 12.98 \text{ (see J.7.6)}$$

$$P_R = 1.35$$

$$\zeta^2 = 1 - (1.35 / 12.98) = .8959$$

$$\zeta = 0.9465$$

$$\eta^2 = \zeta^2 + (v/2) + \sqrt{(v/2)^2 + \zeta^2 v w}$$

$$\eta^2 = 0.896 + (.0082/2) + \sqrt{(0.0082/2)^2 + 0.896(0.0082)w}$$

$$\eta^2 = 0.896 + 0.0041 + \sqrt{0.00001681 + .00734w}$$

$$w = 2[(\eta/\zeta)+1] / [(\eta/\zeta)+2]$$

$$w = 1.345 \rightarrow \eta^2 = 0.999 \text{ \& } w = 1.345, \text{ OK}$$

$$\eta^2 = 0.999 \rightarrow \eta = 0.999$$

$$\zeta = 0.9465$$

$$0 < 0.9465 < .999 < 1 \text{ OK}$$

$$P_Q = (P_A - P_I) \cdot \{1 - 3 \cdot \zeta^2 + 2 \cdot \zeta^3 / \eta + \zeta^2 \cdot \ln \eta^2\} + P_I$$

$$P_Q = (12.98 - 0.0)[1 - 3(0.896) + (2(0.9465)^3 / 0.999) + 0.896 \ln(0.999)] + 0$$

$$P_Q = 0.1125$$

(J.8) Edge bending moments

(J.8.1) $M_A=0$, on both side integral connections

(J.8.2) M_B , the active fluid pressure bending moment

$$b_S = -10.0$$

$$\lambda_S = (2b_S)/d_2 = -2(10)/4230 \text{ (sign of } b_S \text{ must restrictly be observed) see (J.5)}$$

$$= -0.00473 < 0.0$$

$$|\lambda_S| = .00473 < 0.05 \text{ then } M_B = 0 \text{ may be assumed, but more precise:}$$

$$M_B = \{P_S (d_2 - 2b_S) + (P_D - P_R) (d_1^2/d_2^2)\} (b_S/4)$$

$$M_B = \{1(4236 - 2(-10)) + (3 - 1.5) [(4136)^2/4230]\} (-10/4)$$

$$M_B = -25783.85$$

(J.8.3) M_C , the reactive bending moment from connected components

$$M_C = (f_F e_F^2/4)(2b_F/d_2) + (e_C^2/4)\sqrt{f_C^2 - 3(P_T d_C/4e_C)^2} + (e_S^2/4)\sqrt{f_S^2 - 3(P_S d_S/4e_S)^2}$$

$$f_F = f_P = 145 \text{ MPa}$$

$$e_F = 129 \text{ mm}$$

$$b_F = 87 \text{ mm}$$

$$d_2 = 4236 \text{ mm}$$

$$e_C = 87 \text{ mm}$$

$$f_C = 150.5 \text{ MPa}$$

$$P_T = 4.0 \text{ Mpa}$$

$$d_C = 4236 \text{ mm}$$

$$e_S = 67 \text{ mm}$$

$$f_S = 154.66 \text{ Mpa}$$

$$P_S = 1 \text{ Mpa}$$

$$d_S = 4256 \text{ mm}$$

$$M_C = [145(129)^2/4][2(87)/4236] + (87^2/4)\sqrt{(150.5)^2 - 3[4(4236)/4(87)]^2} + (67^2/4)\sqrt{154.66^2 - 3(4256/4(67))^2}$$

$$M_C = 24778.83 + 235873.36 + 170800.16$$

$$M_C = 331452.35$$

(J.8.4) M_D , the reactive bending moment limitation by the tube sheet for all edge configurations

$$M_D = ((f_P e_{P,red}^2)/4) \{1 - (P_R d_2 / 2 f_P e_{P,red})^2\}$$

$$f_P = 145 \text{ MPa}$$

$$e_{P,red} = e_P = 129 \text{ mm}$$

$$P_R = 1.35 \text{ MPa}$$

$$d_2 = 4236 \text{ mm}$$

$$M_D = [(145 (129^2))/4] \{1 - [1.35(4236) / 2(145)(129)]^2\}$$

$$M_D = 589180.29$$

(J.8.5) Resultant bending moment M_2

Due to small plastic deformations, the real value M_2 approximates a value $M_{2,opt}$, being optimum for the limit load.

$$M_{2,max} = \text{Min} \{ M_A + M_B + M_C, M_D \}$$

$$M_{2,max} = \text{Min} \{ 0 - 25783.85 + 331452.35; 589180.29 \}$$

$$M_{2,max} = \text{Min} \{ 305668.5; 589180.29 \}$$

$$M_{2,max} = 305668.5$$

$$M_{2,min} = \text{max} \{ M_A + M_B - M_C; -M_D \}$$

$$M_{2,min} = \text{max} \{ 0.0 - 25783.85 - 331452.35; -589180.29 \}$$

$$M_{2,min} = \text{max} \{ -357236.2; -589180.29 \}$$

$$M_{2,min} = -357236.2$$

$$M_{2,opt} = [-d_1^2 / 8(1 + \lambda_R)] \{ (P_Q / 2(2 + k_P)) + P_R \lambda_R + P_D \lambda_R^2 (1 + \lambda_R / 3) \}$$

$$d_1 = 4136$$

$$\lambda_R = 2b_R / d_1 = 2(47) / 4136 = .0227 \text{ (see J.5)}$$

$$P_D = 3.0 \text{ (see J.7.4)}$$

$$k_P = 0.374 \text{ (see J.5.2.2)}$$

$$k_P = 0.374(1 - \ln \eta^2) = 0.374(1 - \ln 0.9827) \rightarrow k_P = 0.3674$$

$$P_Q = 0.1233 \text{ (see J.7.6.3)}$$

$$P_R = 1.35$$

$$M_{2,opt} = [-(4136)^2 / 8(1 + .0227)] \{ (0.1233 / 2(2 + 0.3674)) + 1.35(.0227) + (3.0)(.0227)^2(1 + (.0227/3)) \}$$

$$M_{2,opt} = -121779$$

$$M_2 = \text{max} \{ M_{2,min}; \text{min}(M_{2,opt}; M_{2,max}) \} = \text{max} \{ -357236.2; \text{min}(-121779; 305668.5) \} \\ = \text{max} \{ -357236.2; -121779 \} = -121779$$

(J.8.6) Pressure representing the moment

$$\begin{aligned}
P_M &= M_2 \cdot 8 \cdot (1 + \lambda_R) / d_1^2 + P_R \lambda_R + P_D \lambda_R^2 (1 + 4 \lambda_R / 3) \\
&= (-121779) (8) (1 + .0227) / (4136)^2 + 1.35(.0227) + 3.0(.0227)^2 (1 + (.0227/3)) \\
&= -0.026
\end{aligned}$$

(J.9.1) Bending within the tubed region

$$\begin{aligned}
L_1 &= 3 \left| P_Q \right| / [(2 + k_p) \Phi_p] \quad (\text{for } \Phi_p \text{ see J.5.2.2}) \\
L_1 &= 3(0.1125) / (2 + 0.3674) (.1683) = 0.847 \\
L_2 &= 3 \left[\left(\left| P_Q + P_M(2 - \lambda_R) \right| \right) + \left| P_M \lambda_R \right| \right] / [(1 + k_p) \Phi_p + \lambda_R] \\
L_2 &= 3 \left[\left(\left| 0.1233 - .026(2 - .0227) \right| \right) + \left| -.026(.0227) \right| \right] / [(1 + .3674) (0.1683) + .0227] \\
&= 0.86 \\
L_3 &= \left[\left| P_Q \right| + \left| P_Q + P_M 6 \right| \right] / (\Phi_p + \lambda_R) \\
L_3 &= [1.1233 + |0.1233 + 6(-0.026)|] / (0.1683 + .0227) = 0.81
\end{aligned}$$

$$\begin{aligned}
\Phi_B &= \max (L_1; L_2; L_3) [d_1^2 / (12 f_p e_p^2)] \leq 1.0 \\
\Phi_B &= \max (0.847; 0.86; 0.81) [(4136^2) / (12(145) (129)^2)] \\
\Phi_B &= (0.86)(0.59078) = 0.51 < 1.0 \quad \text{O.K.}
\end{aligned}$$

(J.9.2) Shear at the boundary of the tubed region

$$\begin{aligned}
\Phi_S &= \left[\left| P_R \right| d_1 \right] / [2 \Phi_p f_p e_p] \leq 1.0 \\
\Phi_S &= (1.35(4136)) / (2) (.1683) (145) (129) = 0.88 < 1.0 \quad \text{O.K.}
\end{aligned}$$

(J.9.3) Local loading on untubed region

$$\begin{aligned}
P_R &= 1.5 \\
P_D &= 3.0 \\
b_u &= (4250 - 4136) / 2 = 57 \\
(3.0)(57) / 4250 &= 0.4 \\
1.5 &> 0.4, \text{ no check is required}
\end{aligned}$$

(J.9.4) Additional effect of weight

$$e_p / d_2 = 129 / 4230 = 0.03 > 0.02, \text{ no check is required}$$

C. Calculation according to ASME Sec. VIII, Div. 1, Appendix AA

All nomenclature is according to the above appendix.

Step 1:

$$d^* = d - 2t(E_t/E)(\%ED/100)(S_t/S)$$

% ED= percent of expanded depth= 0.0 (no expansion)

$$d^* = d, \text{ where } d = \text{tube out diameter} = 57 \text{ mm} = 2.244 \text{ in}$$

$$a = r_c + d^*/4$$

r_c is the radius to outermost tube hole centre

$$r_c = (OTL/2) - (d/2) = (4136/2) - (58/2)$$

$$r_c = 2068 - 29 = 2039 \text{ mm} = 80.27559 \text{ in}$$

$$a = 80.27559 + (2.24/4)$$

$$a = 80.835 \text{ in}$$

$$A_u = 2r_c w_u$$

$$w_u = 0.0 \text{ (no pass partition)}, A_u = 0.0$$

$$t_{\text{tube}} = 2.9 \text{ mm} = 0.11417 \text{ in}$$

$$x = \pi a^2 - A_u = \pi (80.835)^2 - 0.0$$

$$x = 20528.1$$

$$p' = p \sqrt{1 + (A_u/x)}$$

$$p = \text{tube pitch} = 69 \text{ mm} = 2.716 \text{ in}$$

$$p' = p = 69 \text{ mm} = 2.716 \text{ in}$$

$$\eta = 1 - d^*/p'$$

$$\eta = 1 - (2.244/2.716) = 0.173 \text{ (ligment efficiency)}$$

$$e = (E^*/E)(0.91/(1 - v^{*2}))$$

$$\text{Fig. A.2.2.1, } (E^*/E) = 0.16, v^* = 0.46$$

$$e = (0.16)(0.91/(1 - .46^2)) = 0.185 \text{ (flexural efficiency)}$$

$$k = b/a$$

$$b = 4323/2 \text{ mm} = 85.0984 \text{ in}$$

$$k = 85.098/80.835 = 1.052$$

$$k^- = a_1/a$$

a_1 is the imperforated ring outer radius

$$a_1 = A/2 \text{ is the outside diameter of the tubesheet given by } 2205 \text{ mm} = 86.811 \text{ in}$$

$$k^- = 86.811/80.835 = 1.07$$

$$k_c = a_c/a$$

$$a_c \text{ is the radial channel dimension given by } 2160 \text{ mm} = 85.039 \text{ in}$$

$$k_c = 85.0393/80.835 = 1.0517$$

Step 2:

$$\xi = (2/n) (b/d) (h_s/t) (1/(1 - (t/d))) (E_s/E_t)$$

$$E_s = 195000 \text{ MPa} = 28.08(10^6) \text{ PSI}$$

$$E_t = 193387 \text{ MPa} = 27.87(10^6) \text{ PSI}$$

h_s is the shell thickness at the junction to the tubesheet = 67 mm = 2.63779 in

t is the nominal tube wall thickness = 2.9 mm = 0.11417 in

$$\xi = (2/3100)(85.0984/2.244)(67/2.9)(1/(1-(2.9/57)))(195000/193875) = 0.67$$

$$\beta_s = 1.285/\sqrt{bh_s} = 1.285/\sqrt{85.0984(2.63779)} = 0.0857$$

$$\beta_c = 1.285/\sqrt{a_c h_c}$$

h_c is the channel thickness given by 87 mm = 3.42519 in

$$\beta_c = 1.285/\sqrt{(85.039)(3.42519)} = 0.075$$

Step 3:

$$J = 1.0$$

$$\lambda_s = v(b/h_s) + (E_s/E_t)(d/t)[v/2 + (a^2/nd^2)(1/(1-t/d))(1-nd^2/4a^2)]$$

$$\lambda_s = 0.3(85.0984/2.63779) + (2.244/0.11417)(28.08(10^6)/27.87(10^6))[(0.3/2) + ((80.835)^2/3100(2.244)^2)(1/(1-(0.114173/2.244)))(1-(3100(2.244)^2/(4(80.835)^2))]$$

$$\lambda_s = 9.678 + 19.8024[0.15 + 0.41859(1/(1-.0508))(1-0.597)] = 16.17$$

$$\lambda_t = (v/2)(d/t)(1-2t/d) + [a^2/ndt(1-t/d)][1 - (nd^2/4a^2)(1-(4t/d)+(4t^2/d^2))]$$

$$\lambda_t = (0.3/2)(57/2.9)(1-(2(2.9)/57) + [80.856^2/((3100)(57/25.4)(2.9/25.4)(1-(2.9/57)))] [1 - (3100(57/25.4)^2/(4(80.85^2)))(1-(4(2.9)/57) + 4(2.9^2/57^2)]$$

$$= 2.6482 + 8.67[1 - 0.597(0.8088)] = 7.14$$

$$Q_e = J(\alpha_t \Delta T_r - \alpha_s \Delta T_s) + J\lambda_s(p_s/E_s) - (p_t/E)[J\lambda_t + (0.5E_t b/E_s h_s)]$$

$$Q_e = [12.51(10)^{-6}(167.5-20) - 12.42(10)^{-6}(145-20) + 16.17(146/28.08(10^6)) - (584/27.847(10^6))[7.14 + (0.5)(27.847(10^6))(85.0984)/(2.63779(28.08(10^6)))]$$

$$e = .000292725 + 0.000083499 - .0000211[7.14 + 15.996] e = -0.0001119$$

Step 4:

$$h = 129 \text{ mm}$$

L is the tube length given by 4662 mm = 183.56 in

E = tube sheet modulus of elasticity = 193875 MPa

$$X_a = 2.161[(nE_t t(d-t)/(eELa))^{1/4}(a/h)^{3/4}]$$

$$X_a = 2.161[(3100)(0.114173)(2.129)/(27.918(10^6))(0.185)(183.56)(80.835)]^{1/4}(80.835/5.0787)^{3/4} = 12.46$$

$$\mu = (2.198/Eh^3)[\beta_s h_s E_s b(1 + \beta_s h + (\beta_s^2 h^2/2)) + \beta_c h c^3 E_c a_c(1 + \beta_c h + (\beta_c^2 h^2/2))]$$

$$\mu = [2.198/(27.918)10^6(5.0787)^3] \{0.0857(2.63779)^3(28.08(10^6)(85.0984)[1 + 0.0857(5.0787) + (5.0787)^2(.0857)^2/2] + [0.075(3.42519)^3(27.648)(10^6)(85.039)]$$

$$[1 + 0.075(5.0787 + (.075)^2(3.42519)^2/2)]\}$$

$$\mu = [2.198/(27.918)10^6(5.0787)^3] \{0.0857(2.63779)^3(28.08(10^6)(85.0984)(.0947) + [0.075(3.42519)^3(27.648)(10^6)(85.039)](1.42)\} = 6.26$$

$$\gamma_s = 0.25(K^2 - 1)(K - 1) - \bar{\gamma}_s$$

$$\bar{\gamma}_s = \beta_s^2 h_s^2 K^3(1 + \beta_s h)/5.46$$

$$= (0.0857)^2(2.63779)^2(1.052)^3(1 + .0857(5.0787))/5.46_s = 0.016$$

$$\gamma_b = 0.0$$

$$\bar{\gamma}_s = \beta_c^2 h_c^2 K_c^3(1 + \beta_c h)/5.46$$

$$= (0.075)^2(3.425)^2(1.0517)^3(1 + .075(5.0787))/5.46 = 0.0194$$

$$\gamma_i = 0.25(1.0517^2 - 1)(1.0517 + 1) - 0.5(1.0517^3 - 1.0517) + 0.0194 = .019$$

$$\gamma_s = 0.25(1.0517^2 - 1)(1.0517 - 1) - 0.016 = -0.0146$$

Step 5:

$$X_a = 12.46, \text{ and then } Z_v X_a = 0.08, Z_v = 0.08/12.4 = 6.5(10)^{-3} \text{ (out of scale)}$$

$$Z_m = 0.12$$

$$\Phi = (0.91/e)(\ln k + \mu) = (0.91/0.185)(\ln 1.07 + 6.26) = 31.125$$

$$Q_1 = (K - 1 - \Phi Z_v)/(1 + \Phi Z_m)$$

$$Q_1 = (1.0517 - 1 - 96.1(6.5)10^{-3})/(1 + 96.1(0.12)) = -.02249 = -.0318$$

$$Q_2 = [a^2(p_i \gamma_i + p_i \gamma_i + p_s \gamma_s - p_s \gamma_s) + B d \gamma_b]/(1 + \Phi Z_m)$$

$$a = 80.856$$

$$p_i = 584$$

$$\gamma_i = .019$$

$$p_i^* = (E_c h_c / a_c)(\alpha_c \Delta T_c^* - \alpha_{ts} \Delta T_r)$$

$$E_c = 192000, E_s = 195000, E_{tube} = 193875, E_{ts} = 193875$$

$$\alpha_c = 12.7(10)^{-6}, \alpha_s = 12.4(10)^{-6}, \alpha_t = 12.51(10)^{-6}, \alpha_{ts} = 12.51(10)^{-6}$$

$$\text{temperature on channel side} = 190^\circ \text{C}, \text{ temperature on shell side} = 145^\circ \text{C},$$

$$\text{temperature of tubes} = 167.5^\circ \text{C},$$

$$\text{temperature of tubesheet} = 167.5^\circ \text{C}$$

$$\Delta T_c^* = (.5)(\Delta T_c + \Delta T_r) = 158.75^\circ \text{C}$$

$$\Delta T_s^* = .5(\Delta T_s + \Delta T_r) = 136.25^\circ \text{C}$$

$$\Delta T_c = 190 - 20 = 170^\circ \text{C}$$

$$\Delta T_s = 145 - 20 = 125^\circ \text{C}$$

$$\Delta T_{ts} = 167.5 - 20 = 147.5^\circ \text{C}$$

$$\Delta T_r = (.333)(170 + 125 + 147.5) = 147.5^\circ \text{C}$$

$$P_s^* = (E_s h_s / b)(\alpha_s \Delta T_s^* - \alpha_{ts} \Delta T_r)$$

$$P_s^* = [28.08(10^6)(2.63779)/85.0984](12.4(10)^{-6}(136.25) - 12.51(145.5)(10)^{-6})$$

$$P_s^* = -135.5$$

$$P_i^* = (27.648(10^6)(3.425196)(12.7(10)^{-6}(158.75) - 12.51(10)^{-6}(147.5))$$

$$P_i^* = 190.31$$

$$Q_2 = [(80.856^2)(584(.019) + 190.31(.0194) + 146(-.0146) - (-135.5)(.016))]/[1 + 31.125(0.12)]$$

$$Q_2 = 20465.27$$

Step 6:

$$X_a = 12.46, Q_1 = -0.0318 \text{ (out of scale)}$$

$$QZ1/X_a = 0.42, QZ1 = 5.23 \text{ also, } QZ2/X_a^3 = .02, QZ2 = (.02)(12.46)^3 = 38.68$$

$$U_1 = (0.5)(12.46)^4[6.5(10)^{-3} + (1.0517 - 1)(0.12)]$$

$$U_1 = 153.1$$

$$P_e a^2 / 2 = [b E_s h_s Q_e - J \xi Q_2 U_1 - 0.5(p_s - p_t) a^2 (K^2 - 1)]/[1 + J \xi (QZ1 + (K - 1) QZ2)]$$

$$P_e a^2 / 2 = [(85.04)(28.08)(10^6)(2.637795)(-.0001119) - (.67)(20465.27)(153.1) - 0.5(146 - 584)(80.856)^2((1.07)^2 - 1)]/[1 + 0.67[5.23 + (1.07 - 1)(38.68)]]$$

$$= -411056.06$$

$$P_e = -125.75$$

$$Q_3 = Q_1 + Q_2 / (P_e a^2 / 2) = -0.0318 + 20465.27 / (-411056.06) = -0.08$$

$$2F_m = 0.03 \text{ (out of scale)}$$

$$F_m = 0.015$$

$$\sigma_b = (2a/h)^2 (1.5) F_m P_e / \eta$$

$$a = 80.856$$

$$h = 5.0787$$

$$F_m = 0.015$$

$$P_e = -125.75$$

$$\eta = 0.173$$

$$\sigma_b = (2(80.856)/5.0787)^2 [(1.5)(.015)(-125.75)/0.173] = 115 \text{ MPa}$$

allowable stress according to table (2.2.4)

$$\sigma_{allow} = 1.5 \Omega S = 1.5(8/3)(145) = 580 \text{ MPa}$$

Also for the ASME material, the allowable stress, from table (2.2.3), is 138 MPa which results in $\sigma_{allow} = 552 \text{ MPa}$.

Step 7:

Shear stress:

$$\tau = P_e a / (2\eta h)$$

$$\tau = (-125.75)(80.856) / (2(0.173)(5.0787)) = -40.2 \text{ MPa}$$

If temperature effect not to be considered, then

$$d^* = d = 57 \text{ mm}$$

$$a = 2053.7 \text{ mm}$$

$$A_u = 0.0$$

$$x = \pi a^2 = 20535.7$$

$$p' = p = 69 \text{ mm} = 2.716$$

$$\eta = 1 - d^* / p'$$

$$\eta = 1 - (2.244 / 2.716) = 0.173 \text{ (ligament efficiency)}$$

$$e = 0.185 \text{ where } E^* / E = 0.16, \nu^* = 0.46$$

$$b = 85.0984$$

$$k = b / a = 2160 / 2053.7 = 1.0517$$

$$k^- = a_l / a = 1.07$$

$$k_c = 1.05, \xi = 0.67, \beta_s = 0.0857, \beta_c = 0.075, \lambda_s = 16.17, \lambda_l = 7.14$$

$$\text{Recall also, } p_s = 146, p_t = 584$$

$$J = 1.0$$

$$Q_e = J(\alpha_l \Delta T_l - \alpha_s \Delta T_s + J \lambda_s (p_s / E_s) - (p_t / E_t) [J \lambda_l + 0.5(E_t b / E_s h_s)])$$

or with no temperature

$$Q_e = 16.17(p_s / E_s) - (p_t / E_t) [7.14 + 0.5 E_t (85.0984) / 1.22 E_s]$$

$$Q_e = 16.17 [146 / 28.08(10^6)] - [584 / 27.847728(10^6)] / \{7.14 + [0.5(27.87728(10^6)) (85.0984) / [28.08(10^6)(2.63779527)]]\}$$

$$= 0.000084 - 0.00048557 = -0.00040157$$

The following parameters remain the same:

$$X_a = 12.46, \mu = 6.26, \gamma_s = -0.0146, \gamma_t = 0.019, \Phi = 31.125, Q_1 = -0.0318, Z_m = 0.12$$

Then

$$P_i^* = 0.0, P_s^* = 0.0$$

$$Q_2 = (80.856)^2 [584(0.019) + 146(-0.0146)] / [1 + 31.125(0.12)]$$

$$Q_2 = 12377.3$$

$$U_1 = 153.1$$

$$P_e a^2 / 2 = \{ (85.0984) (28.08) (10^6) (2.637795276) (-0.00040157) - (0.67) (12377.3) (153.1) - 0.5 (146 - 584) (80.856)^2 (1.07^2 - 1) \} / \{ 1 + 0.67 [5.23 + (1.07 - 1) 38.68] \} = -568727.94$$

$$P_e = -173.98$$

$$Q_3 = Q_1 + Q_2 / (P_e a^2 / 2)$$

$$Q_3 = -0.0318 + (12377.3 / (-568727.94))$$

$$Q_3 = -0.054$$

$$2F_m = 0.05 \rightarrow F_m = 0.025$$

$$\sigma_b = (2a/h)^2 [1.5 F_m P_e / \eta]$$

$$\sigma_b = [2(80.856)/5.07874]^2 [(1.5)(0.025)(-174)] / 0.173 = -265.53 \text{ MPa}$$

$$\tau = P_e a / 2\eta h$$

$$\tau = (-174)(80.856) / [2(0.173)(5.07874)] = 56 \text{ MPa}$$

13. References

- [1] Timoshenko, S., Woinowsky-Krieger, S.: Theory of plates and shells, McGraw - Hill, 1959.
- [2] Gardner, K. A.: Heat Exchanger Tubesheet Design – Part 2: Fixed Tubesheets. J. Appl. Mech., Trans. ASME, 74 (1952), 215-231.
- [3] Gardner, K. A.: Heat Exchanger Tubesheet Design – Part 3: U-Tube and Bayonet Tubesheets. J. Appl. Mech., Trans. ASME, 27 (1960), 25-32.
- [4] Gardner, K. A.: Tubesheet Design: A Basis for Standardization. Proc. First Intl. Conf. Pressure Vessel Technology: Part I, Design and Analysis, pp. 621-648. ASME New York, 1969.
- [5] WRC Bulletin No. 52, July 1959. Salerno, V. L., Mahoney, J. B.: A Review, Comparison and Modification of Present Deflection Theory for Flat Perforated Plates. Deagle, L.: Correlation of Experimental Data with Theory for Perforated Plates with a Triangular Hole Array.
- [6] Pressure Vessels and Piping: Design and Analysis – A Decade of Progress. Components and Structural Dynamics. Vol. 2. ASME New York, 1976.
- [7] O'Donnell, W. J., Langer, B. F.: Design of Perforated Plates. J. Engng for Industry, 84 (1962), p. 307. ff.
- [8] Meijers, P.: Plates with Doubly-Periodic Pattern of Circular Holes Loaded in Plane Stress or Bending. Proc. First Intl. Conf. Pressure Vessel Technology, Part I, 551-570. ASME New York, 1969.
- [9] Slot, T., O'Donnell, W. J.: Effective Elastic Constants for Thick Perforated Plates with Square and Triangular Penetration Patterns. J. Engng for Industry 93 (1971), p. 935ff.
- [10] O'Donnell, W. J.: A Study of Perforated Plates with Square Penetration Patterns. WRC Bulletin No. 124 (1967).
- [11] Soler, A. I., Caldwell, S. M., Singh, K. P.: Tubesheet analysis – A proposed ASME design procedure. ASME Publication H00343, Thermal/Mechanical Heat Exchanger Design – Karl Gardner Memorial Session, Eds. Singh K. P., Shenkman, S. H., ASME 1986 WAM.
- [12] Soler, A. I., Caldwell, S. M., Soler, S. D.: A proposed ASME Section VIII, Division 1, tube sheet design procedure. Proceedings of the 1990 ASME PVP Conference- Nashville – Vol. 186(H00605).
- [13] ASME Code, Sec. VIII, Div 1 and 2: Pressure Vessel Design Code, American Society of Mechanical Engineers, 2005.
- [14] EN 13445-3: European Standard for Unfired pressure Vessel – Part 3: Design, Annex B: Direct Route for Design by Analysis, European Committee for Standardization, 2002.
- [15] C2- Hydrogenation Reactor Mechanical Data Sheet, Linde, Olefin 6 plant.
- [16] Jones and Gordon: An elastic-plastic flow model for finite element analysis of perforated materials, Transaction of ASME, J. of Pressure Vessel Technology, Vol. 123, No. 3, pp. 265-270, 2001.
- [17] Gerdeen, J.C.: A Critical Evaluation of Plastic Behavior Data and A United Definition of Plastic Load for Pressure Components, WRC Bulletin 24, Nov. 79, ISSN 0043-2326.

- [18] Burgoyne, C. J., Brennan, M. G.: Exact Ilyushin yield surface, International journal of solid structures Vol. 30, No. 8, pp. 1113 – 1131, 1993.
- [19] Zeman, J. L.: Repetitorium Apparatebau: Grundlagen der Festigkeitsberechnung, Oldenbourg Verlag Wien, 1992.
- [20] Osweiller, F.: New common design rules for U-tube heat exchangers in ASME, CODAP and UPV CODES, PVP- Vol. 439, Pressure Vessel and Piping Codes and Standards-2002-1239.
- [21] Preiss, R.: Ratchting and shakedown analysis of pressure equipment using elasto- plastic finite element analysis, PhD Thesis, Vienna University of Technology, Aug. 2000.
- [22] Hamilton, R., Mackenzie, J. Shi & J. T. Boyle: Simplified lower bound limit analysis of pressurised cylinder/ cylinder intersections using generalised yield criteria, Int. J. Ves.& Piping 67 (1996) 219-226.
- [23] Yeom, D.J. & Robinson, M.: Numerical analysis of the elastic –Plastic behaviour of pressure vessel with ellipsoidal and torispherical heads, Int. J. Pres. Ves.& Piping 65 (1996) 147-156.
- [24] Osweiller, F., Robert, D.: New design rules for fixed tube sheets heat exchangers: A comparison of CODAP and ASME approaches, PVP- Vol. 210-2.
- [25] Osweiller, F.: Evaluation and synthesis of the effective constants concept for design of tube sheets, Journal of pressure vessel technology, Aug. 89, Vol.
- [26] Niemi, E.: Stress determinatin for fatigue analysis of welded components, The International Institute of Welding, IIs/IIW-1221-93 (ex doc XIII- 1458-92, XV- 797-92), pp33, 1995.
- [27] Petershagen, Fricke, Massel: Application of the local approach to the fatigue strength assessment of welded structures in ships, International Institute of Welding, IIW-Doc. XIII- 1409- 91, 1991.
- [28] Zeman, J.L., Preiss, R.: The Deviatoric Map – A simple tool in DBA. Intl. J. Pressure Vessel & Piping, 76, 339- 344, 1999.

Khosrow Behseta
No. 34, / Th. Ave.
Nsre(Kisha St.), Tehran, Iran 14467
Ph: 0098-21-88275593
e-mail: behsetaeq@yahoo.com

Feb-01.2006

Personal: Birthday on May 23, 1955 married with two children.

Education:

- Dr. Hashroodi High school, High School Diploma in Mathematics, 1973, Tehran, Iran.
- Tri State University, BSc in Civil (structural) Engineering, 1974 to 1978, Indiana, USA.
- University of Tennessee at Chattanooga, MSc in Mechanical Engineering, 1978 to 1981, Tennessee, USA.
- Vienna University of Technology study for Doktor der technischen Wissenschaften, 2004 to present.

Academic Organization:

- Full member of American Society of Mechanical Engineers.

Work Experience:

- 1980 to 1981, Jordan service Co., application engineer on designing waste heat recovery equipments, Tennessee, USA.
- 1982 to 1983, Ramin Thermal Power Station, site engineer, Ahwaz, Iran.
- 1983 to 1984, Karanj Gas Injection Project, mechanical engineer on pressure vessel section, Sazeh Consulting Engineers, Tehran, Iran.
- 1984 to 1986, Tose and Gazven power station, mechanical design of tank farms, Moshaneir Power Consultant, Tehran, Iran.
- 1986 to 1988, Noshahr Naval University, teaching undergraduate courses on strength of materials, Noshahr, Iran.
- 1988 to 1990, Azarab Manufacturing Company, head of pressure vessel department, Tehran, Iran.
- 1990 to 2001, Oil Industries Engineering and Design Company, head of pressure vessel department, Tehran, Iran.
- 2001 to 2003, Reactor Saz Manufacturing Company, project engineer and engineering manager, Tehran, Iran.

Others:

- Skill on finite element application on pressure vessel components using ANSYS.
- Skill on dome roof design of large diameter refinery and petrochemical storage tanks.
- Skill on design of floating roof tanks.

K. Behseta